2013

cDrake CPIES Data Report November 2007 to December 2011

Karen L. Tracey
Graduate School of Oceanography, University of Rhode Island

Kathleen Donohue
Graduate School of Oceanography, University of Rhode Island

See next page for additional authors

Authors
Karen L. Tracey, Kathleen Donohue, D. Randolph Watts, and Teresa Chereskin

GRADUATE SCHOOL OF OCEANOGRAPHY
UNIVERSITY OF RHODE ISLAND
NARRAGANSETT, RHODE ISLAND

cDrake CPIES Data Report

November 2007 to December 2011

GSO Technical Report 2013-01

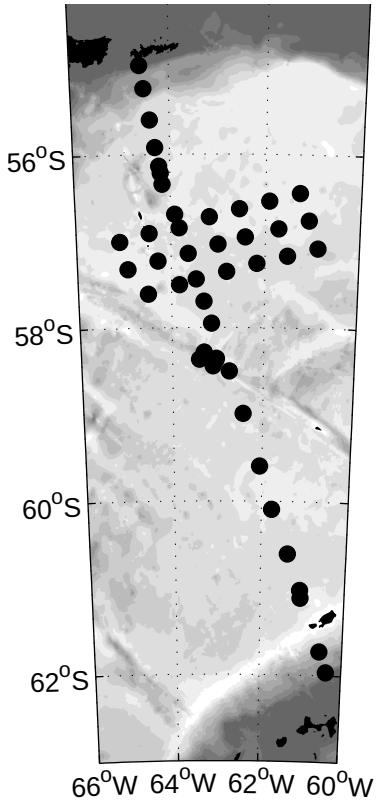

by
Karen L. Tracey
Kathleen A. Donohue
D. Randolph Watts
and
Teresa Chereskin

January 28, 2013

ABSTRACT

The goal of cDrake is to quantify the transport and understand the dynamic balances of the Antarctic Circumpolar Current (ACC) in Drake Passage. For this purpose, a transport line spanning all of Drake Passage and a local dynamics array of CPIES were deployed for a period of four years. A CPIES comprises an inverted echo sounder equipped with a bottom pressure gauge and a current meter tethered 50 m above the bottom.

In addition to the CPIESs, three current meter moorings were deployed along the continental margins for the initial two years of the field program. Subsequently, a current meter comparison mooring was deployed in a region of strong bottom currents for a period of one year. Conductivity-temperature-depth and lowered acoustic Doppler current profiler measurements were taken at each CPIES site. Shipboard acoustic Doppler current profiler measured the velocity structure along the cruise track.

In this report, the CPIES data collected during the field experiment are presented. The collection, processing and calibration of the CPIES are described.

Contents

List of Figures

List of Tables

1 Setting and Experiment Design

1.1 Introduction

This report documents the processing of data collected from an array of inverted echo sounders equipped with bottom pressure gauges and current meters (CPIES) spanning the Drake Passage from November 2007 to December 2011 (Figure 1). The cDrake array consisted of a transport line of 20 CPIESs spanning 800 km across the Drake Passage, and a local dynamics array (LDA) of 21 CPIESs spanning 120 km cross-stream and 240 km downstream. An additional form drag array consisting of 5 CPIESs was maintained along the Shackleton Fracture Zone during the final year of the observational program. The CPIESs were moored in water depths ranging from 500 m on the northern edge of the passage to 4300 m in the middle. Calibration CTDs were taken at each site along with lowered acoustic Doppler current profiles (LADCP).

cDrake was a collaboration between investigators at University of Rhode Island (URI) and Scripps Institution of Oceanography (SIO). The measurements presented here were made with support provided by National Science Foundation Office of Polar Programs grants ANT-0636493 and ANT-0635437.

1.2 CPIES description and sampling schemes

A CPIES is a URI manufactured inverted echo sounder (IES) with a Paroscientific pressure sensor housed in a single glass sphere, and an Aanderaa Doppler current sensor (DCS) tethered 50 m above with additional flotation. The CPIES is kept stationary by an anchor stand to prevent movement from affecting the pressure measurement. Temperatures are measured by both the pressure sensor and the DCS. The cDrake CPIESs were equipped for acoustic telemetry that enabled us to assess data quality immediately after launch and to obtain internally-processed, daily-averaged data throughout the deployment. The telemetered data were collected once per year on annual cruises; acoustic communication with the CPIES was through a hull-mounted 12 kHz transducer.

The IES emits 12 kHz sound pulses, and the round trip travel times to the surface and back of the pulses are recorded internally. During cDrake, four acoustic pulses were transmitted every 10 minutes. After recovery, data processing creates a single value (τ or tau) from the 24 measurements taken during each hour.

The Paroscientific pressure and temperature measurements were taken every 30 minutes, and the CPIES internally corrects the pressure measurements for temperature sensitivity. Two models of pressure sensors were used during cDrake: Model 46k has a rating of 0–6000 psi (about 4100 dbar) and model 410k has a rating of 0–10000 psi (about 6800 dbar). Because the pressure sensor is inside the glass sphere, the associated temperature measurement is not in direct contact with seawater. Nevertheless, the temperature variations are highly correlated (> 0.9) with those measured by the DCS with a lag time of one hour. During the first telemetry cruise in November 2008, we discovered that strong currents produced sufficient drag on the flotation above the current meter to cause the anchor stand (with the attached CPIES) to tip over. When the currents subsided, the instrument self-righted. To minimize the number of tipping events while retaining the self-righting ability, a second ring was added to the anchor stand for CPIESs launched on subsequent cruises.

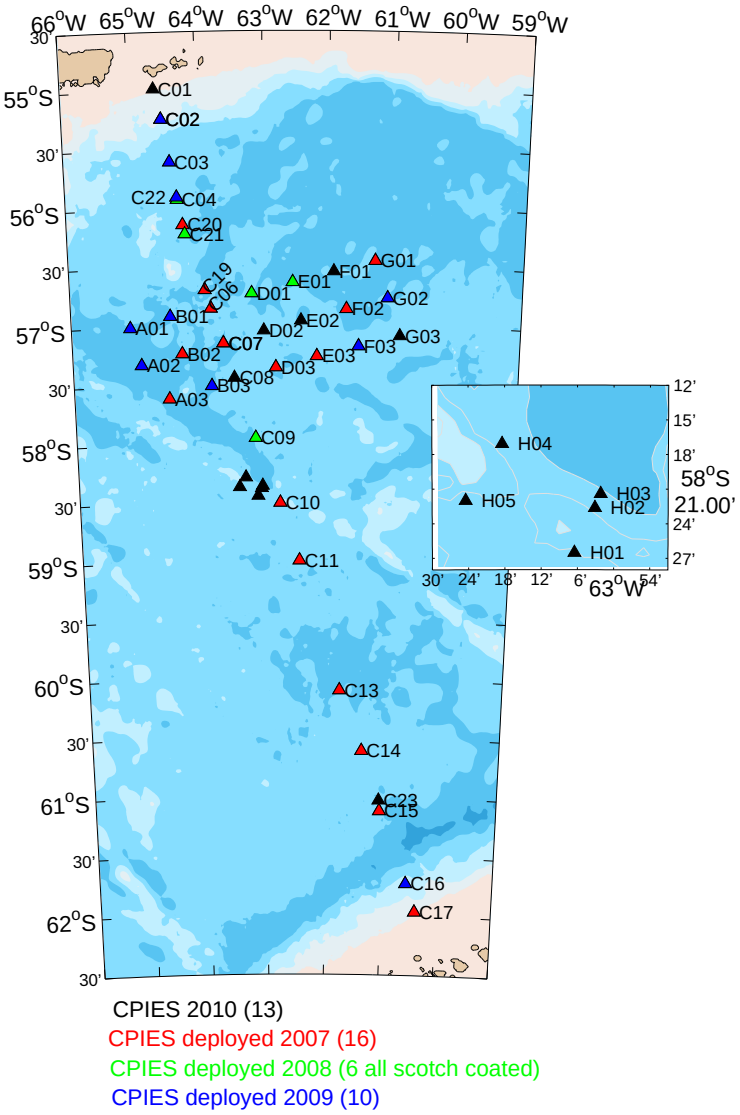

Figure 1: cDrake CPIES sites (triangles) occupied during the final year of the observational program. Bathymetry, derived from Smith and Sandwell (1997), is contoured every 1000 m; tan hues represent shallow depths and transition to blue hues in the deeper parts of the passage. Triangles are color-coded based on the year the CPIES was deployed at that location. Duplicate instruments are not shown. The inset shows an expanded view of the 5 sites in the form drag array located near C10.

Based on the battery capacity of the CPIES for a 4-year experiment, the DCS measurements of velocity and temperature were made once every hour during cDrake. The sampling rate was increased to every 10 minutes for instruments deployed during the final year. Two models of Aanderaa DCS were used during cDrake: Model 3820R (also known as RCM11) was used for all but eight of the deployed instruments. Model 4930R (also known as Seaguard or 'Z-pulse') was used for eight deployments during the final two years of the observational program (see Table 5). Unfortunately, many of the current meter cables deployed in the first year leaked resulting in the loss of data. In many instances just the DCS-measured velocities and temperatures ended early. In other cases, increased energy drain reduced the battery lifetime of the CPIES, which resulted in a system failure and all data collection ended early. Affected instruments were recovered and replaced on the telemetry cruises.

1.3 CPIES locations and data summaries

The cDrake fieldwork consisted of five cruises: deployment, three telemetry, and recovery (Table 1). All cruises were conducted aboard the RVIB Nathaniel B. Palmer which departed from and returned to Punta Arenas, Chile.

Table 1: Cruises aboard the RVIB Nathaniel B. Palmer and their missions.

Cruise Number	Cruise Dates	Cruise Description
NBP0710	13 November–7 December 2007	Deploy CPIES, deep current meter moorings, LADCP/CTD stations
NBP0812	19 November–13 December 2008	CPIES data telemetry, LADCP/CTD stations
NBP0908	19 November–19 December 2009	CPIES data telemetry, deep current mooring recoveries, deploy cook off mooring, LADCP/CTD stations
NBP1004	23 October–15 November 2010	CPIES data telemetry, cook off mooring recovery, LADCP/CTD stations
NBP1107	18 November–11 December 2011	Recover CPIES, LADCP/CTD stations

An array of 38 CPIESs was proposed. At the end of the deployment cruise, several additional instruments were launched to shorten the spacing between sites on the transport line near the LDA. Daily-averaged data were collected on the three telemetry cruises via pulse-delayed telemetry (PDT). To address instrument problems discovered during these cruises, several CPIESs were recovered and replaced. In some cases, where we suspected data quality issues, a second instrument was deployed to ensure continuous data coverage. In 2011, all instruments were recovered.

CPIES locations, shown in Figure 1, are listed in Table 2 together with the duration of deployment and nominal depth. Serial numbers of the IES, pressure, and current sensors are also tabulated. Figure 2 graphically displays the IES serial numbers and dates at each site.

Table 2: Site designators, instrument serial numbers, deployment and recovery dates, locations, and bottom depths. For each instrument package, serial numbers are tabulated for the inverted echo sounder (IES), Paros pressure sensor, and Aanderaa Doppler current sensor (DCS). Paros model 46k has a pressure rating to 6000 psi (∼4100 dbar), and model 410k is rated to 10000 psi (∼6800 dbar).

Site	IES SN	Paros Model	Paros SN	DCS SN	Deployment MMDDYY	Recovery MMDDYY	Latitude (S)	Longitude (W)	Nominal Depth (m)
A01	112	410k	91502	323	11/16/07	11/27/08	57° 00.18′	65° 04.83′	4139
A01	171	410k	92915	174	12/08/08	12/11/09	57° 00.18′	65° 04.84′	4137
A01	166	410k	92042	18	12/11/09	11/26/11	57° 00.30′	65° 04.89′	4130
A02	167	410k	92035	171	11/16/07	11/28/08	57° 19.27′	64° 55.48′	4384
A02	158	410k	92966	318	12/08/08	10/02/10	57° 19.29′	64° 55.45′	4386
A02	109	410k	91523	353	12/10/09	11/26/11	57° 19.39′	64° 55.39′	4455
A03	116	410k	96850	173	11/16/07	11/27/11	57° 36.60′	64° 29.85′	4410
B01	142	410k	92964	759	11/16/07	12/09/09	56° 54.62′	64° 27.35′	3943
B01	168	46k	75157	334	12/10/09	11/26/11	56° 54.59′	64° 27.42′	3943
B02	137	46k	36883	764	11/16/07	11/27/11	57° 13.81′	64° 16.91′	4048
B03	138	410k	92034	348	11/19/07	12/12/09	57° 30.35′	63° 49.54′	4087
B03	105	410k	96841	11	12/12/09	11/27/11	57° 30.36′	63° 49.55′	4093
C01	151	410k	91512	757	11/15/07	12/11/08	54° 58.08′	64° 35.54′	481
C01	151	410k	91512	359	12/11/08	10/25/10	54° 58.08′	64° 35.48′	486
C01	208	46k	75174	359	11/13/10	11/20/11	54° 58.79′	64° 37.08′	525
C02	213	46k	106399	503	11/15/07	11/21/08	55° 14.23′	64° 31.07′	1800
C02	143	46k	75154	354	12/11/08	Lost	55° 14.26′	64° 31.07′	1800
C02	142	410k	92964	348	12/15/09	11/19/11	55° 14.12′	64° 31.27′	1807
C03	168	46k	75157	339	11/15/07	11/22/09	55° 36.05′	64° 24.22′	3818
C03	229	46k	109325	15	11/22/09	11/20/11	55° 36.00′	64° 24.07′	3728
C04	208	46k	75174	353	11/15/07	12/10/08	55° 55.22′	64° 18.28′	3938
C04	144	410k	91525	756	12/11/08	11/21/11	55° 55.23′	64° 18.27′	3938
C05	143	46k	75154	758	11/15/07	12/10/08	56° 20.63′	64° 10.09′	3899
C06	210	46k	106395	344	11/17/07	11/25/11	56° 50.95′	63° 49.33′	4002
C07	121	410k	90551	164	11/19/07	11/28/11	57° 08.68′	63° 38.15′	4216
C07	147	410k	91520	316	11/12/10	11/28/11	57° 08.66′	63° 38.12′	4214
C08	211	46k	106398	760	11/19/07	11/03/10	57° 26.43′	63° 28.04′	3754
C08	107	410k	91509	339	11/02/10	11/28/11	57° 26.37′	63° 28.18′	3751
C09	101	410k	96932	762	11/20/07	11/29/08	57° 57.04′	63° 08.61′	4084
C09	170	410k	91512	503	12/06/08	12/05/11	57° 57.07′	63° 08.49′	4076
C10	102	46k	75161	172	11/20/07	12/04/11	58° 30.13′	62° 45.26′	2541
C11	217	46k	106389	165	11/20/07	12/04/11	58° 59.48′	62° 26.51′	3912
C12	109	410k	91523	165	11/20/07	11/29/09	59° 35.75′	62° 03.39′	4084
C12	208	46k	75174	349	11/29/09	12/08/09	59° 35.73′	62° 03.42′	4061
C13	115	410k	90776	343	11/20/07	12/02/11	60° 05.50′	61° 45.87′	4031
C14	209	46k	75163	351	11/21/07	12/02/11	60° 36.21′	61° 22.44′	3735
C15	111	410k	91510	501	11/21/07	12/02/11	61° 06.69′	61° 02.76′	3908
C16	149	410k	91500	341	11/21/07	11/30/09	61° 43.42′	60° 32.94′	2549

Continued on new page

Table 2 – *Continued from previous page*

Site	IES SN	Paros Model	Paros SN	DCS SN	Deployment MMDDYY	Recovery MMDDYY	Latitude (S)	Longitude (W)	Nominal Depth (m)
C16	153	410k	91869	12	11/30/09	12/03/11	61° 43.41′	60° 32.94′	2547
C17	157	410k	92972	504	11/21/07	12/03/11	61° 57.70′	60° 22.50′	1282
C18	132	410k	91508	342	11/26/07	12/06/08	57° 41.79′	63° 18.29′	3673
C19	119	410k	91144	337	12/01/07	11/25/11	56° 41.46′	63° 54.71′	3506
C20	162	410k	91866	313	12/03/07	11/21/11	56° 08.15′	64° 13.70′	3904
C21	213	46k	106399	305	12/10/08	11/25/11	56° 13.31′	64° 12.00′	3963
C22	218	46k	106838	174	12/15/09	11/21/11	55° 54.05′	64° 18.65′	3917
C23	138	410k	92034	352	11/06/10	12/02/11	61° 01.26′	61° 03.69′	3923
D01	144	410k	91525	756	11/17/07	12/08/08	56° 43.42′	63° 11.18′	4083
D01	167	410k	92035	338	12/08/08	11/25/11	56° 43.40′	63° 11.24′	4084
D02	147	410k	91520	352	11/19/07	11/23/08	57° 02.30′	63° 00.10′	3990
D02	148	410k	92040	357	11/23/08	Lost	57° 02.35′	63° 00.04′	3985
D02	132	410k	91508	17	12/13/09	10/31/10	57° 02.24′	63° 00.11′	3999
D02	173	410k	91519	171	10/31/10	11/28/11	57° 02.41′	63° 00.16′	3997
D03	216	46k	106839	340	11/19/07	11/29/11	57° 21.22′	62° 48.98′	3995
E01	153	410k	91869	305	11/17/07	12/09/08	56° 37.89′	62° 33.09′	4126
E01	112	410k	91502	762	12/09/08	11/22/11	56° 37.86′	62° 33.17′	4104
E02	156	410k	92909	316	11/18/07	10/27/10	56° 57.36′	62° 25.51′	4105
E02	124	410k	91136	349	10/27/10	11/24/11	56° 57.37′	62° 25.46′	4104
E03	214	46k	106397	166	11/19/07	11/22/11	57° 15.53′	62° 10.44′	3982
F01	152	410k	91498	346	11/17/07	10/29/10	56° 32.32′	61° 55.09′	4234
F01	149	410k	91500	758	10/29/10	11/23/11	56° 32.31′	61° 55.04′	4237
F02	118	410k	92036	307	11/18/07	11/22/11	56° 51.44′	61° 43.10′	4121
F03	218	46k	106838	517	11/18/07	11/26/09	57° 10.30′	61° 31.32′	3813
F03	101	410k	96932	13	11/26/09	11/23/11	57° 10.33′	61° 30.99′	3822
G01	110	410k	91854	311	11/17/07	11/24/11	56° 26.72′	61° 16.92′	4407
G01	147	410k	91520	—	12/09/08	10/29/10	56° 26.70′	61° 17.08′	4401
G02	124	410k	91136	763	11/18/07	11/25/09	56° 45.62′	61° 04.83′	4065
G02	230	46k	109319	16	11/25/09	11/23/11	56° 45.56′	61° 04.90′	4065
G03	212	46k	106396	761	11/18/07	10/30/10	57° 04.74′	60° 52.80′	3655
G03	171	410k	92915	757	10/30/10	11/24/11	57° 04.74′	60° 52.81′	3644
H01	114	410k	91506	355	11/07/10	12/05/11	58° 26.51′	63° 06.48′	3849
H02	152	410k	91498	33	11/08/10	12/05/11	58° 22.63′	63° 03.11′	3834
H03	211	46k	106398	760	11/08/10	12/05/11	58° 21.42′	63° 02.15′	4406
H04	132	410k	91508	25	11/08/10	12/05/11	58° 17.08′	63° 18.42′	3922
H05	212	46k	106396	761	11/07/10	12/05/11	58° 22.00′	63° 24.45′	3803

Instrumentation problems and noteworthy information about data quality are summarized in Table 3. Two instruments were lost: No communication could be established with one CPIES deployed at C02 because of a faulty acoustic command system (ACS). That instrument could not be recovered nor could its data be retrieved. One instrument at D02 rose very slowly after being released from the seafloor; it failed to reach the surface and was not recovered. Fortunately, we retrieved the daily-averaged data via telemetry prior to releasing the CPIES from the seafloor. The most common instrumental issues affecting the CPIESs included the current meter cable leaks

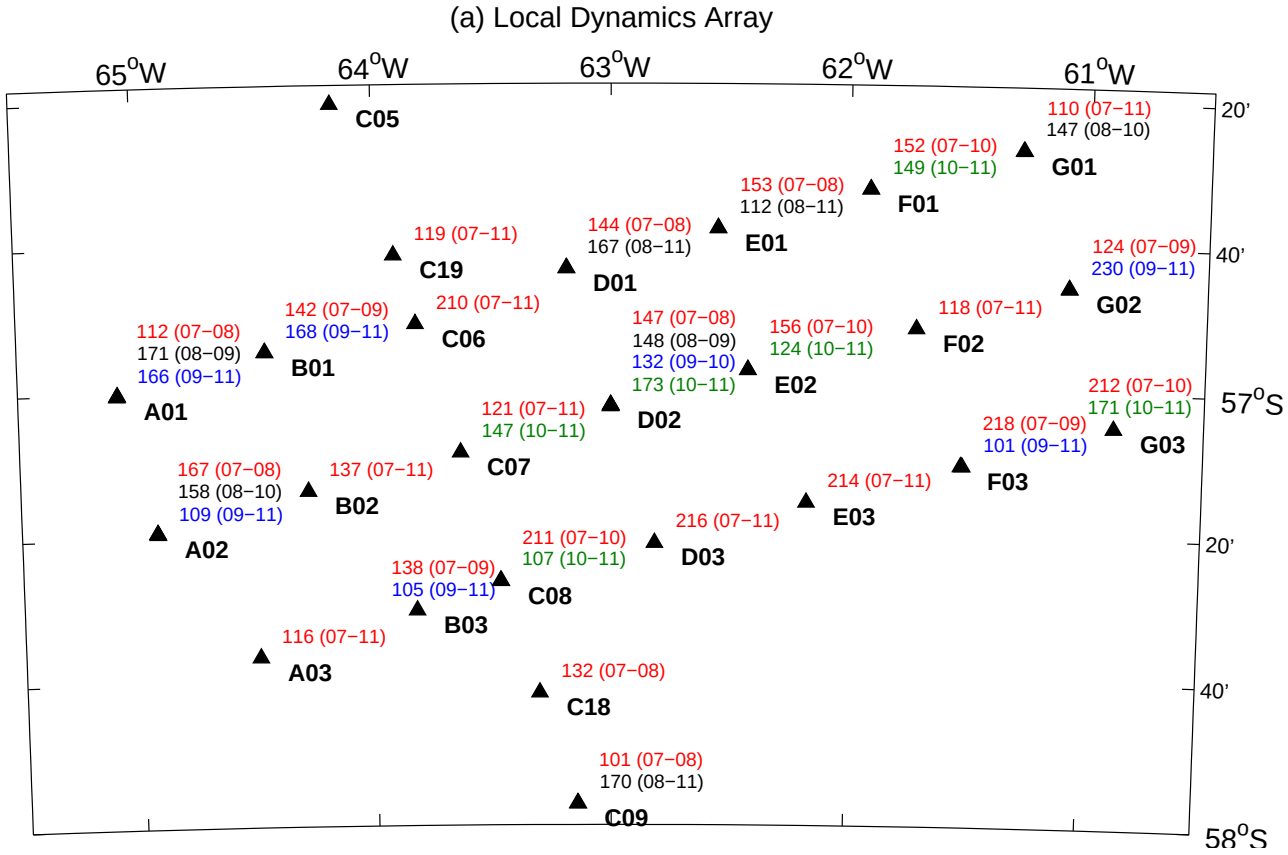

Figure 2: Graphical display of the instruments deployed in the (a) LDA, (b) northern and (c) southern portions of the transport line. Except for a few locations, site designators appear to the lower right of the location markers (triangles). CPIES serial numbers and years of deployment are listed to the upper right. Text is colored according to the year the CPIES was launched: 2007 (red), 2008 (black), 2009 (blue), and 2010 (green).

(noted above) and highly scattered (noisy) travel time measurements.

Two problems affected the pressure data quality at many sites. These included down-slope sliding and tipping events; both issues were caused by strong bottom currents. Sliding events were identified by abrupt changes in pressure to higher values ('jumps') when instruments located on steep topography changed depth. In general, the jumps were removed by adjusting the pressures so that the mean values before and after the jumps agreed. Dates listed in Table 3 for the sliding events at each site are approximate. Sliding events also affected the travel time measurements because they lengthened the distance traveled by the acoustic pulses. Adjustments to travel times were made by scaling the pressure adjustments. Tipping events were identified by large pressure changes concurrent with bottom current speeds in excess of 40 cm s^{-1}. Our hypothesis is that strong currents tipped the CPIES in its anchor stand horizontally, and the resulting change in the orientation of the pressure sensor caused the pressure spike. Often during the tipping events, the

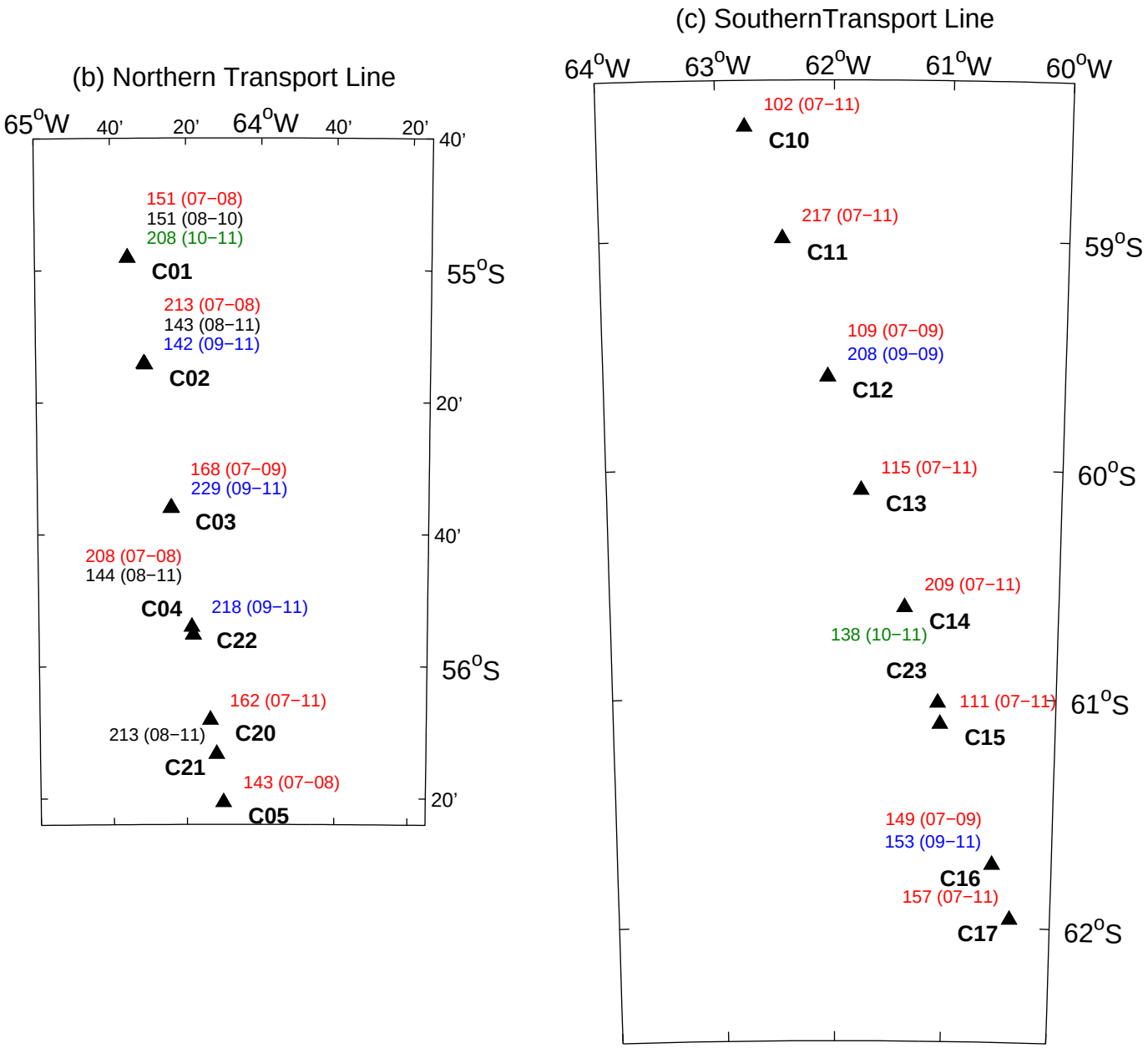

Figure 2: Continued.

travel time signals were also lost because the transducer was not directed upwards. Because we cannot determine what the actual pressures should be during these tipping events, they have been excised.

Figure 3 summarizes the data coverage in time line format, after all processing had been completed. While the temperature data are not displayed, in general, the Paroscientific temperature measurements have the same coverage as the pressure data, and the DCS temperatures have the same coverage as the velocities. Gray lines indicate sites that were intentionally left unoccupied. Blank (white) spaces indicate missing or excised data. This figure was generated using the 3-day low-pass filtered data, which have larger gaps than the unfiltered (hourly) data.

Table 3: Summary of the instrumentation deployed at each site. Rationale for instrument recovery and notable issues with the data are provided. Also listed are the dates (day relative to the deployment year) and adjustments applied to the pressure records to correct for down-slope sliding.

Site	IES SN	Launched	Recovered	Status at Recovery	Data issues/Notes
A01	112	2007	2008	No currents	1. Tipping events 2. Currents end in Jan 2008
	171	2008	2009	Noisy tau	1. Tipping events 2. Truncated noisy tau at end of record
	166	2009	2011	Okay	
A02	167	2007	2008	No currents	1. Pressure Jumps: 426, 0.4647 dbar 687, 0.2103 dbar 2. Tipping events 3. Currents end in Oct 2008 4. Noisy tau
	158	2008	2010	Noisy tau	1. Pressure Jump: 381, 0.1297 dbar 2. Tipping events
	109	2009	2011	Okay	1. Duplicate site 2. Tipping events 3. Fixed 12 hr timebase error
A03	116	2007	2011	Okay	Tipping events
B01	142	2007	2009	No currents	1. Currents end in Feb 2009 2. Tipping events
	168	2009	2011	Okay	
B02	137	2007	2011	Okay	1. Pressure Jump: 1731, 0.1117 dbar 2. Tipping events
B03	138	2007	2009	Noisy tau	1. Pressure jumps: 361, 0.1190 dbar 418, 0.1531 dbar 2. Pressure: big exponential drift; excised initial 2 days 3. Tipping events

Continued on new page

Table 3 – *Continued from previous page*

Site	IES SN	Launched	Recovered	Status at Recovery	Data issues/Notes
	105	2009	2011	Okay	
C01	151	2007	2008	No currents Cable cut	1. Pressure Jumps: 482, 0.0856 dbar 517, 0.2495 dbar 598, 0.1474 dbar 653, 0.1184 dbar 664, 0.2696 dbar 710, 0.7788 dbar 2. Tipping events 3. Currents end in Apr 2008
	151	2008	2010	Bad pressures caused by heavy algal growth on cable	1. Pressure used to dejump tau, then discarded
	208	2010	2011	Not working Cable cut	1. Currents end in Dec 2010 2. Tau and Pressure end in Jan 2011
C02	213	2007	2008	No currents	1. Currents end in Oct 2008 2. Tipping events 3. Fixed 12 hr timebase error
	143	2008	Lost	No communication, bad ACS	No data
	142	2009	2011	Okay	
C03	168	2007	2009	No currents	1. Pressure Jumps: 331, 0.2165 dbar 499, 1.8065 dbar 2. Tipping events 3. Currents end in Nov 2008
	229	2009	2011	Okay	1. Pressure: big exponential drift; excised first day 2. Tipping events
C04	208	2007	2008	No currents	1. Currents end in Feb 2008 2. Tipping events
	144	2008	2011	Okay	Tipping events
C05	143	2007	2008	No currents	1. Pressure Jumps: 340, 0.579 371, 0.961 577, 15.566 2. Pressure: used to dejump tau, then discarded values after day 577 3. Tipping events 4. Currents end in Oct 2008 5. Site abandoned due to topography, relocated to C21
C06	210	2007	2011	Okay	1. Tipping events 2. Fixed 12 hr timebase error

Continued on new page

Table 3 – *Continued from previous page*

Site	IES SN	Launched	Recovered	Status at Recovery	Data issues/Notes
C07	121	2007	2011	Okay	Tipping events
	147	2010	2011	Okay	Duplicate site
C08	211	2007	2010	No currents	1. Pressure: big exponential drift; excised initial 10 days 2. Currents end in Jan 2010
	107	2010	2011	Okay	
C09	101	2007	2008	Bad Tau	1. Tau: discarded 2. Tipping events
	170	2008	2011	Okay	Tipping events
C10	102	2007	2011	Okay	1. Pressure Jumps: 331, 0.1153 dbar 914, 0.1049 dbar 1064, 0.5547 dbar 1204, 1.1932 dbar 2. Tipping events 3. DCS temperatures bad; discarded
C11	217	2007	2011	Okay	Pressure: big exponential drift; excised data prior to day 339
C12	109	2007	2009	No currents	1. Currents end in Nov 2008 2. Site abandoned
C13	115	2007	2011	Okay	
C14	209	2007	2011	Okay	
C15	111	2007	2011	Not working	All data ended in Oct 2011
C16	149	2007	2009	No currents	Currents end in Jul 2009
	153	2009	2011	Okay	
C17	157	2007	2011	Okay	Pressure: big exponential drift; excised initial 6 days
C18	132	2007	2008	Okay	Site abandoned
C19	119	2007	2011	Okay	Tipping events
C20	162	2007	2011	Okay	1. Tau: bad; very little salvagable 2. Tipping events
C21	213	2008	2011	Okay	1. Tau gap caused by interference with site C20 (9 km apart) 2. Tipping events 3. Replaced site C05
C22	218	2009	2011	Okay	Duplicate site for C04
C23	138	2010	2011	Okay	1. Fixed 4 day timebase error 2. Near neighbor of C15
D01	144	2007	2008	Noisy tau	Tipping events
	167	2008	2011	Okay	Tipping events
D02	147	2007	2008	DCS concern	Tipping events

Continued on new page

Table 3 – *Continued from previous page*

Site	IES SN	Launched	Recovered	Status at Recovery	Data issues/Notes
	148	2008	Lost	Bad currents	1. Rose slowly and never surfaced 2. PDT data only; no temperatures 3. Currents discarded
	132	2009	2010	No currents	Currents end in Dec 2009
	173	2010	2011	Not working	All data end in Oct 2011
D03	216	2007	2011	Okay	
E01	153	2007	2008	Noisy tau	
	112	2008	2011	Okay	Tipping events
E02	156	2007	2010	Noisy tau	Tipping events
	124	2010	2011	Not working; battery pack problem	1. All data ended 2 days early 2. Fixed one month timebase error
E03	214	2007	2011	Okay	1. Pressure: big exponential drift, excised initial 8 days 2. Tipping events
F01	152	2007	2010	No currents	1. Currents end in Apr 2010 2. Tipping events
	149	2010	2011	Okay	
F02	118	2007	2011	Okay	Tipping events
F03	218	2007	2009	No currents	1. Currents end in Aug 2009 2. Tipping events
	101	2009	2011	Okay	
G01	110	2007	2011	Okay	1. Noisy tau during first winter 2. Tipping events
	147	2008	2010	Okay	1. PIES; no currents 2. Duplicate site
G02	124	2007	2009	No currents	1. Currents end in Sep 2009 2. Tipping events
	230	2009	2011	Okay	
G03	212	2007	2010	No currents	1. Currents end in Nov 2009 2. Tipping events
	171	2010	2011	Not working; battery pack problem	All data end in Oct 2011
H01	114	2010	2011	Okay	
H02	152	2010	2011	Okay	Pressure jump: 403–413, 0.0768 dbar
H03	211	2010	2011	Okay	1. Currents stopped working for one month, late Jun–late Jul 2011 2. Pressure: big exponential drift, no data excised
H04	132	2010	2011	Okay	
H05	212	2010	2011	Okay	

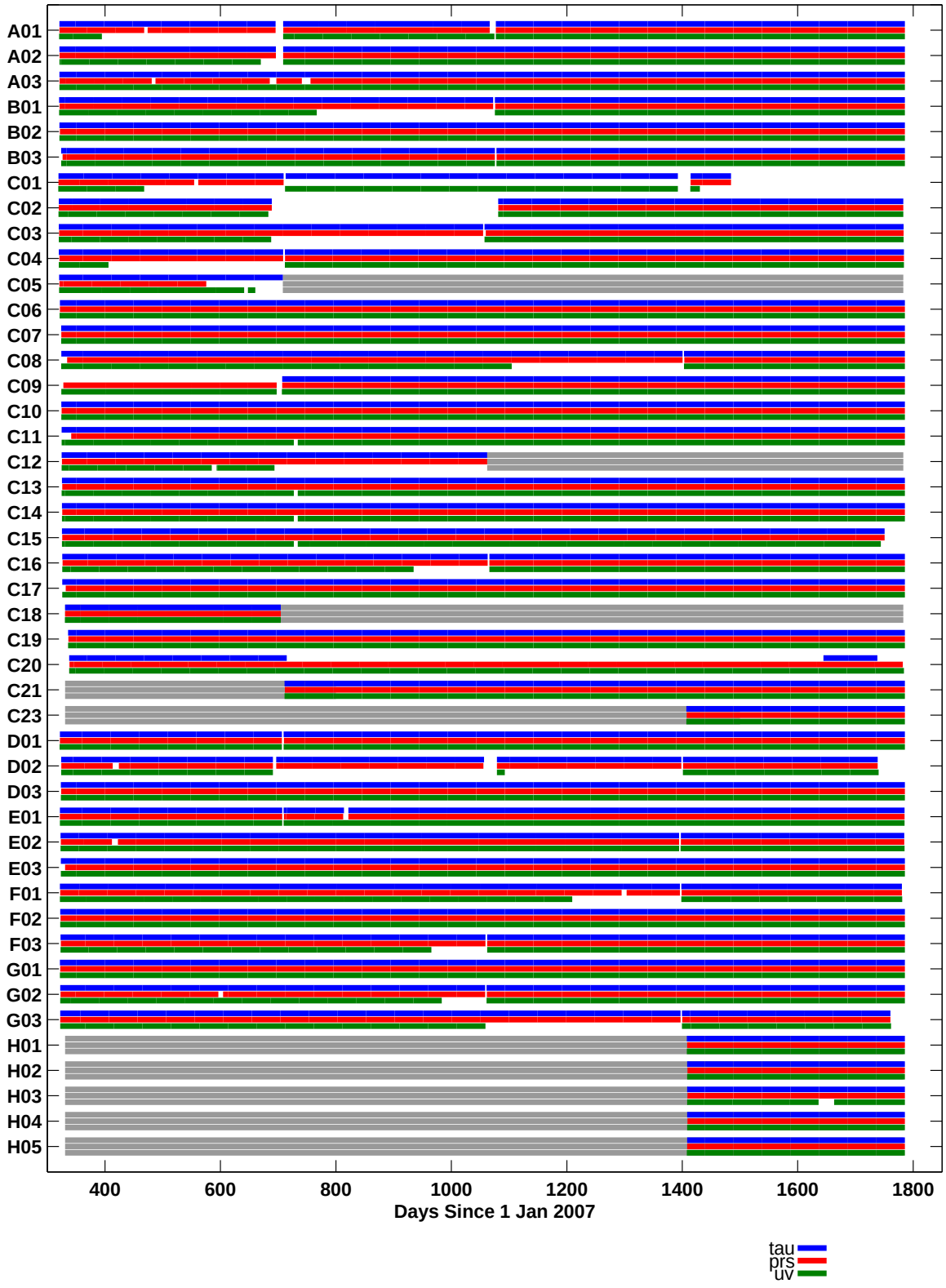

Figure 3: Time line showing periods of data coverage of low-pass filtered τ (blue), pressure (red), and velocity (green) after all processing. Duplicate sites are excluded. Gray lines indicate time periods when sites were not occupied. White spaces indicate missing or excised data.

2 Data Processing and Calibration

2.1 Overview

The basic data processing is accomplished by a series of MATLAB routines specifically developed for the CPIES (*Kennelly et al.,* 2007). The steps are briefly summarized here and described in more detail in the subsections below. Travel times, pressures, temperatures, and velocities were windowed and outliers removed (despiked). Tidal signals and instrumental drifts were removed from the pressure measurements. All variables were low-pass filtered and then subsampled at 12 hour intervals (0000 and 1200 UT).

After the initial processing was completed, several processing steps are performed on all the instruments together. Each pressure record was simultaneously dedrifted and leveled with a more robust method that uses the array-wide velocity measurements. Travel times were adjusted to remove the effects of pressure variations on path length. Additionally, travel times were calibrated to τ_{index} using CTDs taken at each CPIES location throughout the field program. 'Site Best' files were constructed to attain a single four-year-long record of measurements at each site. If duplicate instruments were deployed at a location, the site best file consists of the best quality records. Subsequently, the twice-daily leveled pressures and currents and τ_{index} data were gridded using optimal interpolation (*Firing,* 2012).

In the above mapping procedure, the near-bottom pressures and currents were treated as though they were all measured at the same depth level based on the assumption of no deep shear. In reality, there is deep shear in the Drake Passage, and with the exception of the instruments located on the continental margins and the SFZ, instrument depths listed in Table 2 range from 3500 to 4400 m. To remove the effects of deep shear, the near-bottom pressures and currents were adjusted to a common level of 4000 m using maps of τ_{index} and its gradients along with the Φ GEM look-up table (*Firing,* 2012). Finally, the array-wide processing procedures listed in the above paragraph were repeated.

After each cDrake cruise, a new version of the CPIES data set was created to incorporate the most recent data retrieved via acoustic telemetry or instrument recovery. This report documents the processing performed on the data records after the final cruise when all the instruments were recovered. The initial processed versions of the recovered records were reviewed at a workshop held at SIO during June 2012, and they were subsequently updated to incorporate the recommended changes. The latest version of the data set, documented in this report, is referred to in-house as 'year 4 version 2' (which retains only the adjusted pressure and velocity records), and also as 'year 4 version 3' (which retains unadjusted pressure and velocity records in addition to the adjusted records).

2.2 Pressure

Before processing the pressure data, the records were modified to remove 'jumps' that resulted when instruments changed depth, and to excise tipping events. For instruments that slid down the topography, the mean pressures before and after each jump were determined, and their difference determined the magnitude of the jump (Table 2). The entire record after each jump was offset

by subtracting this amount to correct the pressures. Tipping events change the orientation of the pressure sensor producing large spikes in the measured pressures. Since we were unable to separate changes due to orientation from the true ocean signals, tipping events were identified by the timing of strong current events and the pressures were deleted. Subsequently, the pressure and velocity data were objective mapped excluding the measured pressures from one site at a time to produce a time series of pressure at that site. The measured and mapped records were compared to identify additional jumps and tipping events.

Table 4: Tidal constituents at four CPIES sites along the transport line listed from north to south. Amplitudes are in decibars; phases are in degrees.

Site		O1	K1	Q1	P1	M2	K2	N2	S2
C03	ampl	0.1671	0.1748	0.0357	0.0602	0.4784	0.0244	0.1041	0.1077
	phase	53.2800	99.4480	27.3680	96.0940	262.9410	315.2590	228.3770	309.0010
C07	ampl	0.1733	0.1758	0.0360	0.0605	0.4080	0.0230	0.0849	0.0972
	phase	54.0770	94.7220	33.1450	91.5680	261.2940	326.0230	225.3040	316.7200
C11	ampl	0.1872	0.1862	0.0403	0.0643	0.3622	0.0278	0.0662	0.1081
	phase	54.9670	86.2820	35.7580	84.5290	264.2290	341.0320	223.8330	330.3500
C15	ampl	0.2163	0.2192	0.0456	0.0749	0.3355	0.0394	0.0528	0.1441
	phase	54.1540	76.0350	42.6700	74.6700	273.6150	351.4150	229.8830	343.0440

The semidiurnal and diurnal tidal constituents were determined using the response analysis method (*Munk and Cartwright,* 1966) and removed from the hourly pressures. The amplitudes and phases of the eight major constituents for the CPIES in the LDA are contoured in Figures 4 and 5. The constituents for four sites spanning the north-south extent of the transport line are listed in Table 4.

Next, the pressures were simultaneously leveled and dedrifted using the current measurements. This is an extension of the method described by *Watts et al.* (2001) in which previously-dedrifted pressures were leveled (referenced to a common geopotential) with objectively-interpolated mean currents. Our present method uses the velocity time series, rather than the means, to determine if the leveling offsets change systematically over time; such changes would indicate drifting of the pressure sensors. Following *Watts et al.* (2001), absolute pressure at a given site s and time t is

$$P(t,s) + P_0(s) = p_{cm}(t,s) + p_0(t)$$

where $P(t,s)$ and $P_0(s)$ are measured pressure and its site-dependent unknown reference, and $p_{cm}(t,s)$ and $p_0(t)$ are the objectively-interpolated pressure and its time-dependent unknown offset. *Watts et al.* (2001) eliminated the time-dependent offset $p_0(t)$ by subtracting the above equation for one site from the equations for all other sites, yielding

$$\Delta P_0(s) = \Delta p(t,s) - \Delta P(t,s)$$

where Δ is the spatial difference operator. The term $\Delta P_0(s)$ should be constant over time; any long term changes (such that $\Delta P_0(s,t)$) result from sensor drift.

For this application, both the pressure and velocity data were low-passed filtered using a Butterworth filter with a 15 day cutoff period to eliminate higher frequency fluctuations not associated with drift. Next, the measured velocities were objectively mapped to produce time series of stream

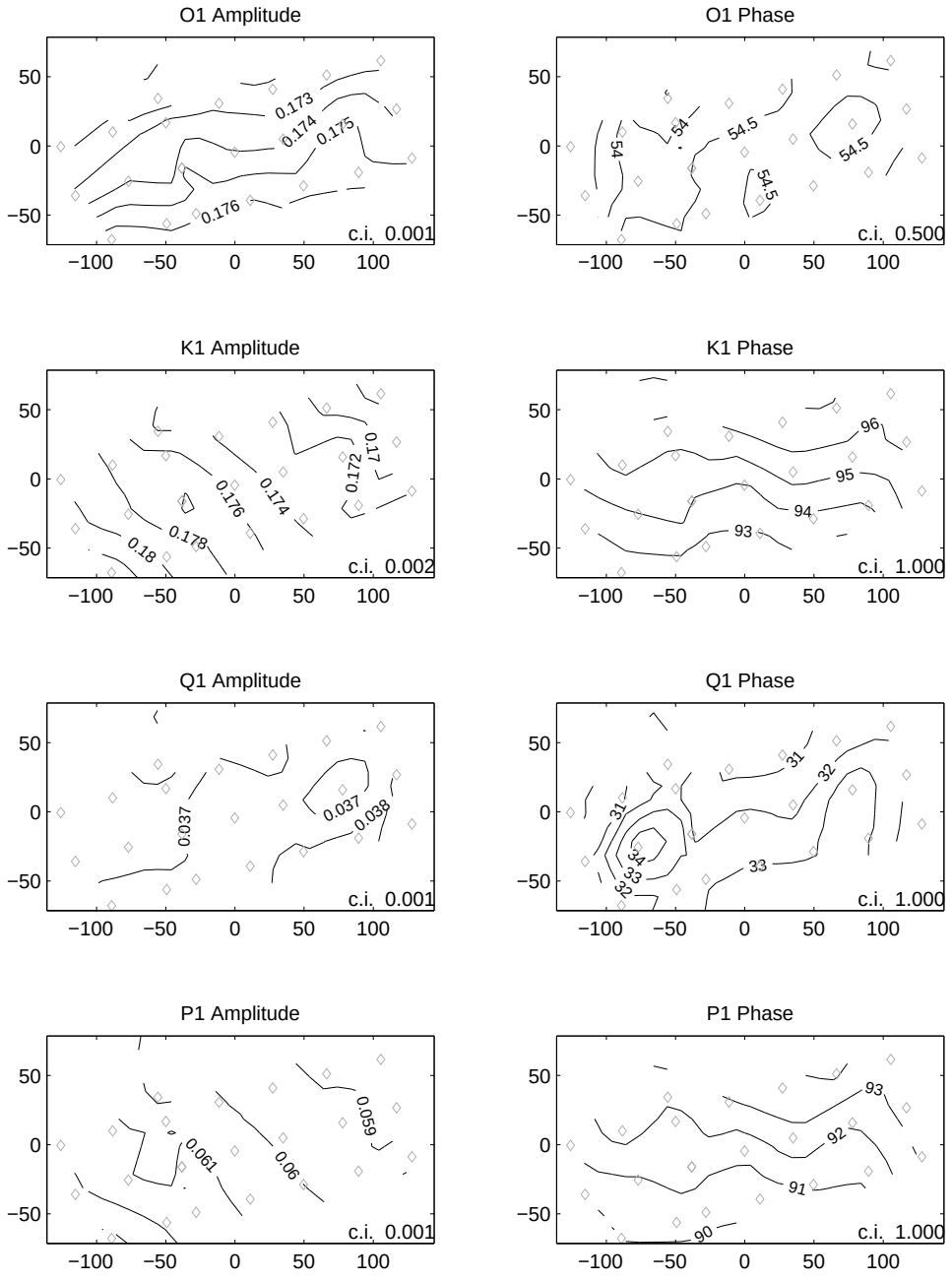

Figure 4: Amplitudes (dbar) and phases (degrees) of the major diurnal tidal constituents in the cDrake LDA. CPIES sites are denoted by the diamonds.

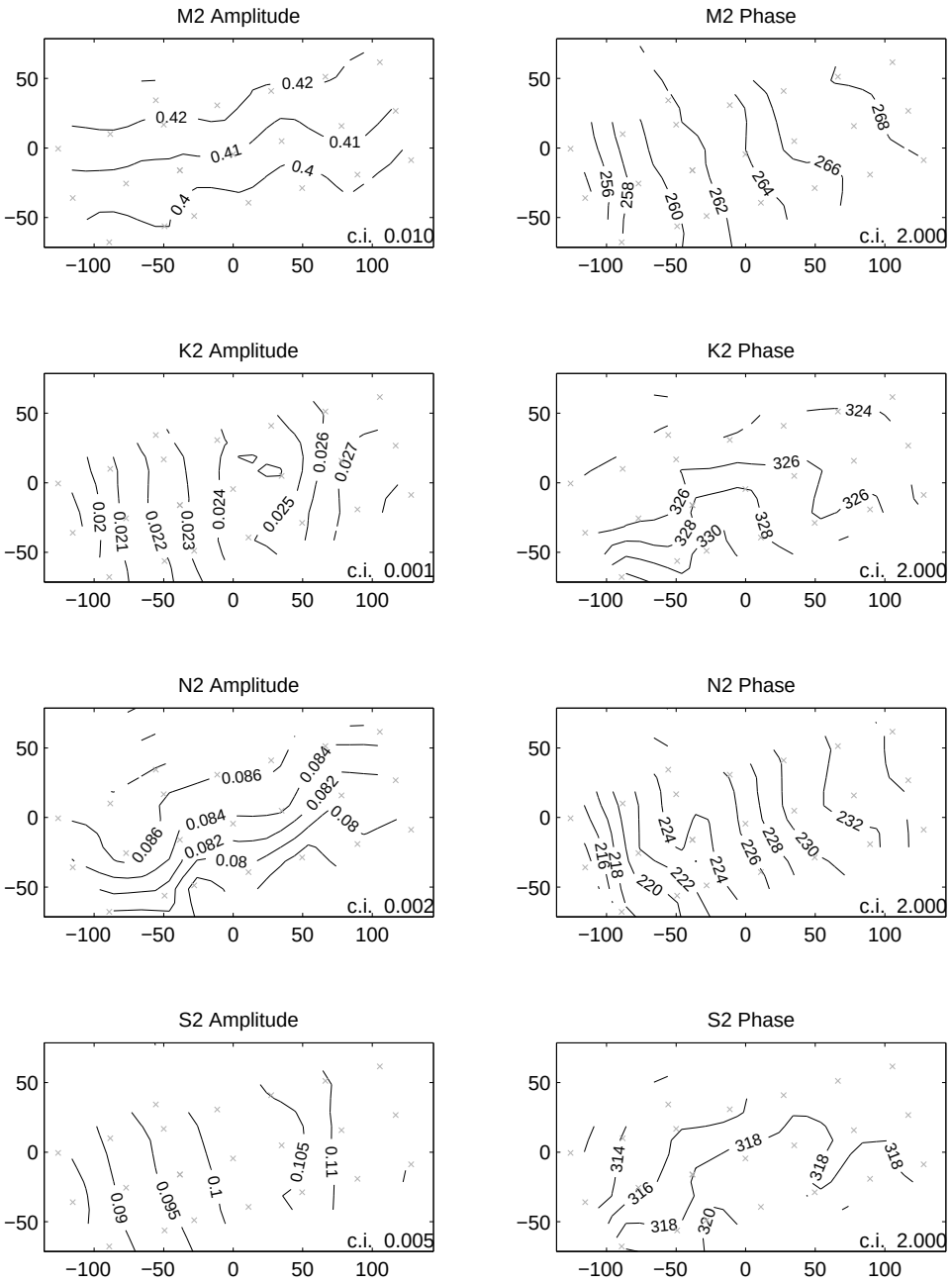

Figure 5: Amplitudes (dbar) and phases (degrees) of the major semi-diurnal tidal constituents in the cDrake LDA. CPIES sites are denoted by the diamonds.

function at each site that were subsequently scaled to pressure units. The cDrake instruments were separated into two groupings prior to mapping: Sites located north of the Shackleton Fracture Zone and sites located to the south. For leveling the northern sites, the average of sites B02 and C07 were subtracted to eliminate $p_0(t)$. For leveling the southern sites, only C15 was subtracted. If the slope of $\Delta P_0(s,t)$ was smaller than $\pm 10^{-5}$ dbar day^{-1}, it was considered to be constant over time and the measured pressure was deemed free of drift. If not, pressure drift was determined by fitting either linear or exponential-linear curves to $\Delta P_0(s,t)$. Dedrifted and leveled pressure records were produced by subtracting the drift curves from the measured hourly pressures.

2.3 Travel Time

The travel time records of instruments that changed depth contain small offsets (or 'jumps') which were typically difficult to identify visually. Instead, they were identified by the timing and magnitude of pressure jumps. Adjustments to travel times ($\Delta\tau$) were made by scaling the pressure adjustments (Δp) as $\Delta\tau = 2\Delta p/\rho g c$ where ρ is mean density, g is gravitational acceleration, c is the mean speed of sound at the seafloor. These fixes were applied to the individual acoustic pings prior to other processing.

During the initial processing steps, a single representative travel time measurement is determined from a burst of 24 pings taken during each hour. Details of the method, which first windows the τ values to remove outliers and reduce noise, are provided in *Kennelly et al.* (2007). The travel times were referenced to a common pressure level (τ_{index}) for subsequent analyses. The steps to convert measured travel time (τ_m) to τ_{index} are described next; more comprehensive descriptions can be found in *Donohue et al.* (2010) or *Kennelly et al.* (2007).

Contributions to τ_m arise from two sources: a steric component (τ_s) and a mass-loading or path length component. We wish to remove the path length contribution from τ_m so that variations in τ_s are solely due to fluctuations of the upper baroclinic structure. The path lengths are affected by both atmospheric and bottom pressure fluctuations, which partially compensate each other. High atmospheric pressure shortens the path length by depressing the sea surface whereas high bottom pressure (such as tides) lengthens the path. The contribution due to bottom pressure fluctuations (τ_p) was estimated as

$$\tau_p = 2 \cdot p/(\rho \cdot g \cdot c)$$

where p is the dedrifted and demeaned bottom pressure time series. The magnitude of τ_p was O(1–2 ms). Surface pressure was obtained from the ERA Interim Re-analysis via the ECMWF data server. The gridded re-analysis product, with 1.5 degree spatial and 6 hour temporal resolution, was interpolated in both space and time to each CPIES location. Its contribution to path length (τ_{IB}) was estimated by substituting surface pressure into the above formula. The magnitude of τ_{IB} was O(0.5 ms). Finally, we determined the steric contribution as $\tau_s = \tau_m - \tau_p + \tau_{IB}$.

Next, we removed the latitudinal and depth dependence of g from τ_s to obtain a dynamic τ (designated τ_s^*) using

$$\tau_s^* = \tau_s \cdot \frac{g(\lambda, z)}{9.8(1 - \gamma P_b)}$$

where λ is the latitude and P_b is the average mean bottom pressure (scaled from decibars to Pascals)

at the CPIES site, and depth $z = 0$ m. The constant γ is determined as

$$\gamma = \frac{1}{\overline{\rho}\ \overline{g}\ a}$$

where $\overline{\rho}$ and $\overline{g}$ are regional averages of density and gravity, respectively, and $a = 6371000$ is the earth's radius in meters. For cDrake, the scale factor ranged 1.0021–1.0028, producing O(0.014 s) changes in τ.

Ocean temperature changes due to seasonal warming and cooling also cause variations in the travel times measured by the CPIES. To minimize these variations, *Cutting* (2010) estimated the average seasonal variation in τ for the upper 150 dbar from a suite of expendable conductivity, temperature, and depth (XCTD) probes (*Sprintall et al.,* 2012). The annual curve, with an amplitude of about 0.6 ms, was subtracted from τ_s^* producing $\tau_{s,ds}^*$.

In previous experiments, measured travel times were projected onto a common pressure level (τ_{index}) using a linear relationship and coincident hydrographic measurements (see *Meinen and Watts,* 1998). Due to the deep-reaching baroclinic thermal structure in the Drake Passage, the cDrake $\tau_{s,ds}^*$ were scaled to τ_{index} using a 2nd order polynomial relationship

$$\tau_{index} = A(\tau_{s,ds}^*)^2 + B\tau_{s,ds}^* + C$$

where coefficients A, B and C are determined from historical hydrography. The offset C was subsequently adjusted with calibration CTDs taken at each CPIES site. To estimate the coefficients, τ_{index} was determined by integrating the available casts between 0–2000 dbar. The 2000 dbar integration limit was chosen in order to include data from profiling floats that transited the Drake Passage. A series of relationships were determined between τ_{index} and τ at other pressure levels. Relationships were determined at 10 m increments for pressure levels ranging from 400 dbar to 4500 dbar; several examples are shown in Figure 6. Coefficients A, B, and C were determined by fitting a 2nd order polynomial to each relationship. The three coefficients were plotted as a function of pressure level and smoothed (Figure 7). Using these coefficients, travel times measured by the CPIES at any depth can be projected onto the common pressure level. For shallow sites C01 and C17, the integration limit was shortened to 1000 dbar in order to include water masses confined closer to the continental margins. The coefficients were recalculated using the shallower common pressure level (not shown).

The C coefficients were subsequently adjusted using calibration CTDs taken at each CPIES site. Each CTD was integrated to τ_{index} (τ_{ctd}) and the offset (C_{offset}) from the τ_{index} record was determined as

$$C_{\text{offset}} = \tau_{ctd} - < \tau_{index} >$$

where $< \tau_{index} >$ is the average of 12 hourly measurements centered on the time of the CTD. In general, more than one calibration CTD was available at each site, so the C_{offset} values were averaged. Finally, the τ_{index} records were modified by adding these averaged values.

2.4 Currents

Most of the cDrake CPIESs measured currents once every hour. For the instruments deployed during the final year, sampling was more frequent and these were averaged to produce

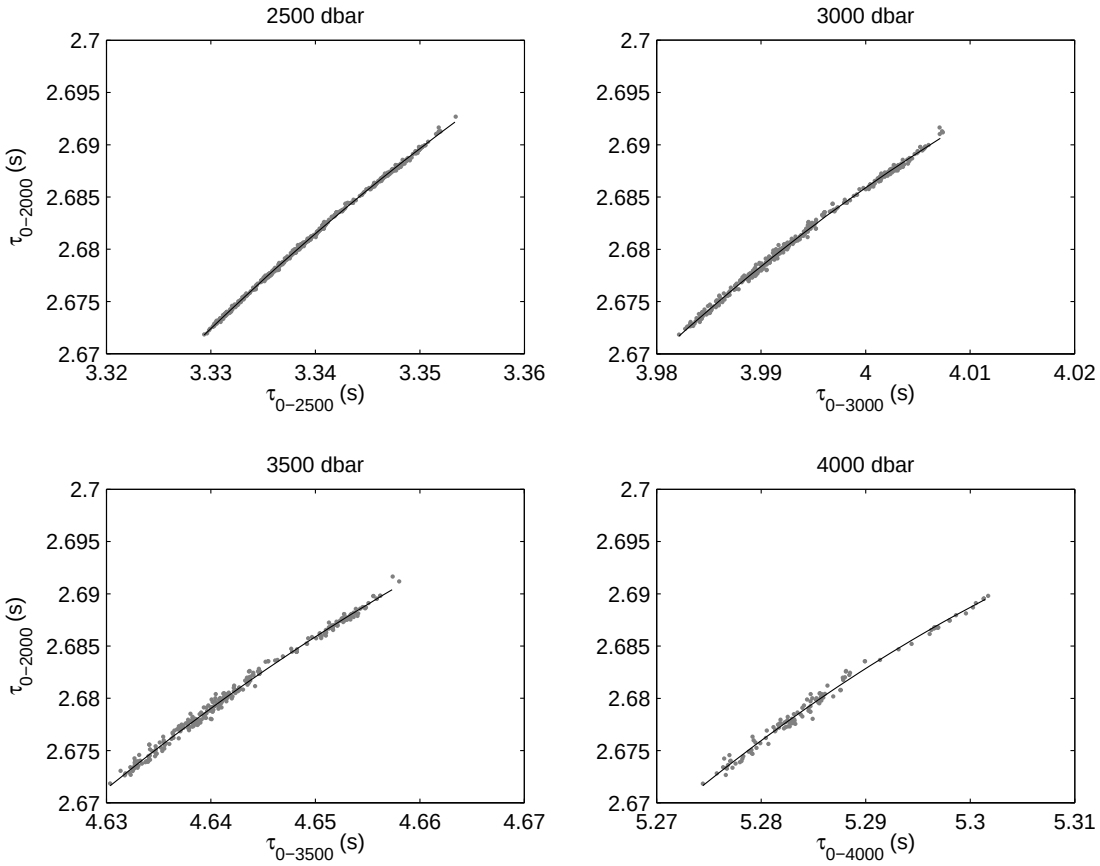

Figure 6: Polynomial relationships for τ at four pressure levels and τ_{index} (τ_{0-2000}) calculated from historical CTD casts.

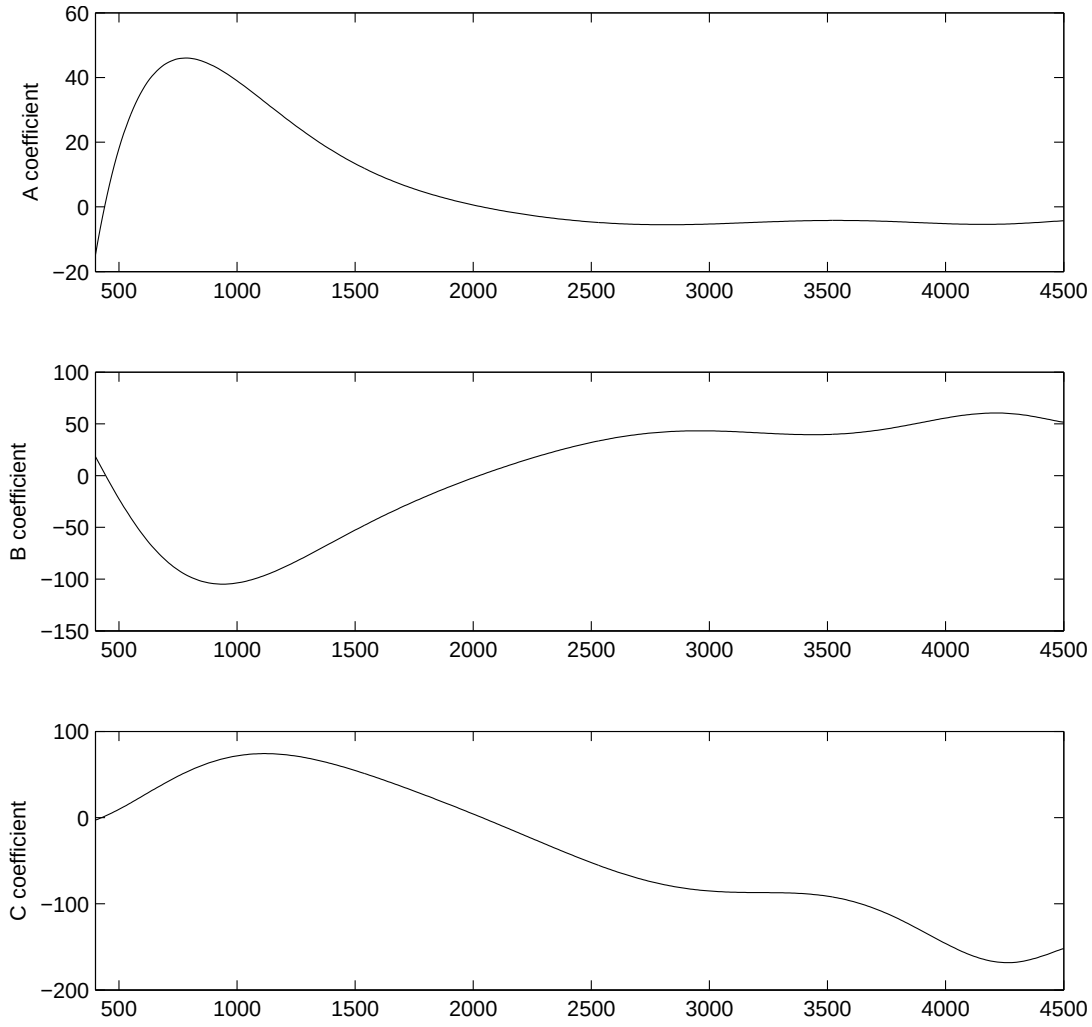

Figure 7: Coefficients A, B, and C for τ_{index} (τ_{0-2000}) as a function of bottom pressure.

hourly values. Two corrections were applied to the velocities after converting the components to speed and direction. First, the directions were adjusted for magnetic declination using codes written by the University of Hawaii to apply time-dependent declination corrections obtained from http://www.ngdc.noaa.gov/geomag. Mean corrections for cDrake ranged from 9° to 11°. Second, the measured speeds were multiplied by a speed of sound scale factor. This adjustment was necessary because a default sound speed value of 1500 m s^{-1} was used when the currents were measured. The scale factor is a ratio of the true sound speed to the default value. For cDrake instruments at depths of 500–4300 dbar, deep mean sound speeds ranged 1468–1525 m s^{-1}, and the scale factors ranged 0.9792 to 1.0165. After applying the corrections, speed and direction were converted back to velocity components, u and v (positive eastward and northward, respectively).

Hogg and Frye (2007) found that RCM11 current meters recorded consistently lower speeds than other conventional current meters, and recommended that the measured speeds be scaled to high values (by roughly 10%). In their study region, however, the maximum recorded current speeds were less than 35 cm s^{-1}. During the first year of cDrake, currents in excess of 60 cm s^{-1} were recorded. A current meter comparison mooring was deployed during the second year between site E01 and F01 to determine if the speed correction factor was applicable to strong currents. *Kennelly et al.* (2012) found that both Aanderaa models (RCM11 and Seaguard) agreed with vector-measuring current meters within 2% in high current ($\geq$ 35 cm s^{-1}) events. Because of this good agreement, no speed-correction factor was applied to the cDrake currents.

2.5 Temperature

A quartz crystal with temperature sensitivity is incorporated into the Paroscientific pressure sensor. Because the pressure sensor is located inside the glass housing of the CPIES, it does not provide an accurate measurement of the instantaneous water temperature. Nevertheless the temperatures were averaged to create hourly values. Typically, it takes roughly 12 hours for the temperature inside the housing to equilibrate with the surrounding water. Temperature and pressure measurements taken prior to reaching equilibrium were discarded.

The temperature sensor associated with the DCS current sensor is in direct contact with the surrounding water. Thus it reaches equilibrium more rapidly than the Paroscientific temperature sensor. Typically only the first hour of post-launch data were discarded.

Temperature measurements from both types of sensors are available at all sites throughout the observational program with the following exceptions. DCS temperature records at several sites ended early when the current meter cables leaked (Table 3 and Figure 3). At site C10 (SN 102), the DCS temperature sensor failed at launch. At C02 (SN 143) year 2 (November 2008–November 2009), communication with the CPIES was lost and no data could be retrieved. At D02 (SN 148) year 2, the CPIES failed to surface, so the internally recorded data could not be retrieved. While daily averages of travel time, pressure, and currents were obtained via telemetry, no temperature data were telemetered. At G01, the duplicate instrument (SN 147) was only a PIES, thus no temperatures were measured by a DCS.

The absolute accuracy of the Paroscientific temperature measurements is quite poor, roughly ±2°C. The stated accuracy of the DCS temperature measurements in 0.05°C, but we observed offsets of ±1°C between instruments deployed consecutively at several sites. These temperature

offsets could not be accounted for by differences in the bottom depth between deployments. Therefore, both the Paroscientific and DCS temperature measurements require additional calibration if the absolute temperatures are to be used for scientific analyses. No calibrations have been performed. The resolution of both temperature sensors is good, however, so the variability may be examined with confidence. The resolution of the Paroscientific temperatures recorded by the CPIES is 0.0002°C. The two models of Aanderaa DCS used during cDrake have different temperature resolutions. Temperatures measured with model 3820, which was used almost exclusively in cDrake, have a resolution of 0.012°C. Temperatures measured with model 4390, used at a few sites (Table 5), have a resolution of 2×10^{-5}°C.

A preliminary comparison was made between the Paroscientific and DCS temperatures measured at a few sites. The records were highly correlated ($> 90\%$) with the internal Paros temperatures lagging the DCS measurements by one hour.

Table 5: CPIES sites with model 4390 (or 'Z-pulse') current meters. Temperatures measured by these DCS models have very high resolution.

Site	IES SN	Launch Year
A01	116	2009
B03	105	2009
C03	229	2009
C16	153	2009
F03	101	2009
G02	230	2009
H02	152	2010
H04	132	2010

2.6 D02 SN 148 Telemetered Data

The daily averaged data were collected via pulse-delay telemetry from the CPIES at D02 early on the cruise in November 2009. Initial processing at sea revealed that the current meter was beginning to fail. We returned to the site and attempted to recover the instrument, which was unsuccessful.

It was not necessary to run the response analysis program on the pressure data, because the measured pressures were processed internally by the CPIES with a *Godin* (1972) filter to remove the semi- and diurnal tides prior to averaging. The pressures were, however, dedrifted and leveled following the same procedures used on the other instruments.

A comparison between the D02 telemetered currents with the velocity measurements of neighboring sites revealed that the D02 currents were bad. They have been discarded.

2.7 Low-pass Filtering

All records (including the PDT data from D02) were convolved with a 4th order Butterworth filter with a cut-off period of 3 days. Data gaps smaller than 3 days were interpolated prior to

filtering. The records were broken into segments if there were remaining gaps, and filtering was performed on each segment separately. The filter was applied forward and backward to eliminate phase offsets. In addition, the first and last hour of each segment were excluded to minimize the effects of start-up transients. The filtered records were subsampled at 12 hour intervals (0000 and 1200 UTC).

2.8 Site Best Records

For upcoming scientific analyses, it is useful to consolidate the data measured by multiple instruments at each site into a single four-year-long record for each variable. 'Site Best' files were constructed using the low-pass filtered records, after the travel times were calibrated into τ_{index} and after the pressures were leveled, which allows multiple records to easily be appended. Because the temperature records have not been calibrated nor shifted to a uniform depth horizon, offsets occur when multiple temperature records are appended. If duplicate instruments were deployed at a location, the Site Best file consists of the highest quality records.

2.9 Adjustments to 4000 dbar

After the above processing steps were completed, preliminary maps of bottom pressure and current were produced using optimal interpolation (*Firing,* 2012). The assumption of no deep vertical shear was made, and the leveled pressures and currents were mapped as if they were all measured at the same depth level. Because vertical shear extends all the way to the seafloor in the Drake Passage, improved maps of the bottom fields can be obtained by adjusting the measured pressures and currents to a constant level; thus eliminating the need for the no shear assumption. For cDrake, the 4000 dbar level was chosen since most CPIES were located within ±500 dbar. At sites C02, C10, and C16 adjustments were made to pressure but not to the velocities, because the instruments were deployed at depths shallower than 2500 m. No adjustments were made to sites C01 and C17, which were close to shore in water depths shallower than 1500 m.

To adjust the pressures at a given site, the τ_{index} time series was used together with the Φ GEM look-up table (*Firing,* 2012) to determine the time-dependent steric contribution $\Phi_p^{4000}(t)$, which is the geopotential anomaly between the mean pressure (p) at the site and 4000 dbar. The pressure adjustments (δ_p) in decibars, obtained by scaling $\Phi_p^{4000}(t)$ by $\rho = 1053$ kg m^{-3}, were added to the measured hourly pressures.

To adjust the measured currents at a given site, geostrophic shears were estimated using the methods described in *Sun and Watts* (2001) and *Donohue et al.* (2010). This method invokes the chain rule such that two-dimensional spatial gradients of τ_{index} ($\partial\tau_{index}/\partial x$) are multiplied by the τ_{index} gradient of the Φ GEM ($-\partial\Phi_{GEM}/\partial\tau_{index}$). Time series of $\partial\tau_{index}/\partial x$ were determined at each CPIES site by optimal interpolation. The u, v adjustments (δ_u, δ_v) were subtracted from the hourly values. Note, however, that along the northern and southern portions of the transport line, the single line of instruments only resolves the flow normal to the line. So these adjustments effectively only correct the velocity in one direction at those sites.

The largest adjustments were made at the sites where the instrument depths differed from 4000 dbar by nearly 500 dbar. Examples of these adjustments for a shallower site (C19) and a deeper

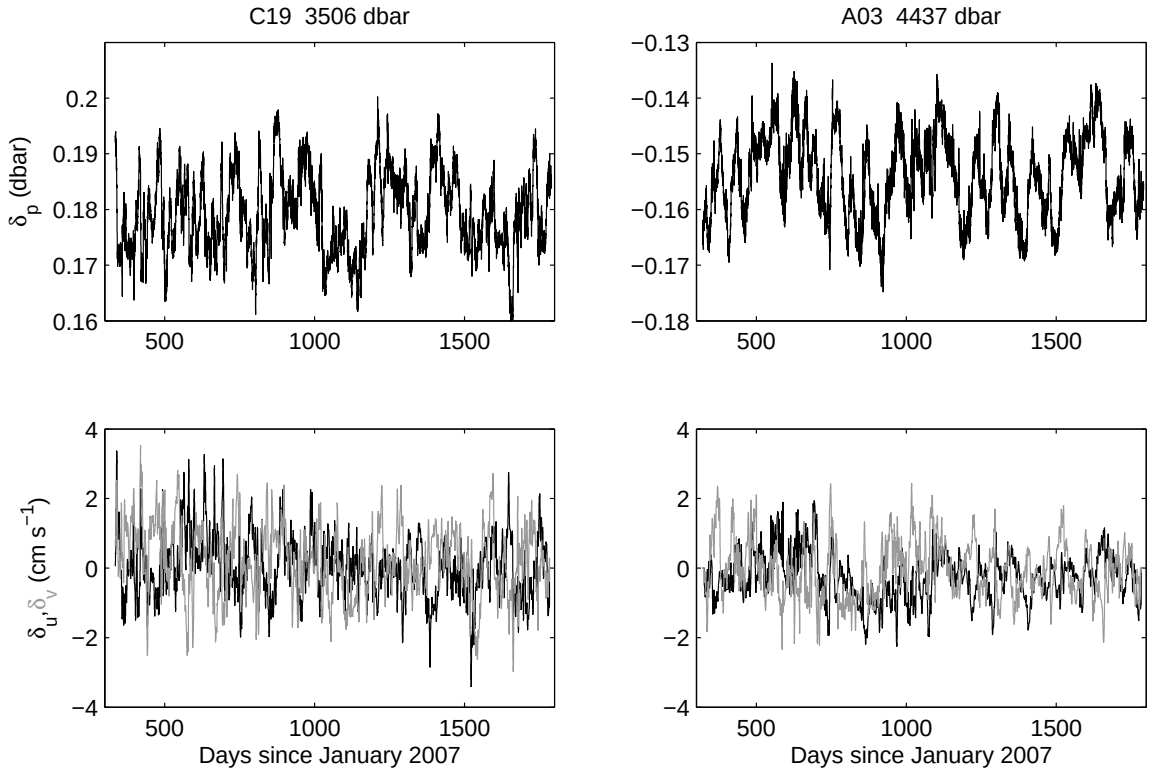

Figure 8: Pressure (δ_p) and velocity (δ_u, δ_v) adjustments for two sites, C19 and A03, are among the largest calculated, because their instrument depths were approximately 500 dbar from the common level of 4000 dbar.

site (A03) are plotted in Figure 8.

After applying the adjustments to the pressures and currents, several of the processing steps described above were repeated. All pressure records were leveled and dedrifted again using the adjusted currents. Measured travel times were converted to τ_{index} using the adjusted pressures to determine an improved estimate of the steric contribution τ_p. The updated records were low-pass filtered and used to create final Site Best files.

3 Site Best Records

Fourteen of the CPIES deployed on the initial cruise in 2007 remained in place for the full four-year observational program. Those sites included A03, B02, C06, C10, C11, C13, C14, C15, C17, C19, C20, D03, E03, and F02. At the most of remaining sites, instruments were replaced when problems arose, so the individual records were of shorter duration. By appending the data measured by instruments deployed consecutively at each site, a single continuous four-year-long time series was obtained for each variable at each location. These consolidated records are termed 'Site Best' files and are plotted in this section. If more than one instrument was deployed at a single location at the same time, the Site Best file consists of the highest quality records for each variable. Some sites were abandoned, relocated, or only occupied for a short period of time; the longest available records for those sites are plotted.

The data are organized here by site. All variables have been 3-day low-pass filtered, and data gaps less than 3 days have been linearly interpolated. The records span from 15 November 2007 to 21 November 2011, and the time axis is expressed in days since 1 January 2007 at 0000 UTC.

The plotted travel times have been calibrated to τ_{index}. For all sites except C01 and C17, the integration limits were between the surface and 2000 dbar. For shallow sites C01 and C17, the deep integration limit was 1000 dbar.

Two versions of pressure and current are plotted. The panels on the left side show the measured pressures and currents at their in situ depth; these are labeled p_{bot}, u_{bot}, and v_{bot}. The panels on the right side show the pressures and currents after they have been adjusted to the common level of 4000 m; these are labeled p_{4000}, u_{4000}, and v_{4000}. For both p_{bot} and p_{4000}, the records have been leveled (referenced to a common geopotential), and therefore have small mean values. The u-component is positive eastward, and the v-component is positive northward.

The temperature measured by the Paroscientific pressure sensor is plotted at the bottom left, and the temperature measured by the Aanderaa Doppler current sensor is plotted at the lower right. No attempt has been made to remove offsets that arose when instruments were replaced. Therefore, large offsets (in either direction) occur when these temperature records are appended to create four-year-long records. It is important to note that both temperature measurements require additional calibration if the absolute temperatures are to be used for scientific analyses.

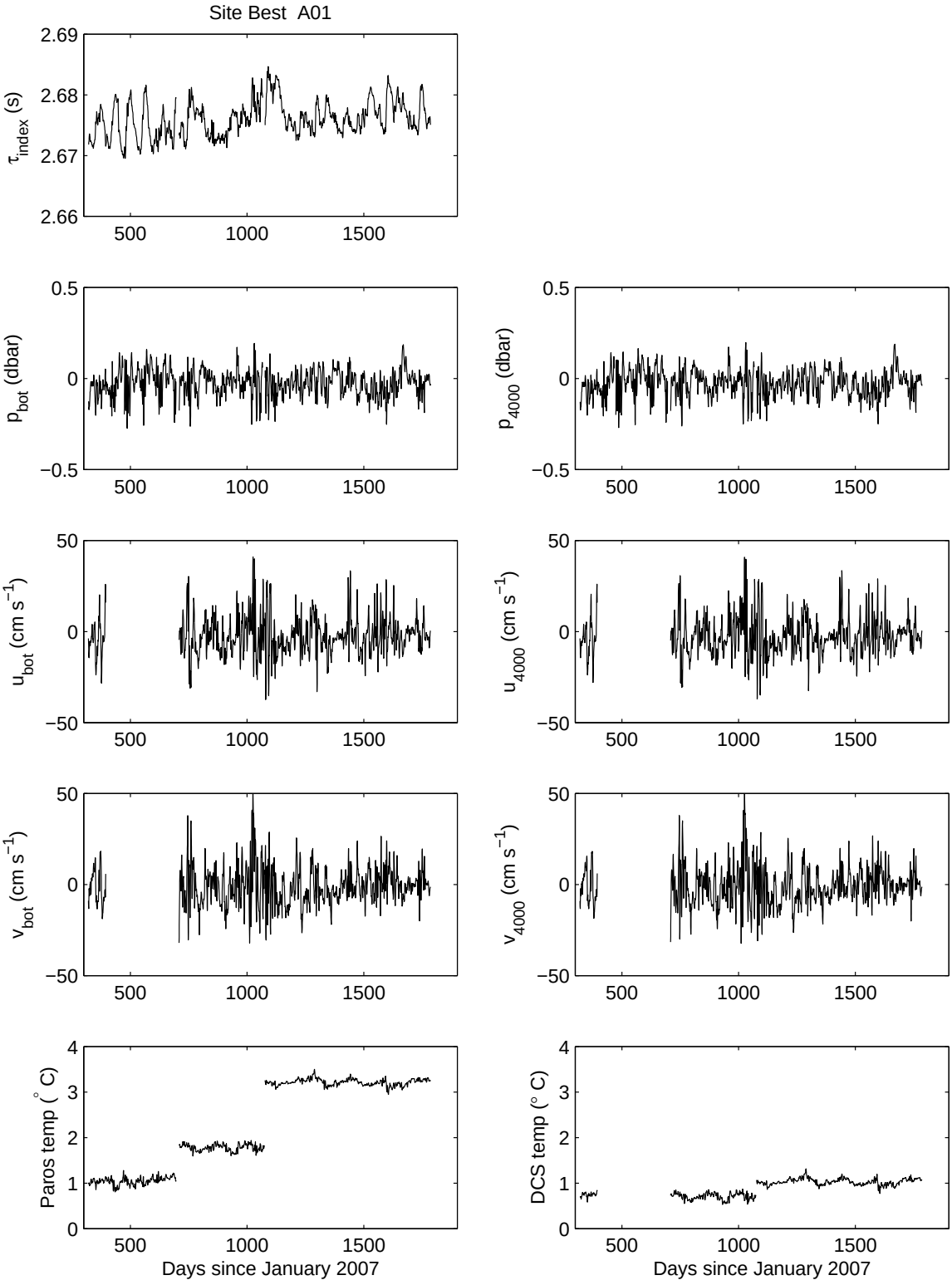

Figure 9: Time series of the 3-day low-pass filtered data obtained at site A01.

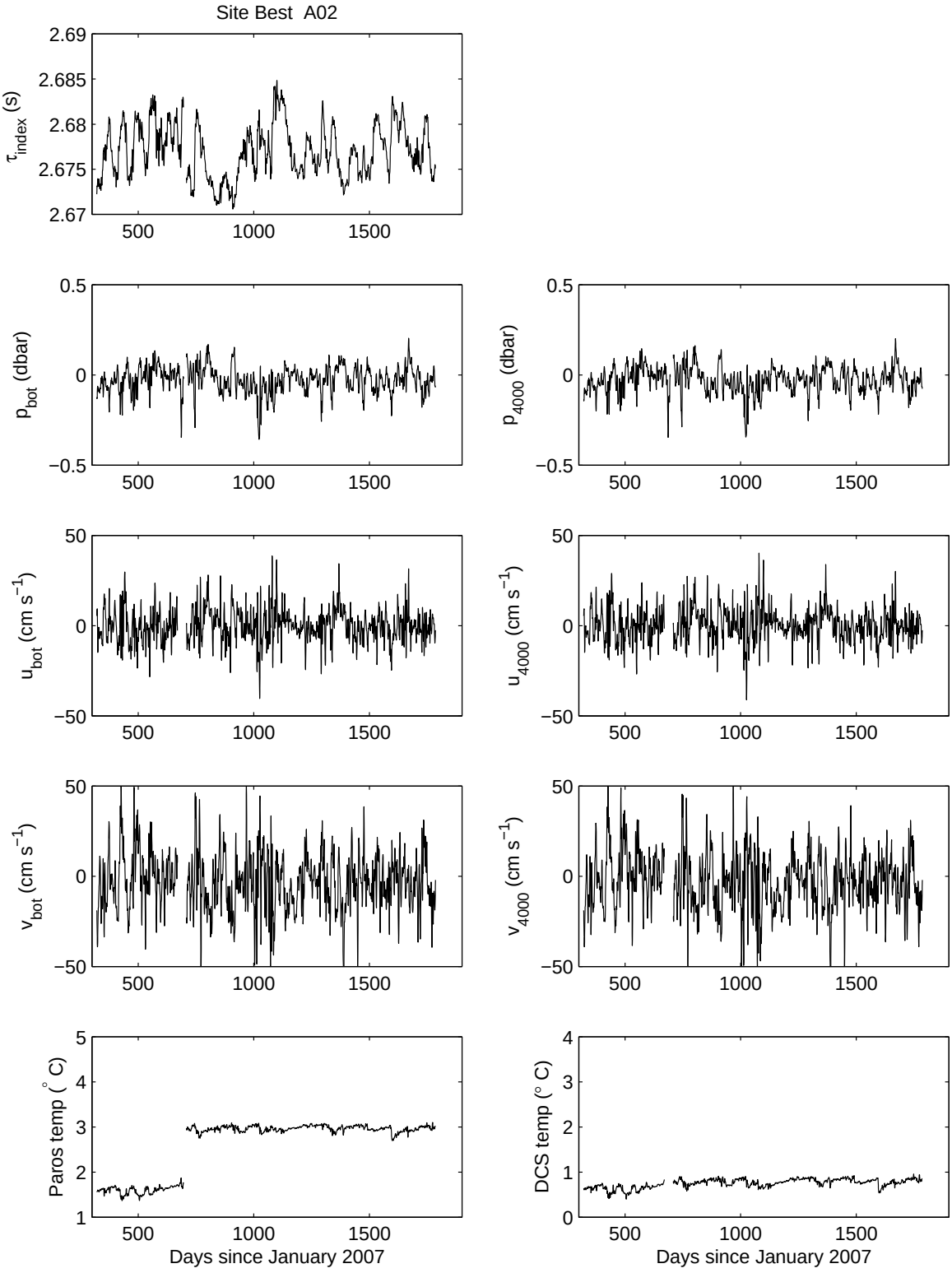

Figure 10: Time series of the 3-day low-pass filtered data obtained at site A02.

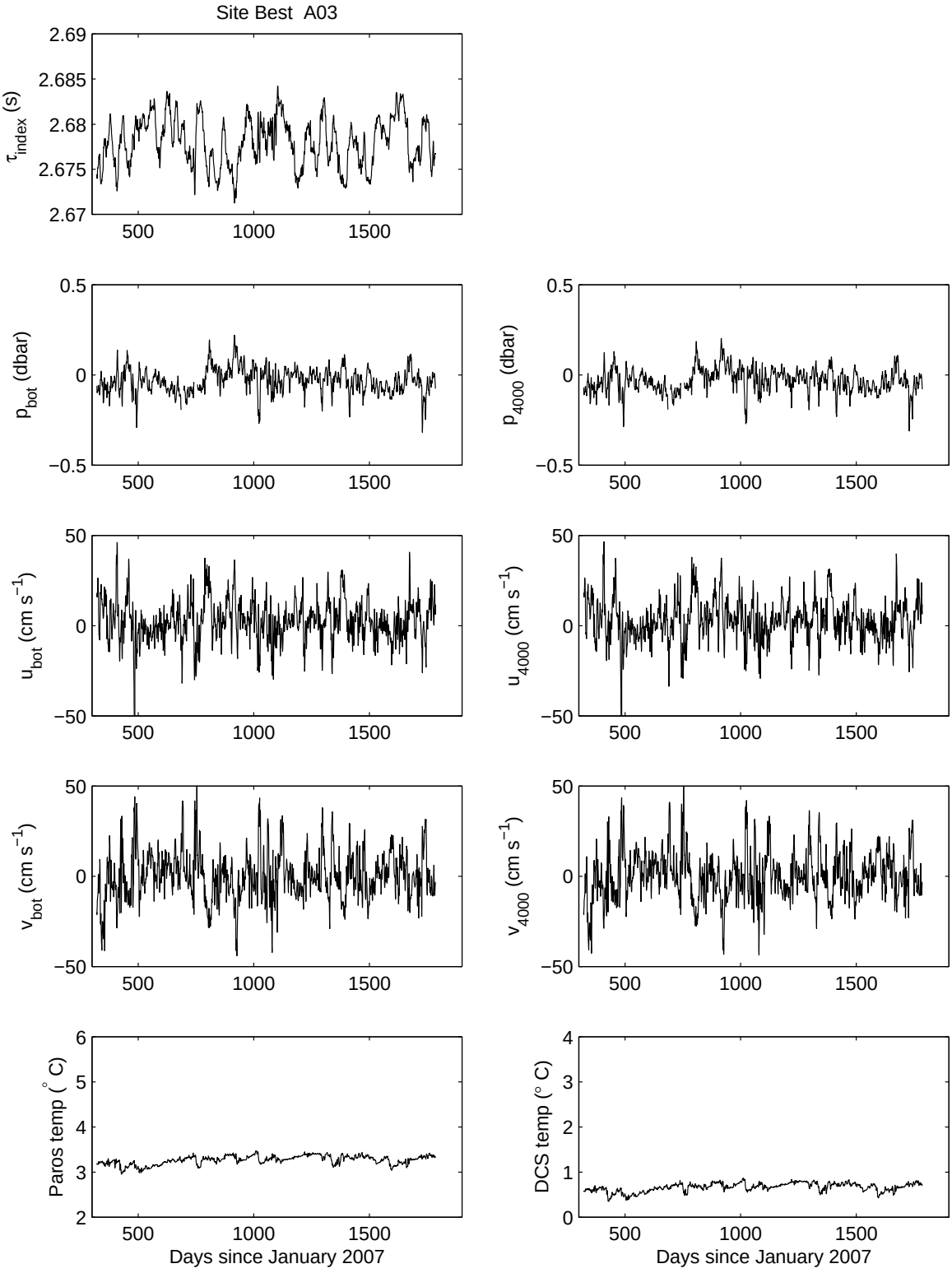

Figure 11: Time series of the 3-day low-pass filtered data obtained at site A03.

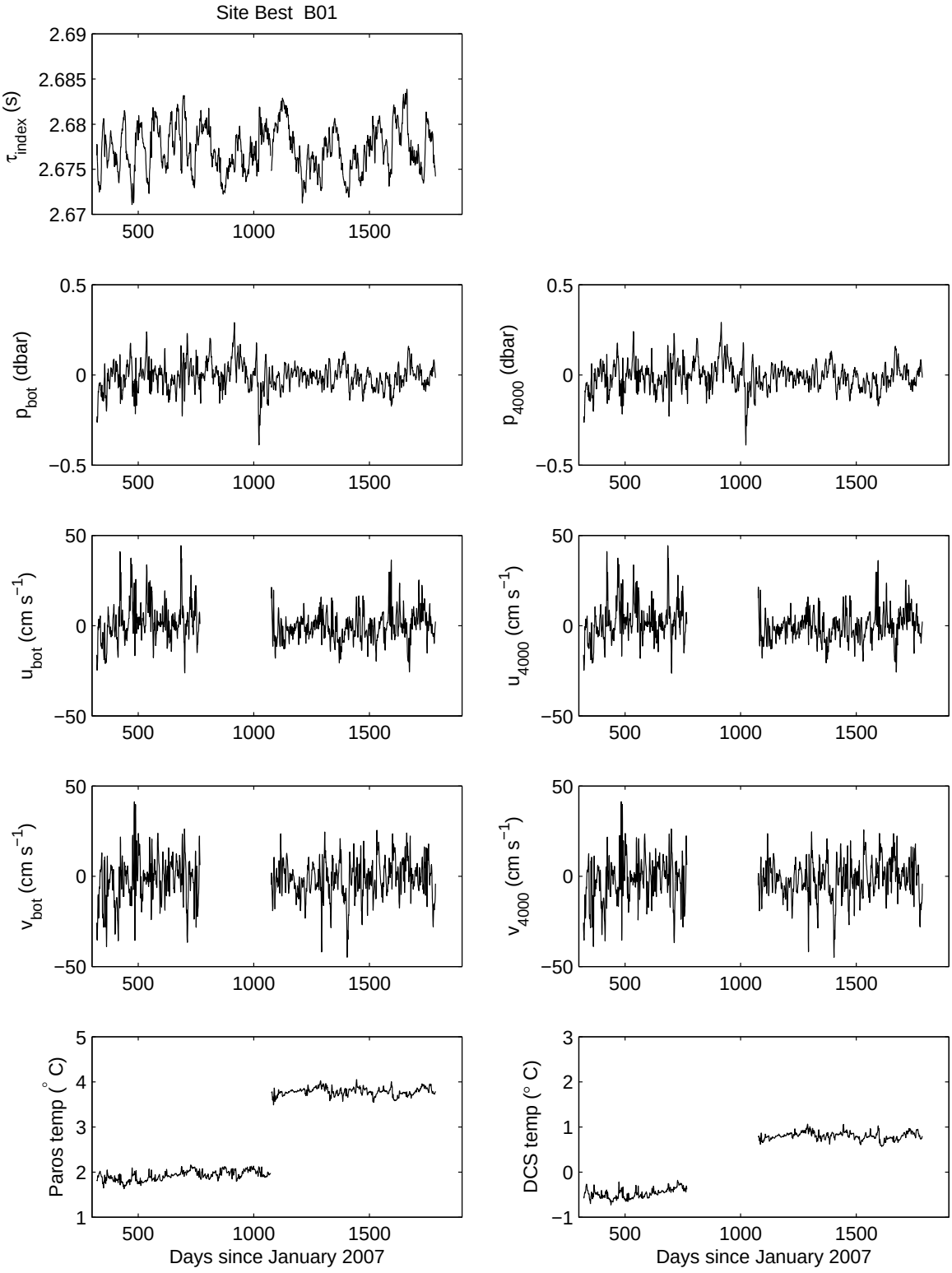

Figure 12: Time series of the 3-day low-pass filtered data obtained at site B01.

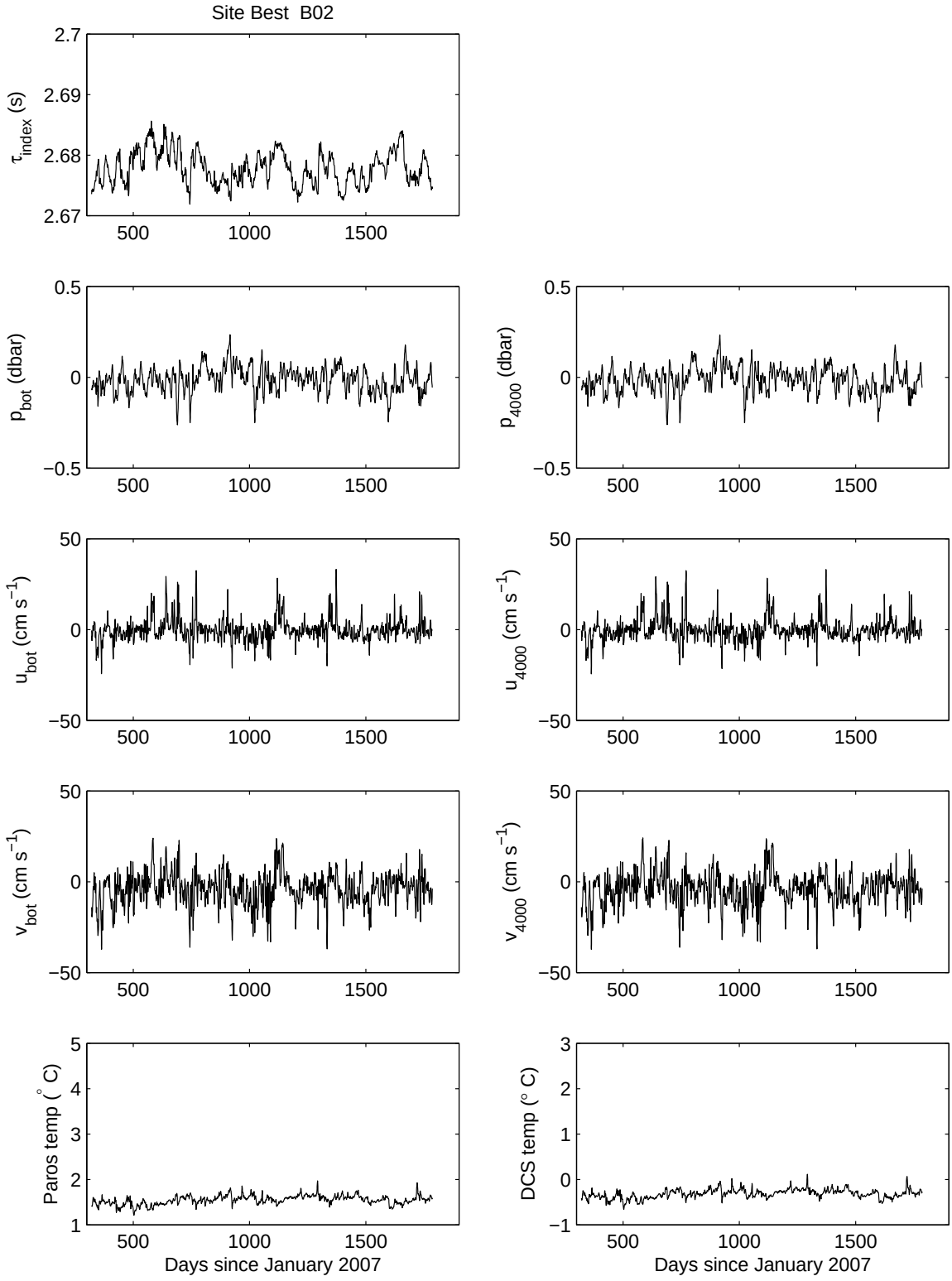

Figure 13: Time series of the 3-day low-pass filtered data obtained at site B02.

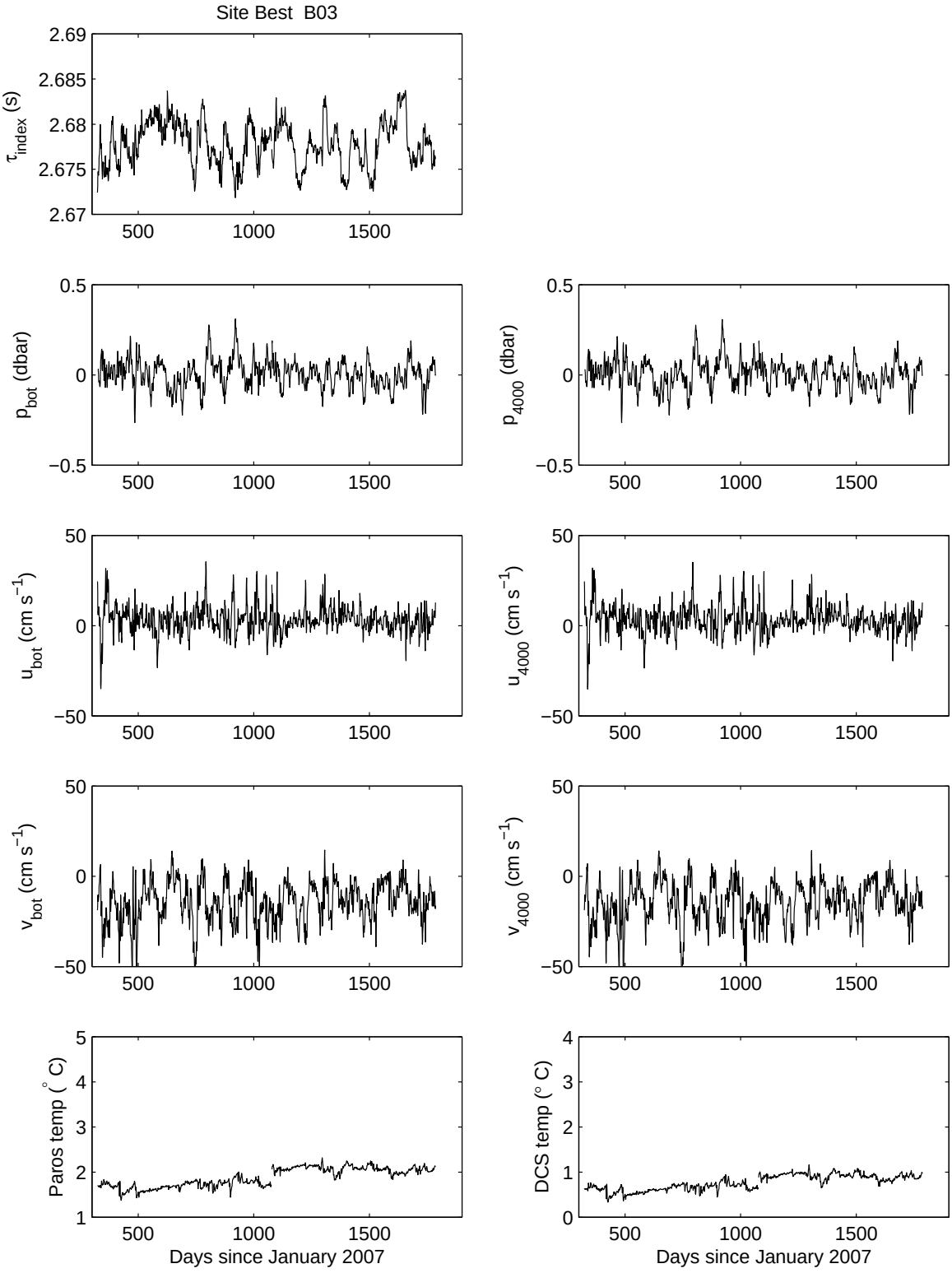

Figure 14: Time series of the 3-day low-pass filtered data obtained at site B03.

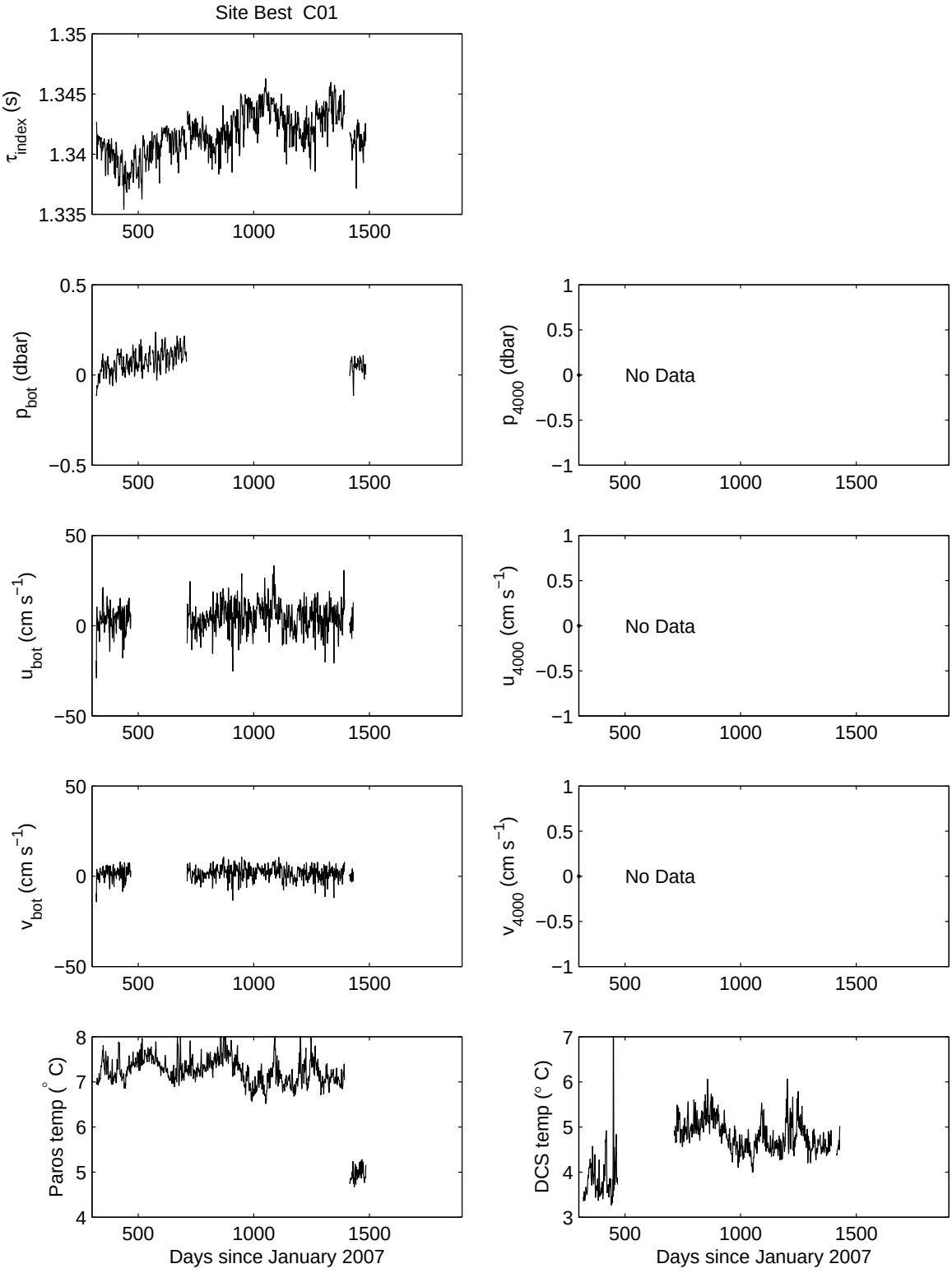

Figure 15: Time series of the 3-day low-pass filtered data obtained at site C01.

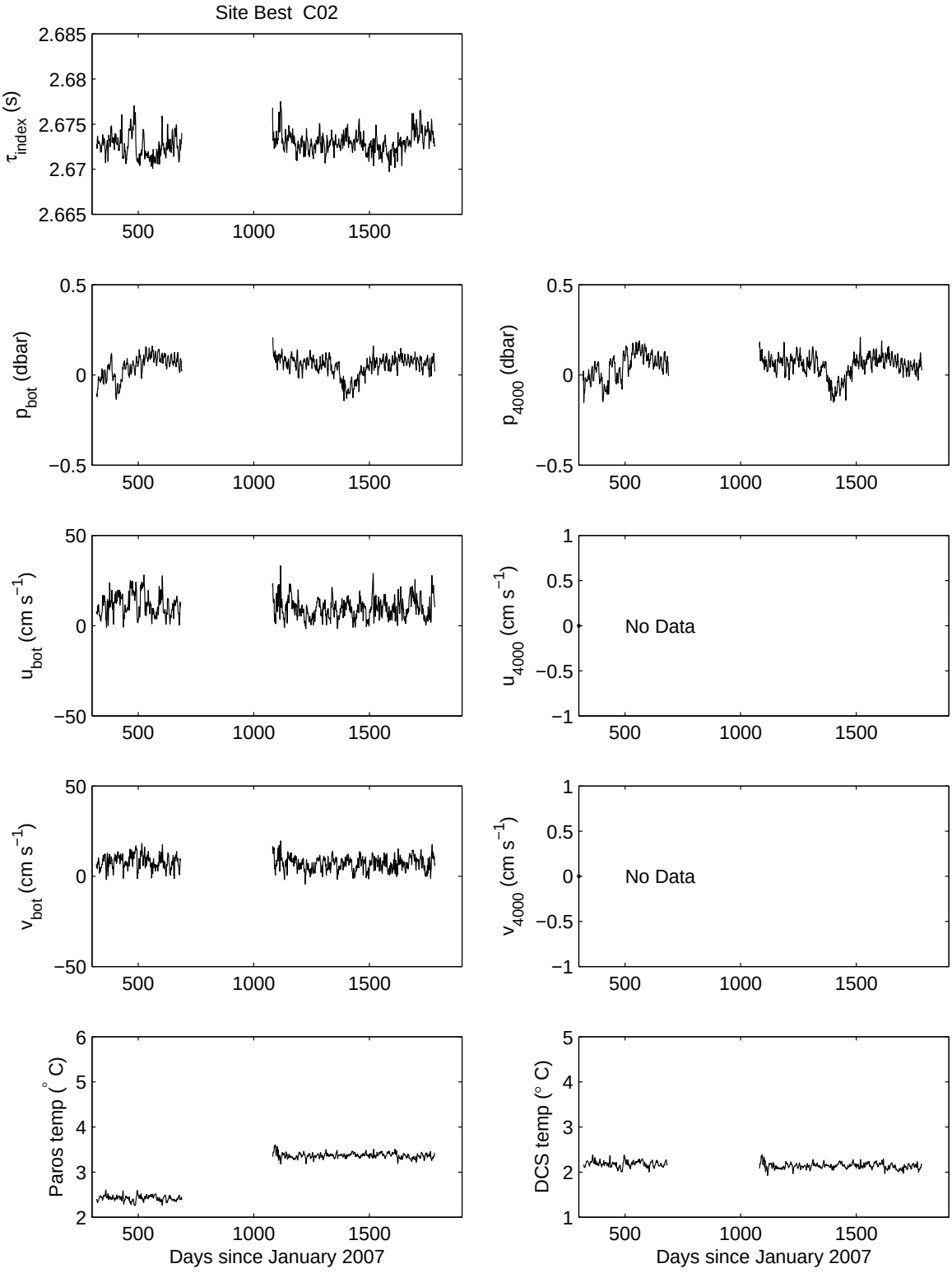

Figure 16: Time series of the 3-day low-pass filtered data obtained at site C02.

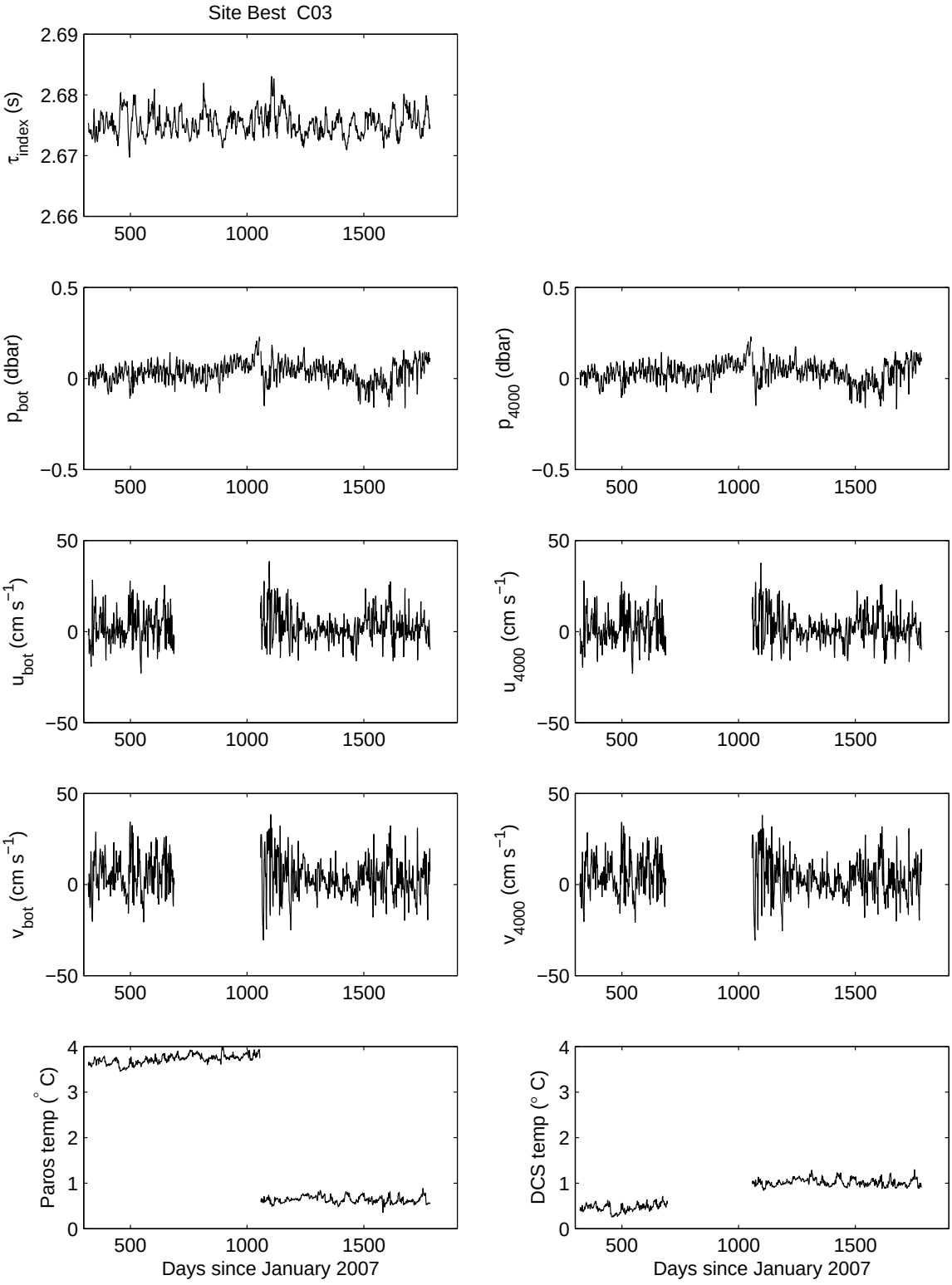

Figure 17: Time series of the 3-day low-pass filtered data obtained at site C03.

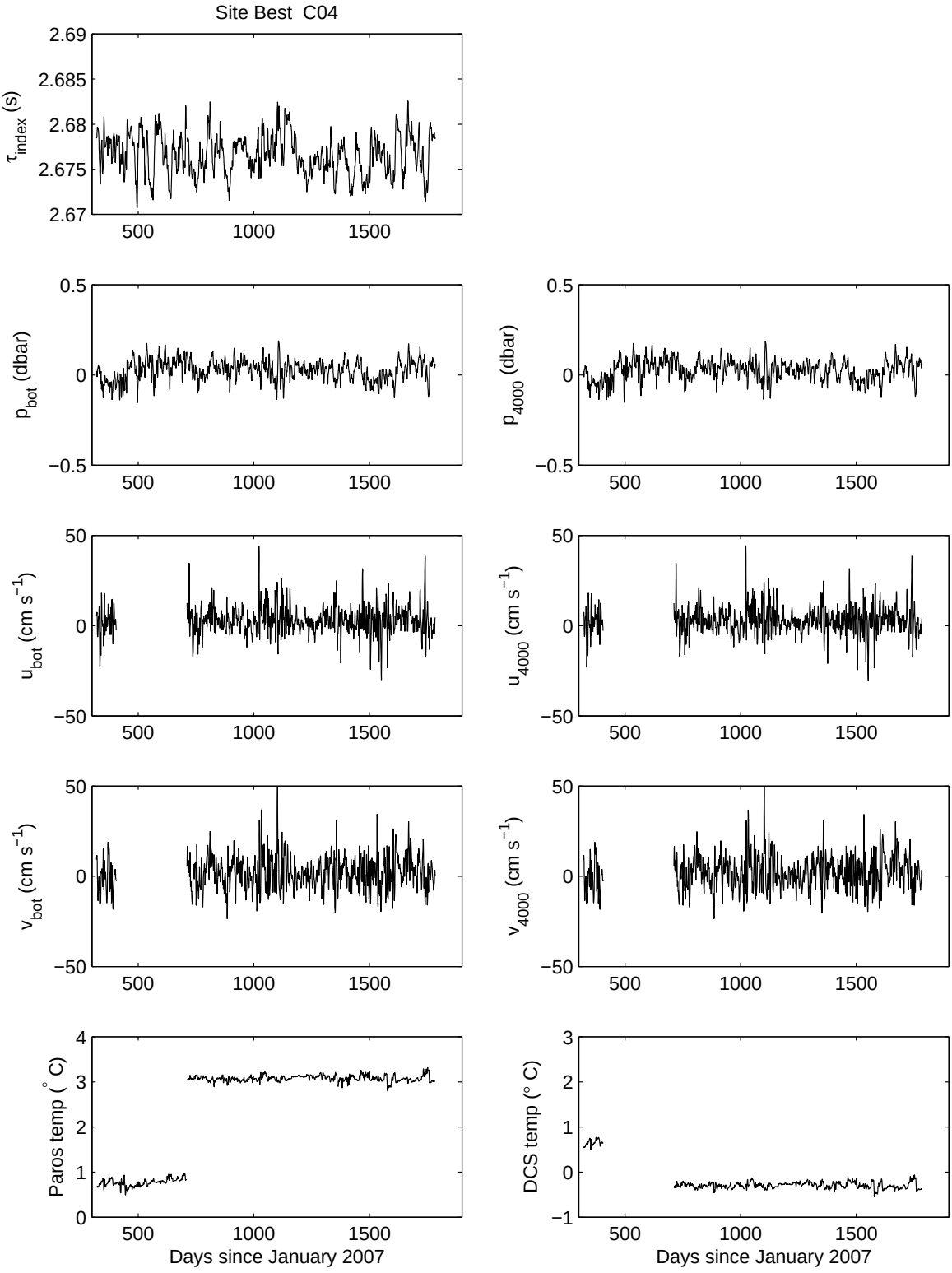

Figure 18: Time series of the 3-day low-pass filtered data obtained at site C04.

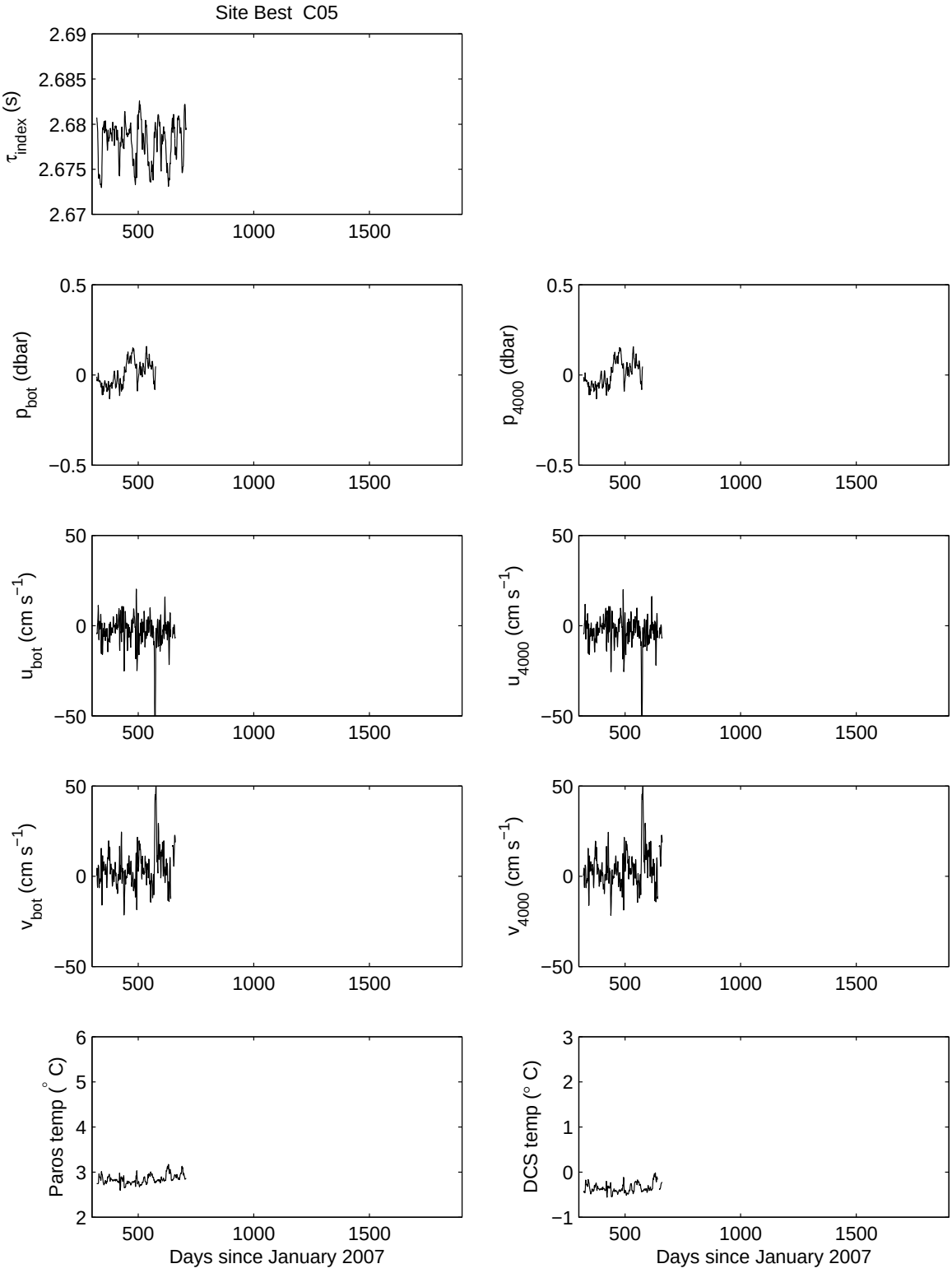

Figure 19: Time series of the 3-day low-pass filtered data obtained at site C05.

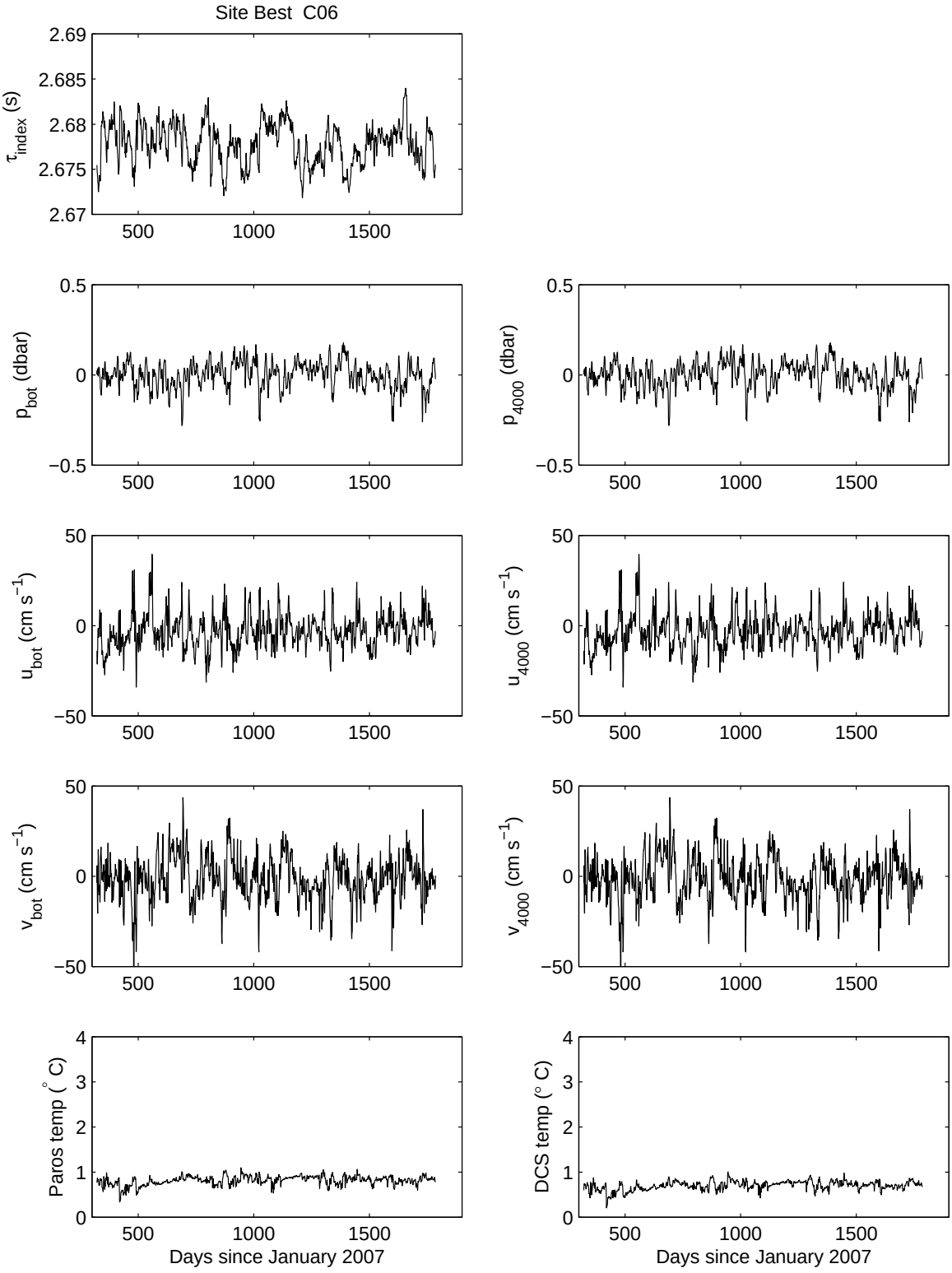

Figure 20: Time series of the 3-day low-pass filtered data obtained at site C06.

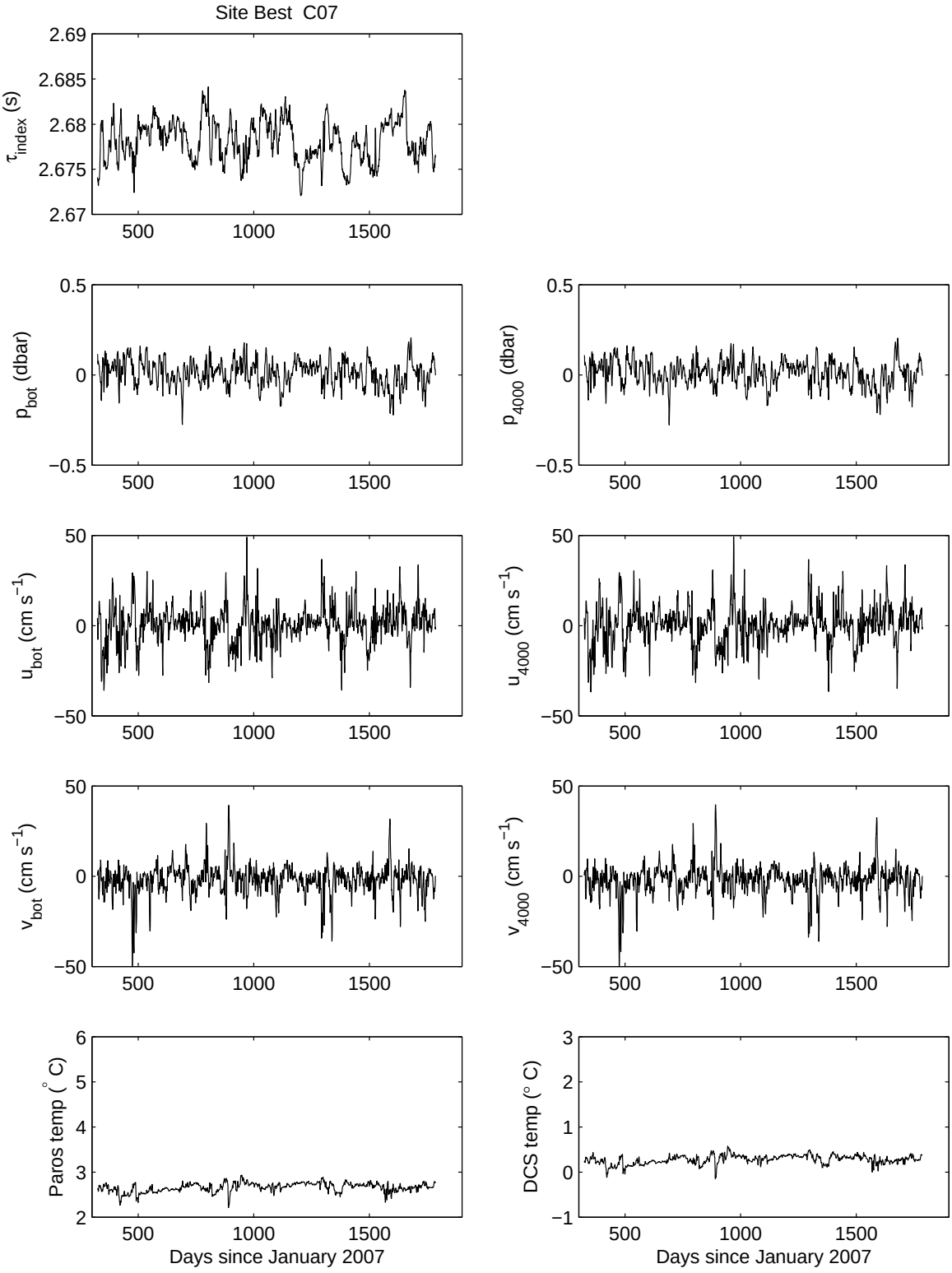

Figure 21: Time series of the 3-day low-pass filtered data obtained at site C07.

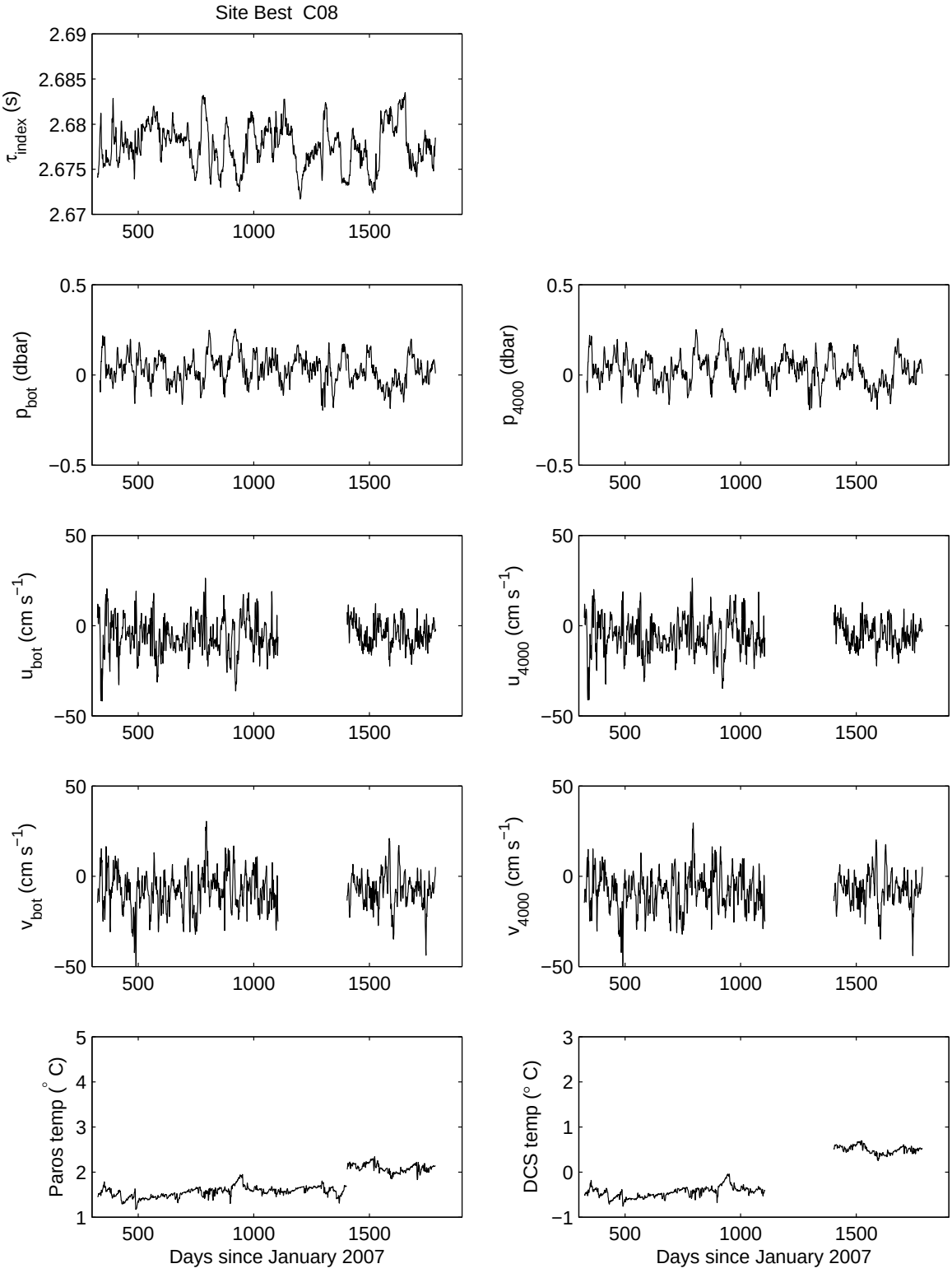

Figure 22: Time series of the 3-day low-pass filtered data obtained at site C08.

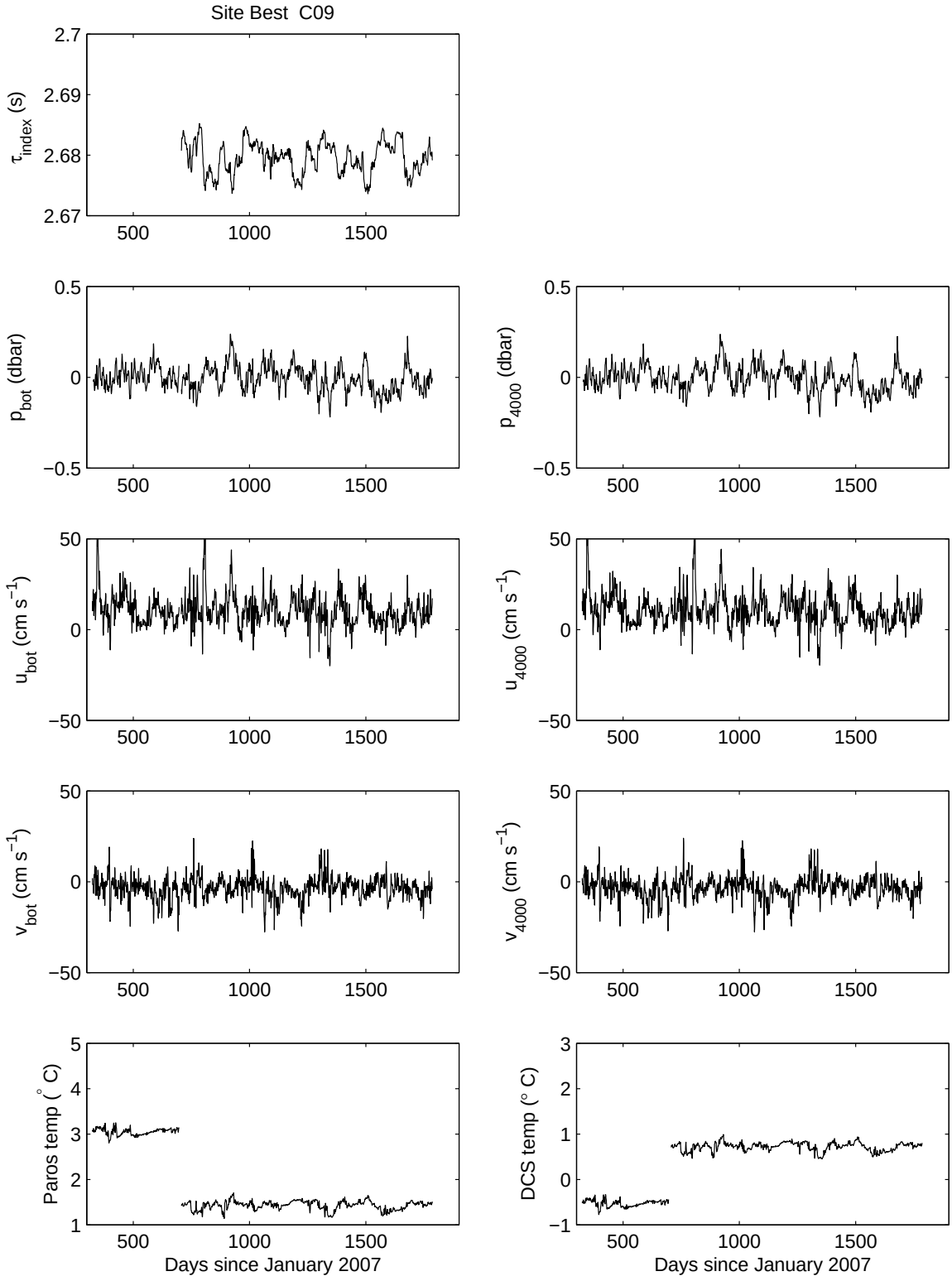

Figure 23: Time series of the 3-day low-pass filtered data obtained at site C09.

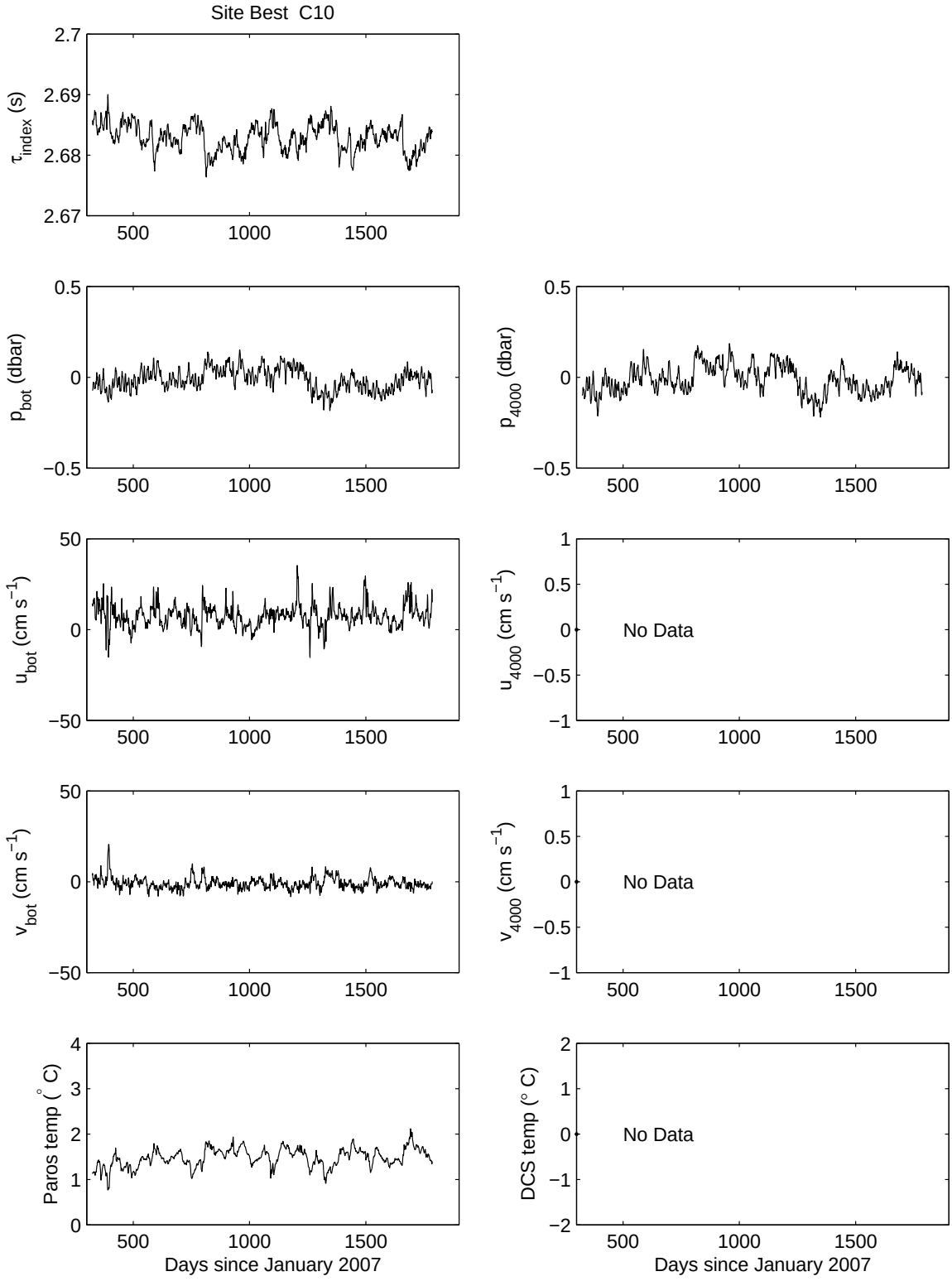

Figure 24: Time series of the 3-day low-pass filtered data obtained at site C10.

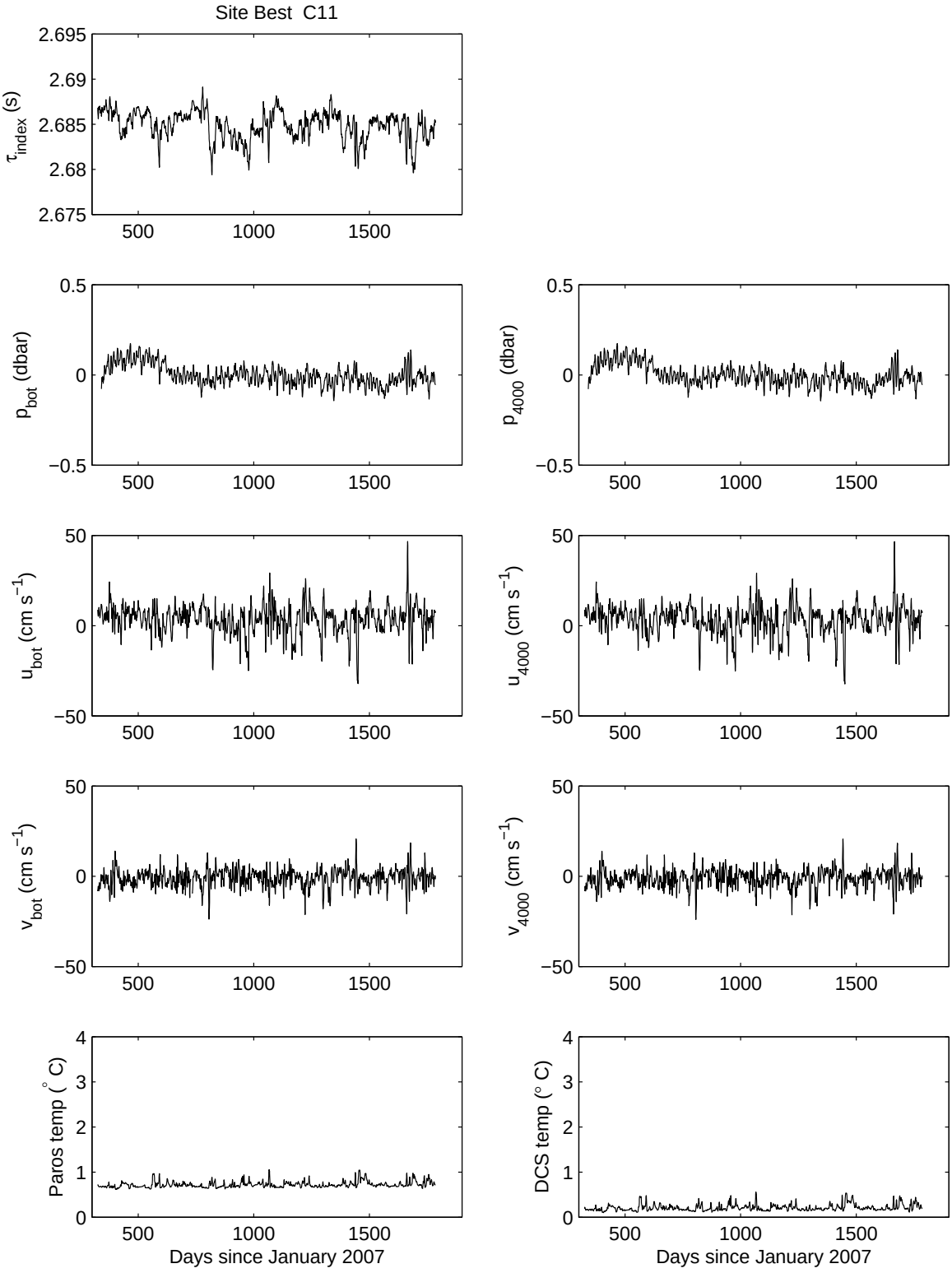

Figure 25: Time series of the 3-day low-pass filtered data obtained at site C11.

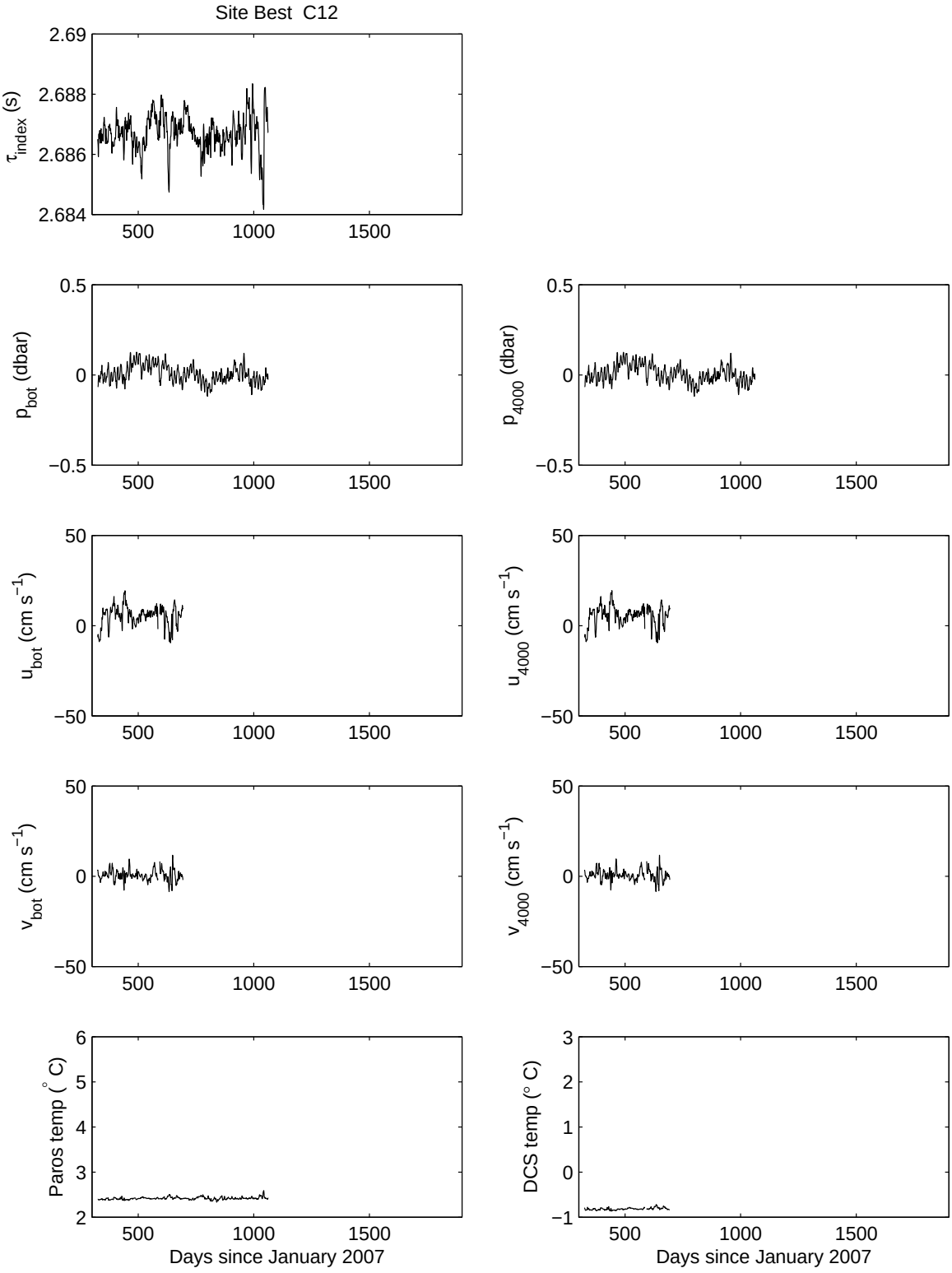

Figure 26: Time series of the 3-day low-pass filtered data obtained at site C12.

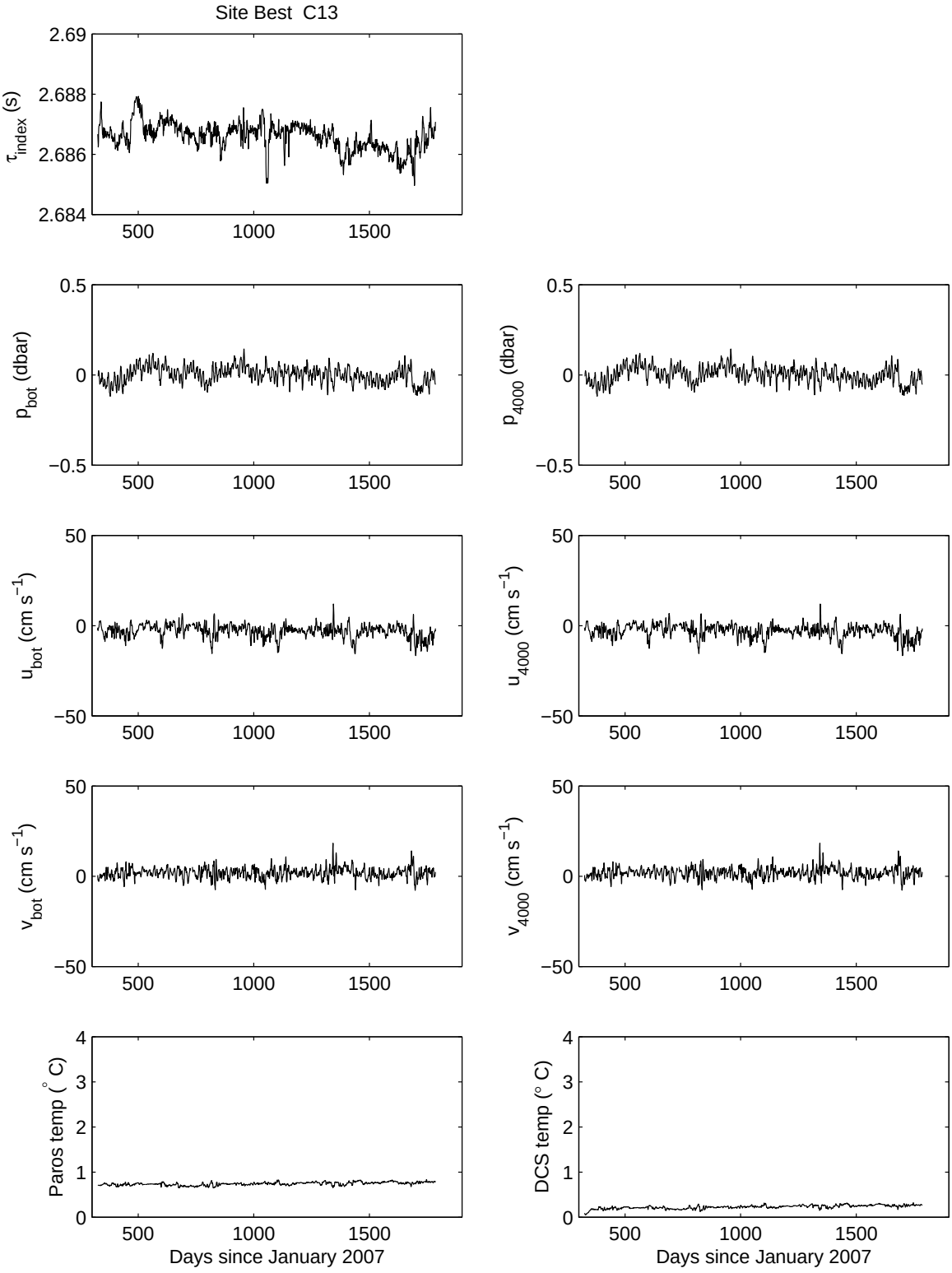

Figure 27: Time series of the 3-day low-pass filtered data obtained at site C13.

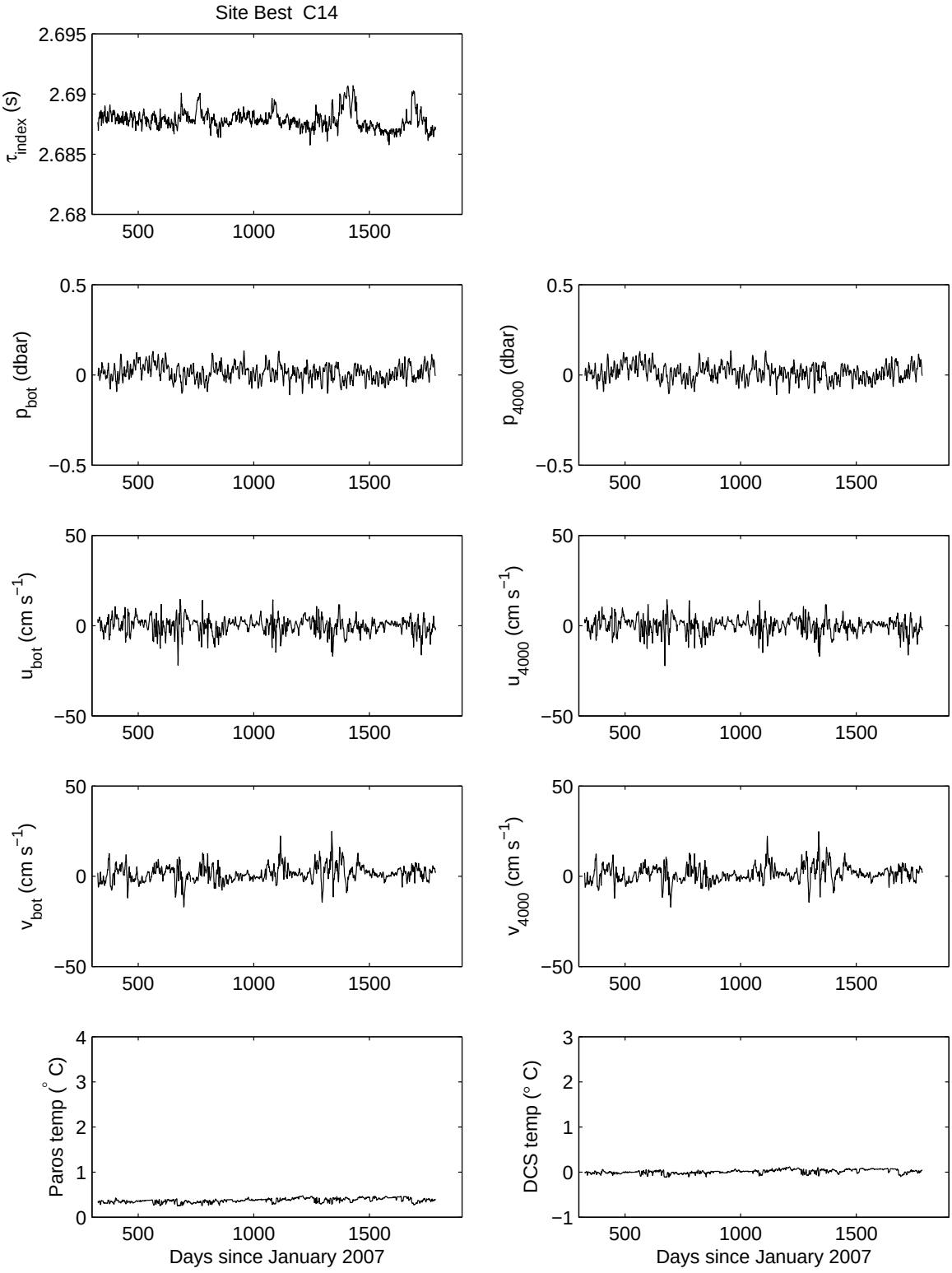

Figure 28: Time series of the 3-day low-pass filtered data obtained at site C14.

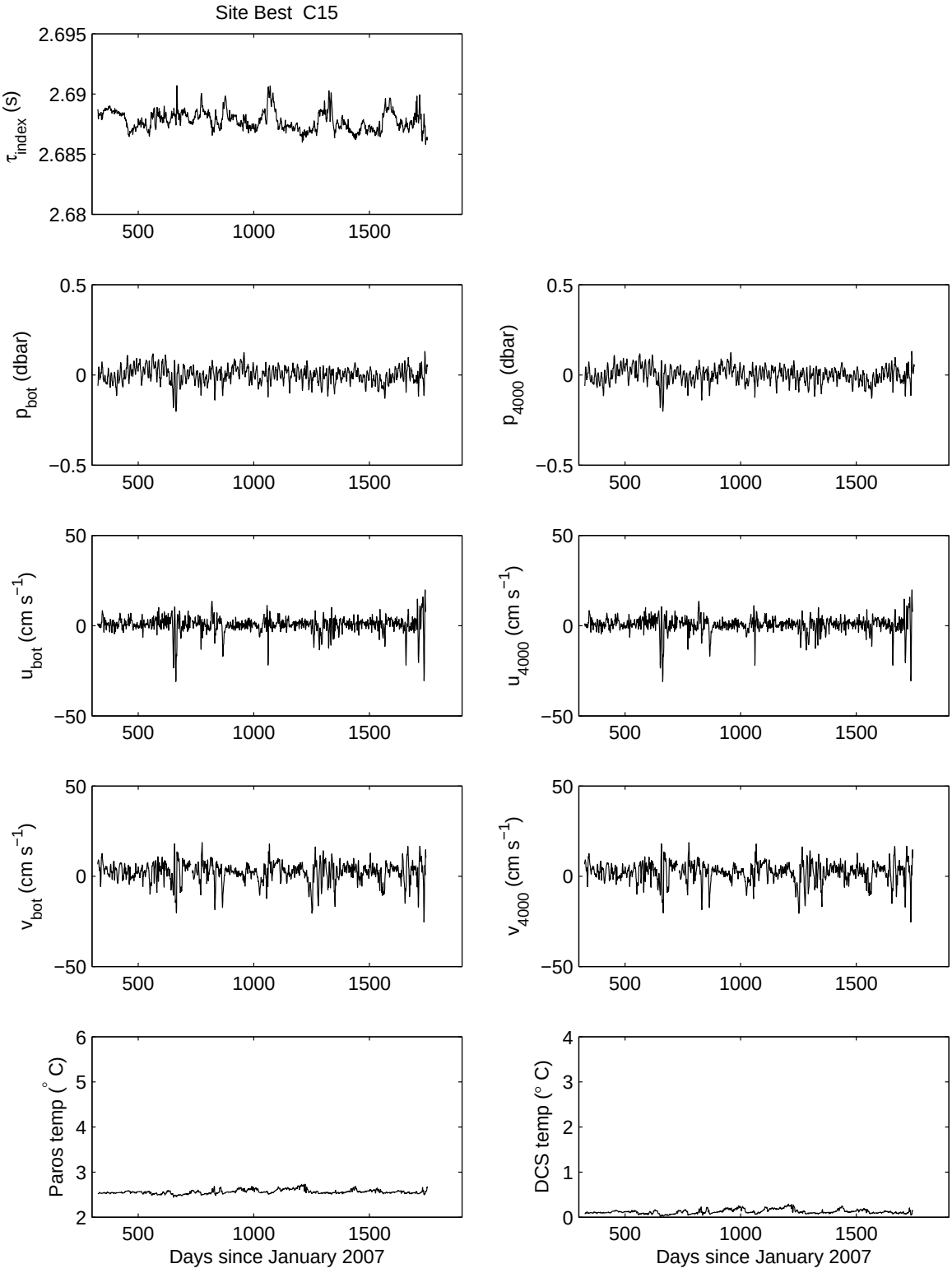

Figure 29: Time series of the 3-day low-pass filtered data obtained at site C15.

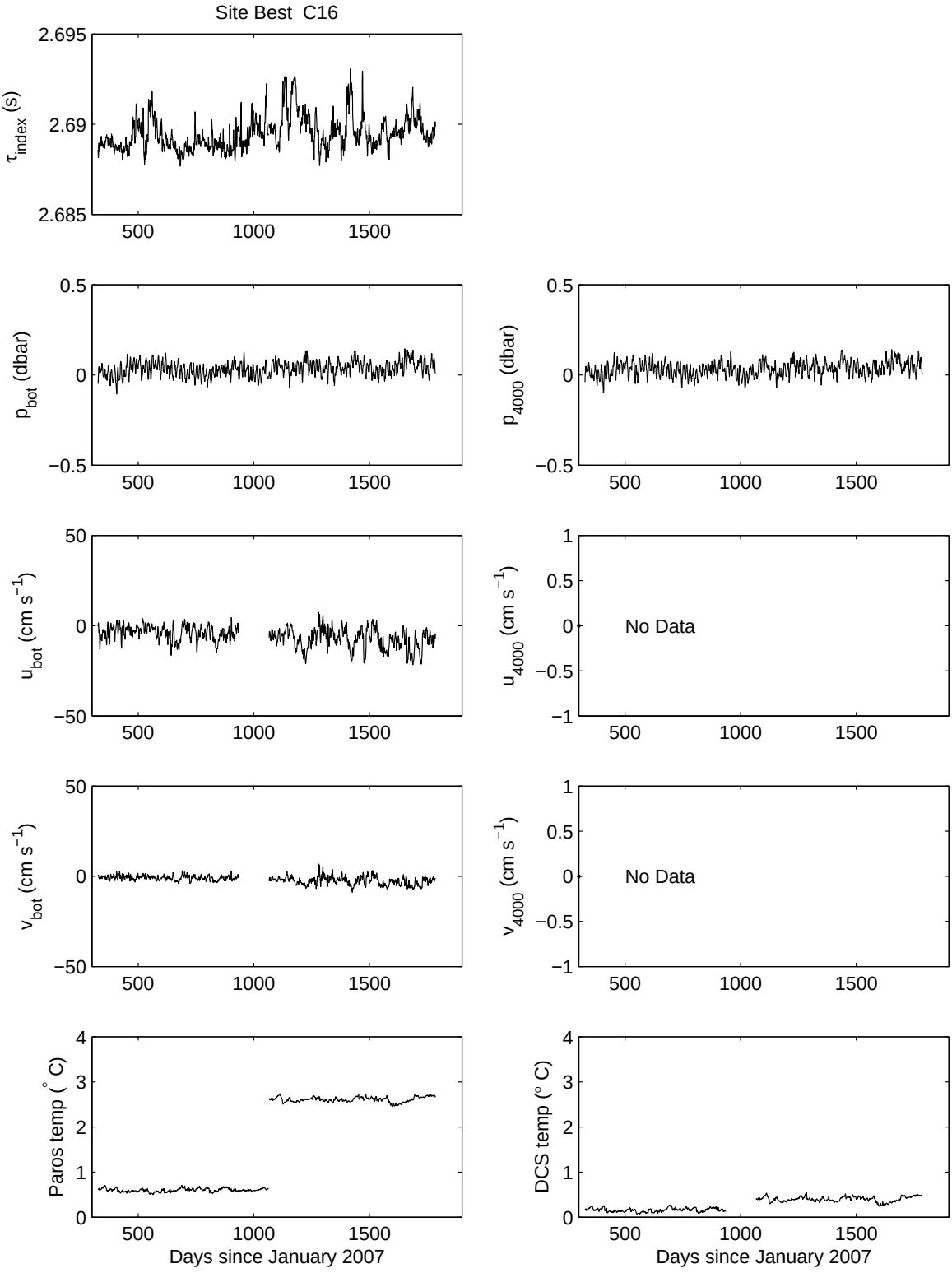

Figure 30: Time series of the 3-day low-pass filtered data obtained at site C16.

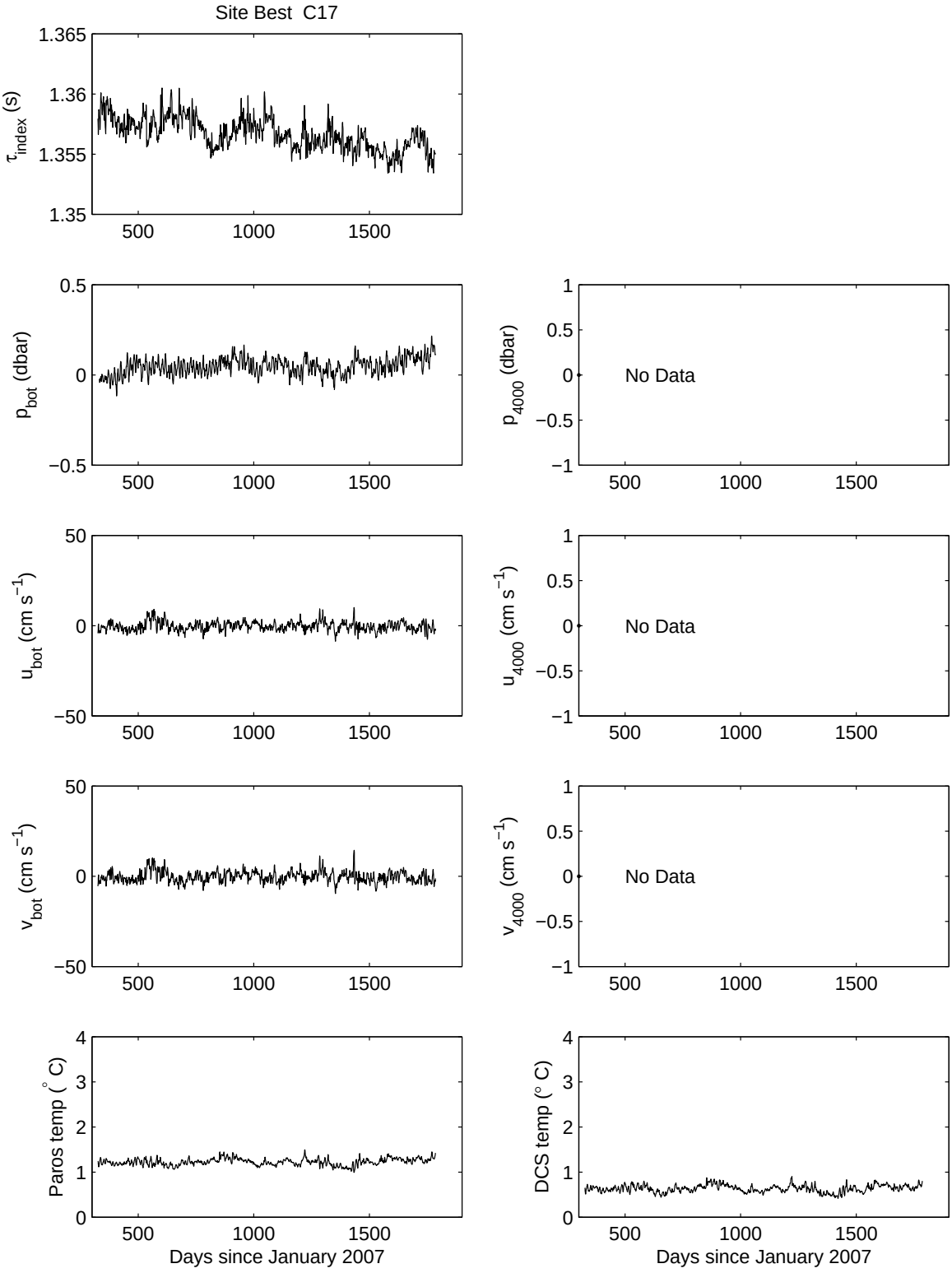

Figure 31: Time series of the 3-day low-pass filtered data obtained at site C17.

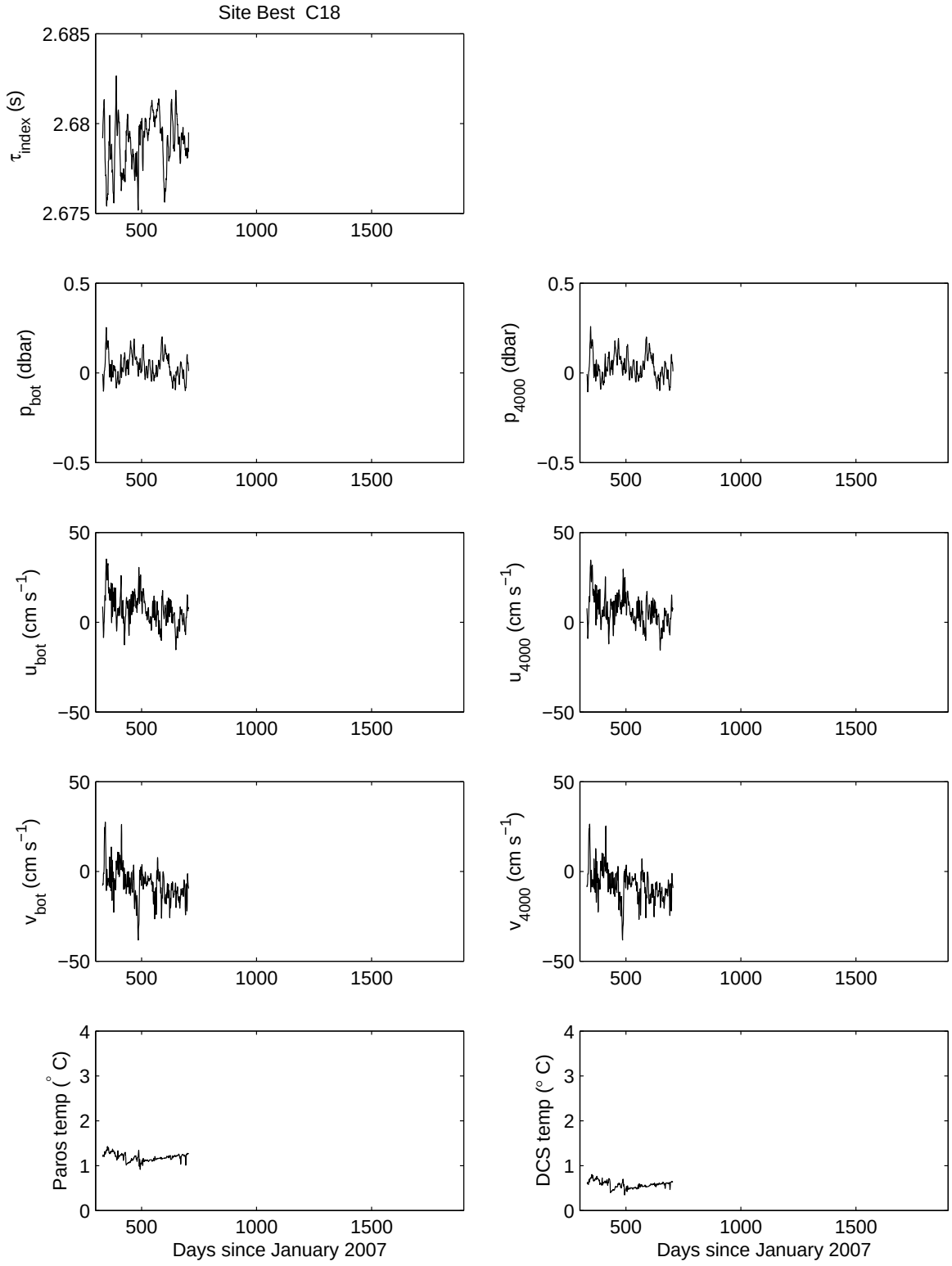

Figure 32: Time series of the 3-day low-pass filtered data obtained at site C18.

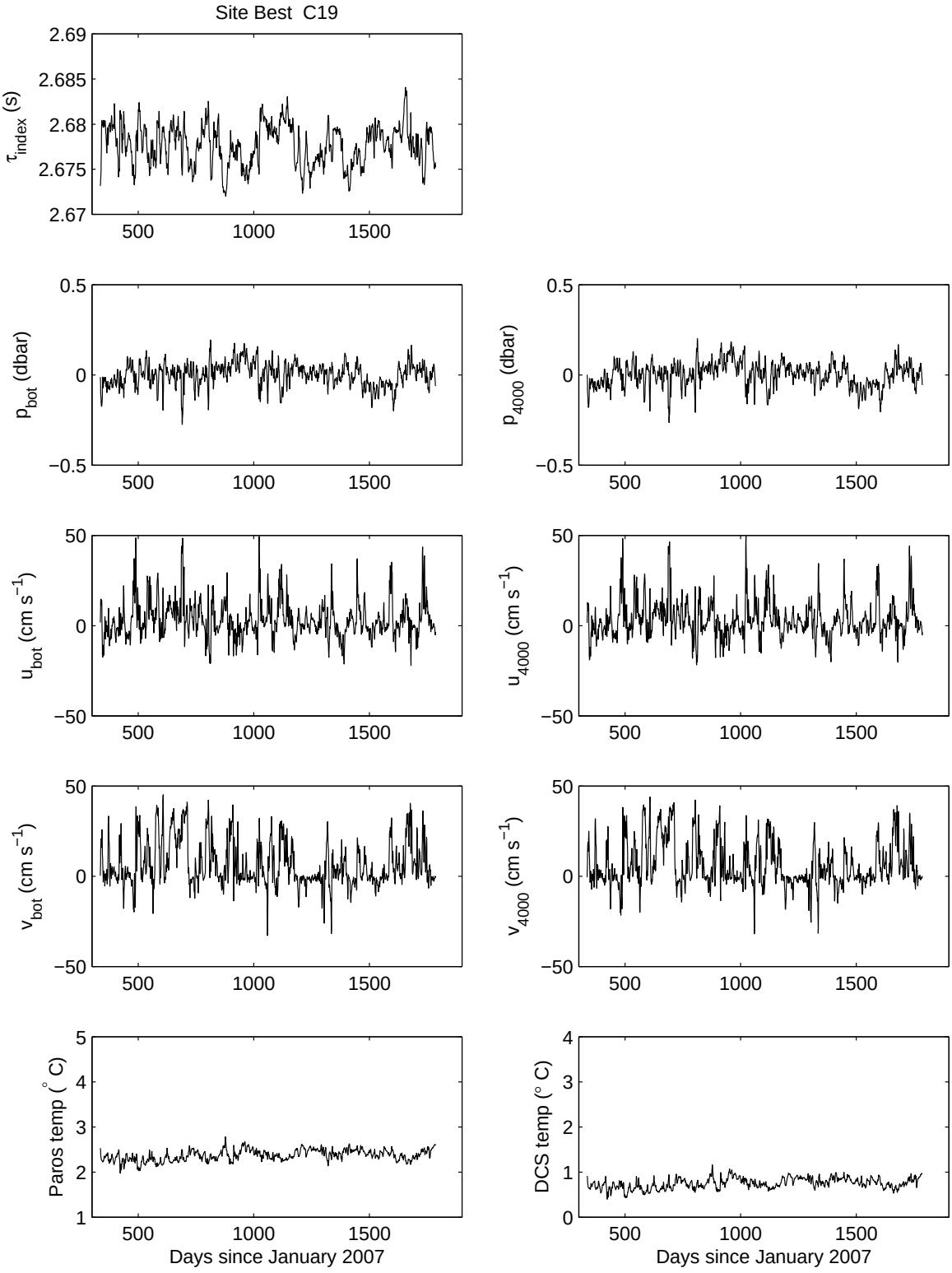

Figure 33: Time series of the 3-day low-pass filtered data obtained at site C19.

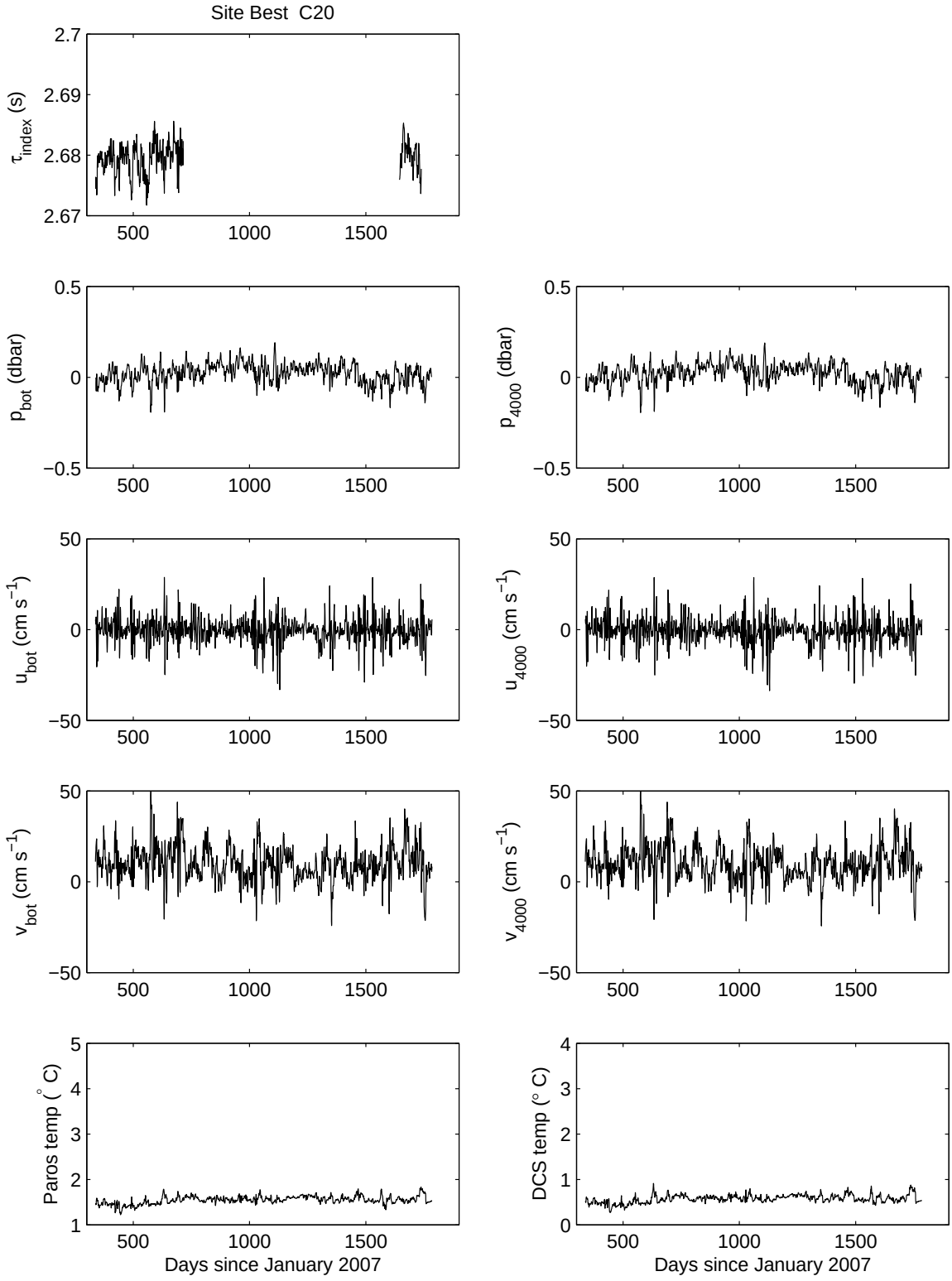

Figure 34: Time series of the 3-day low-pass filtered data obtained at site C20.

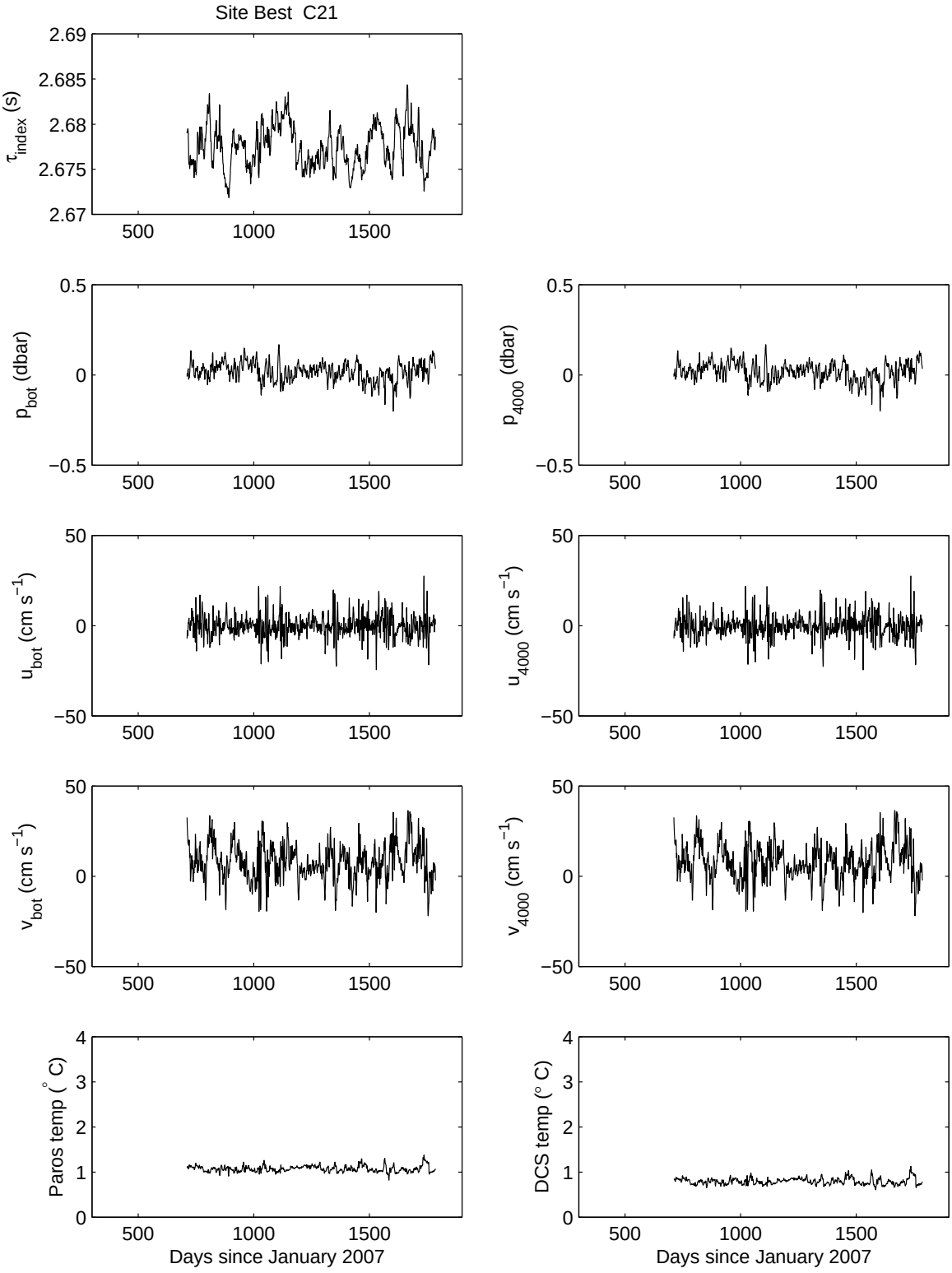

Figure 35: Time series of the 3-day low-pass filtered data obtained at site C21.

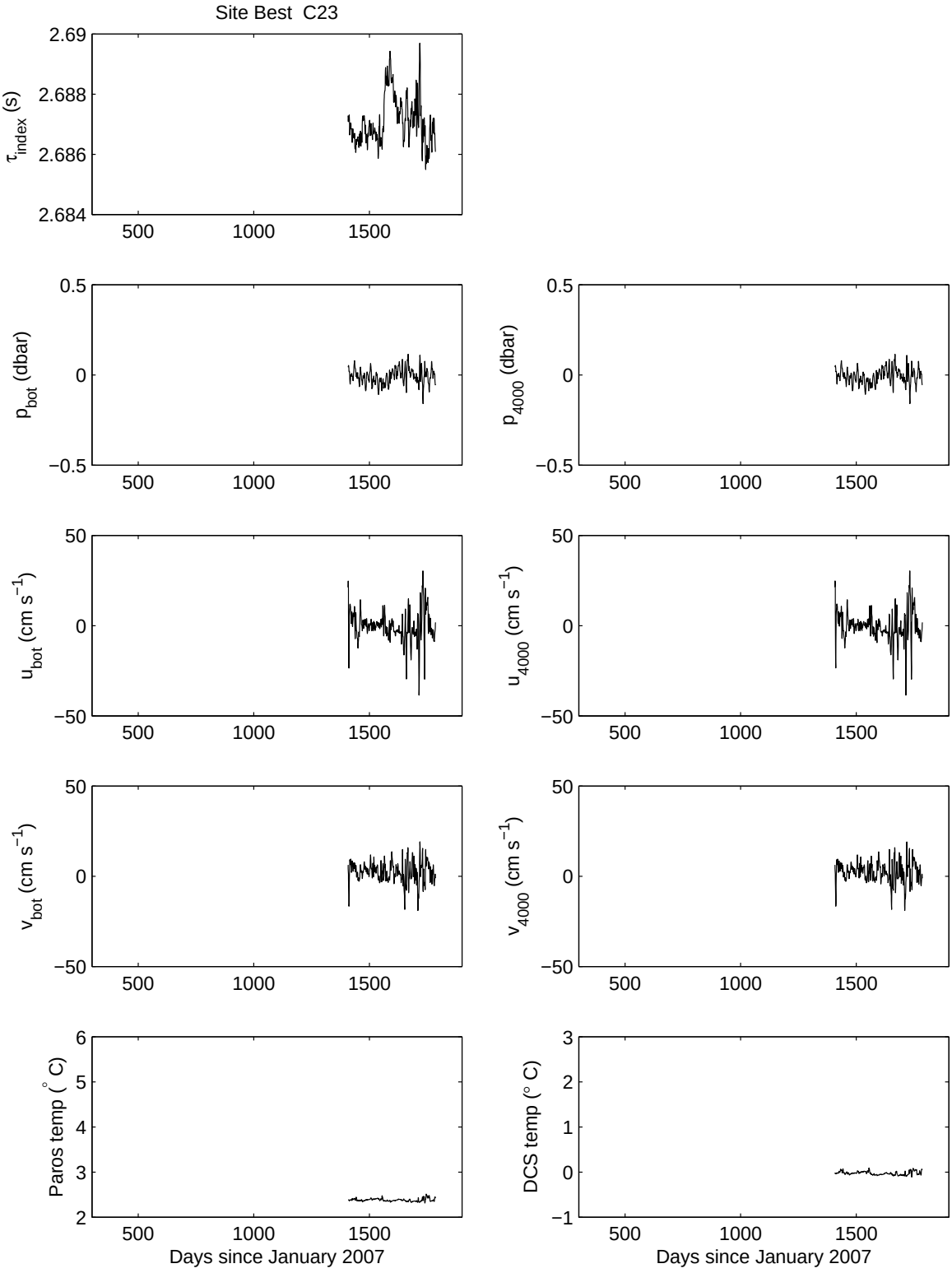

Figure 36: Time series of the 3-day low-pass filtered data obtained at site C23.

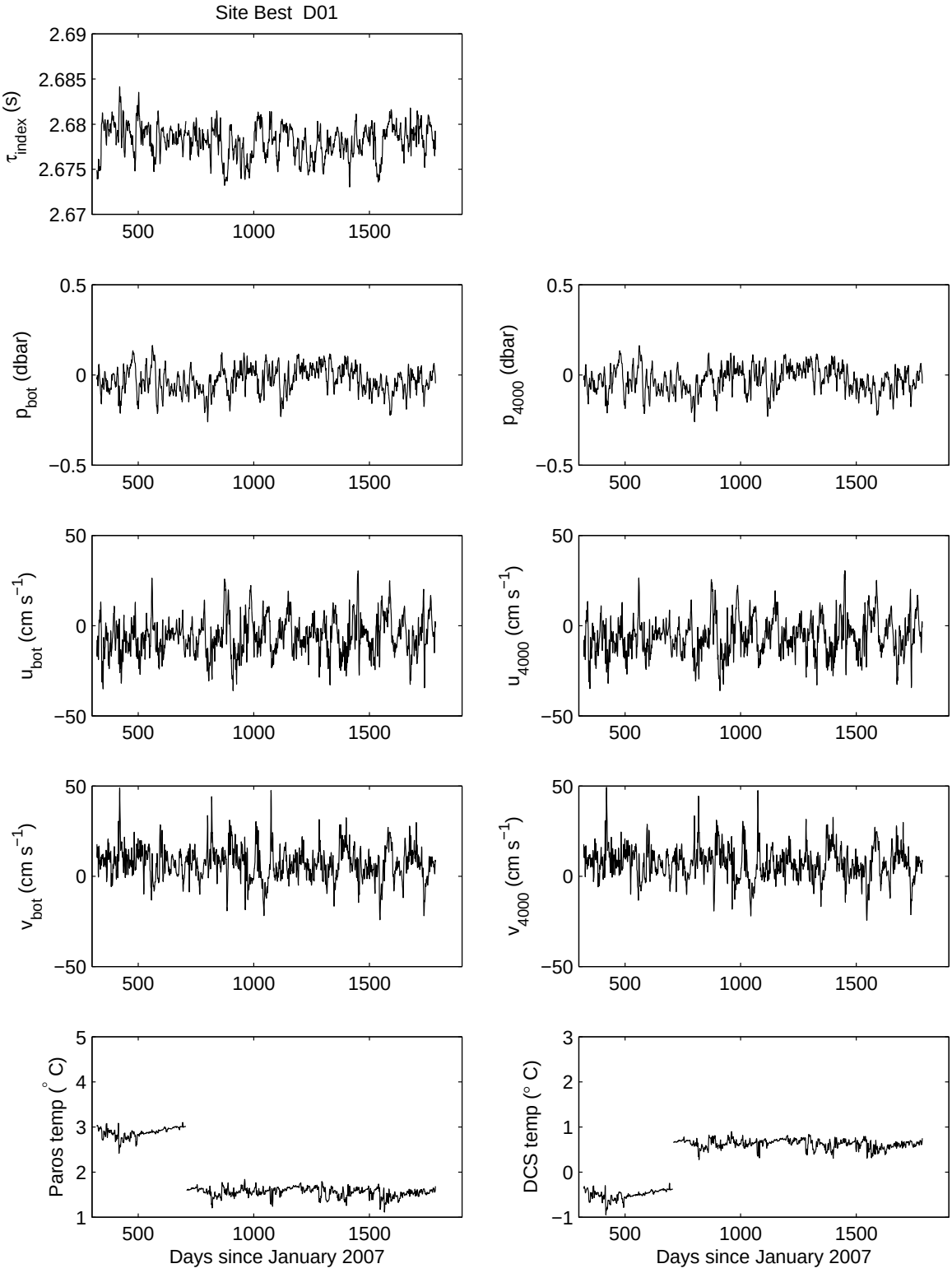

Figure 37: Time series of the 3-day low-pass filtered data obtained at site D01.

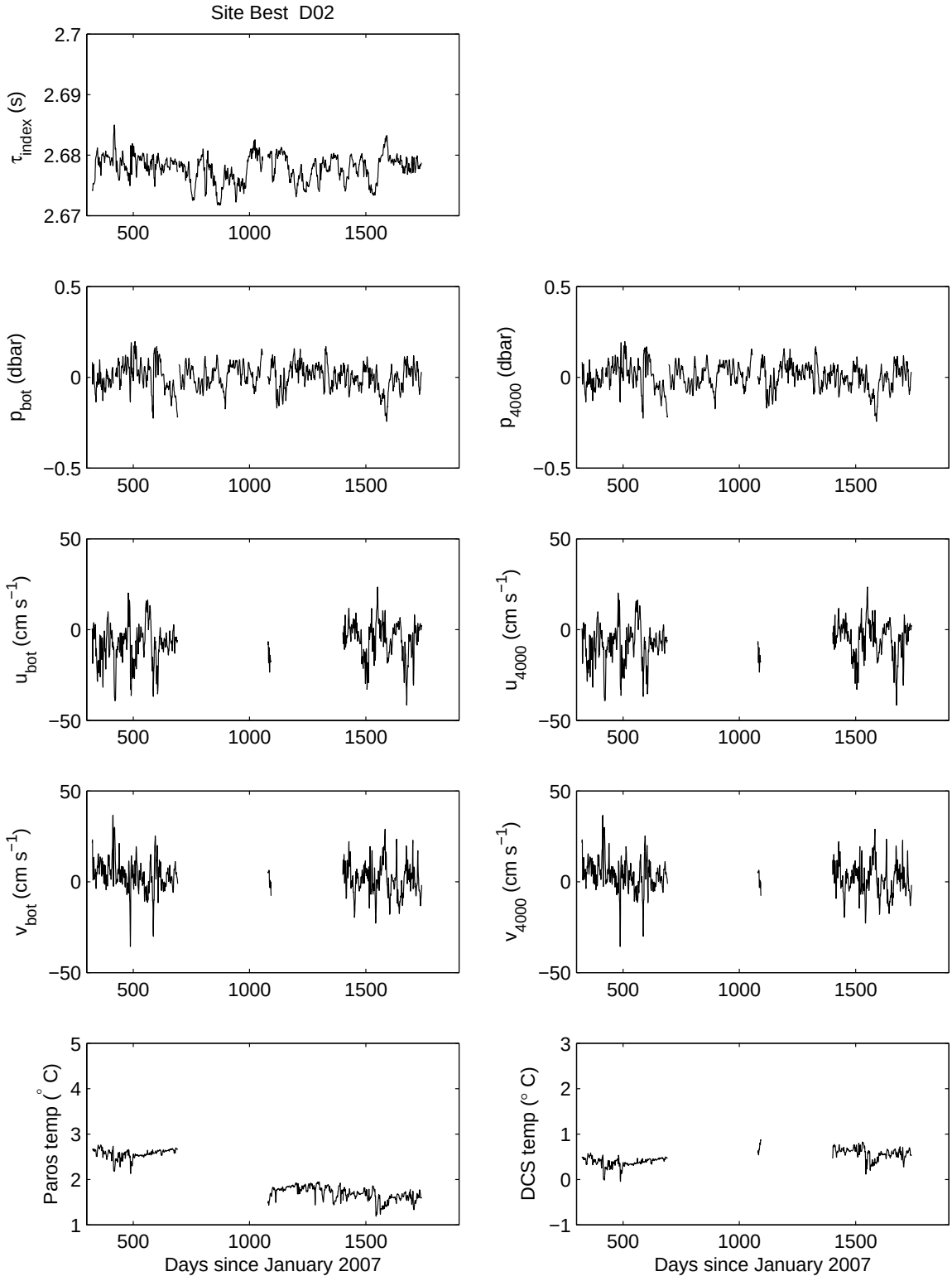

Figure 38: Time series of the 3-day low-pass filtered data obtained at site D02.

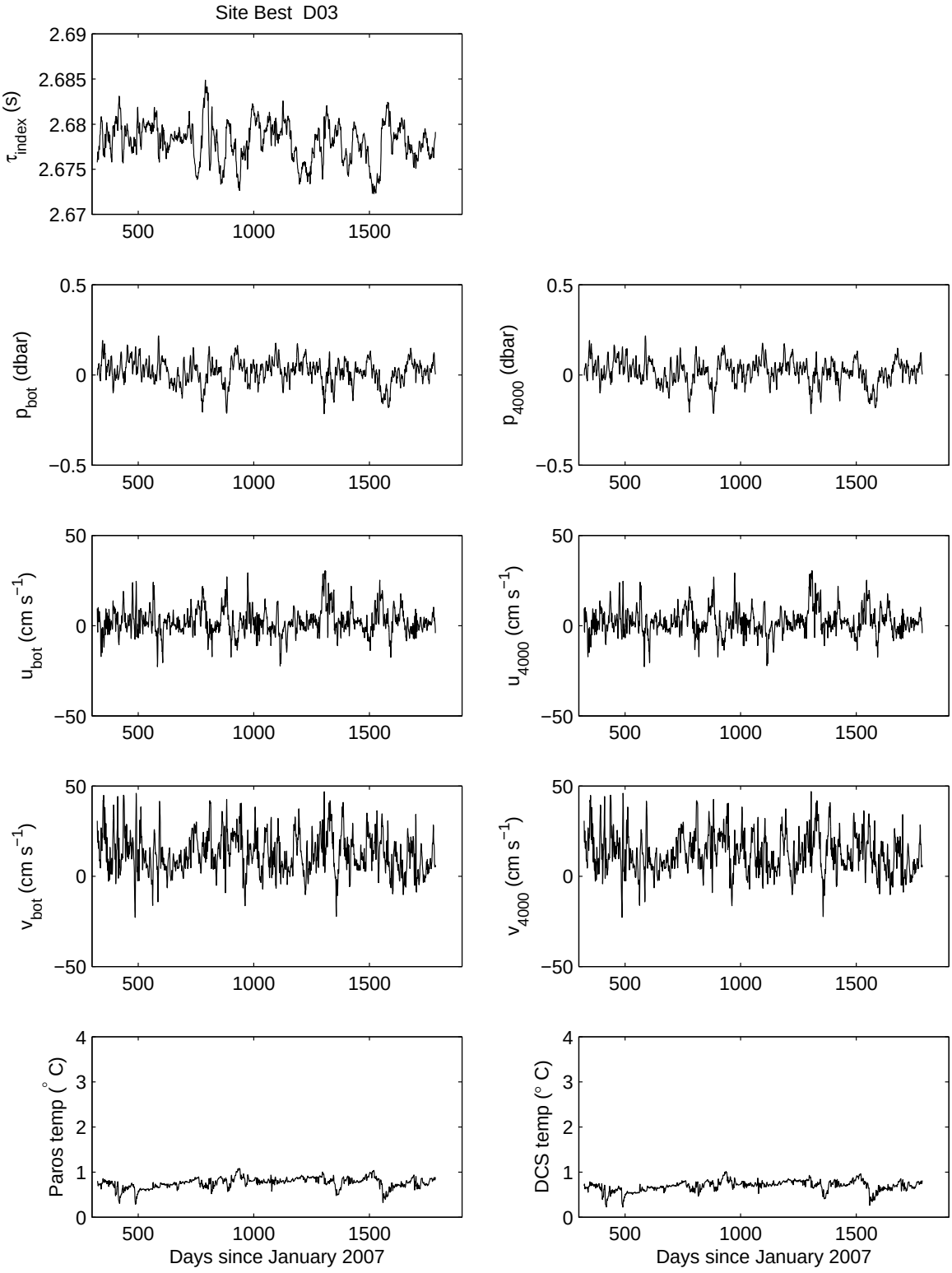

Figure 39: Time series of the 3-day low-pass filtered data obtained at site D03.

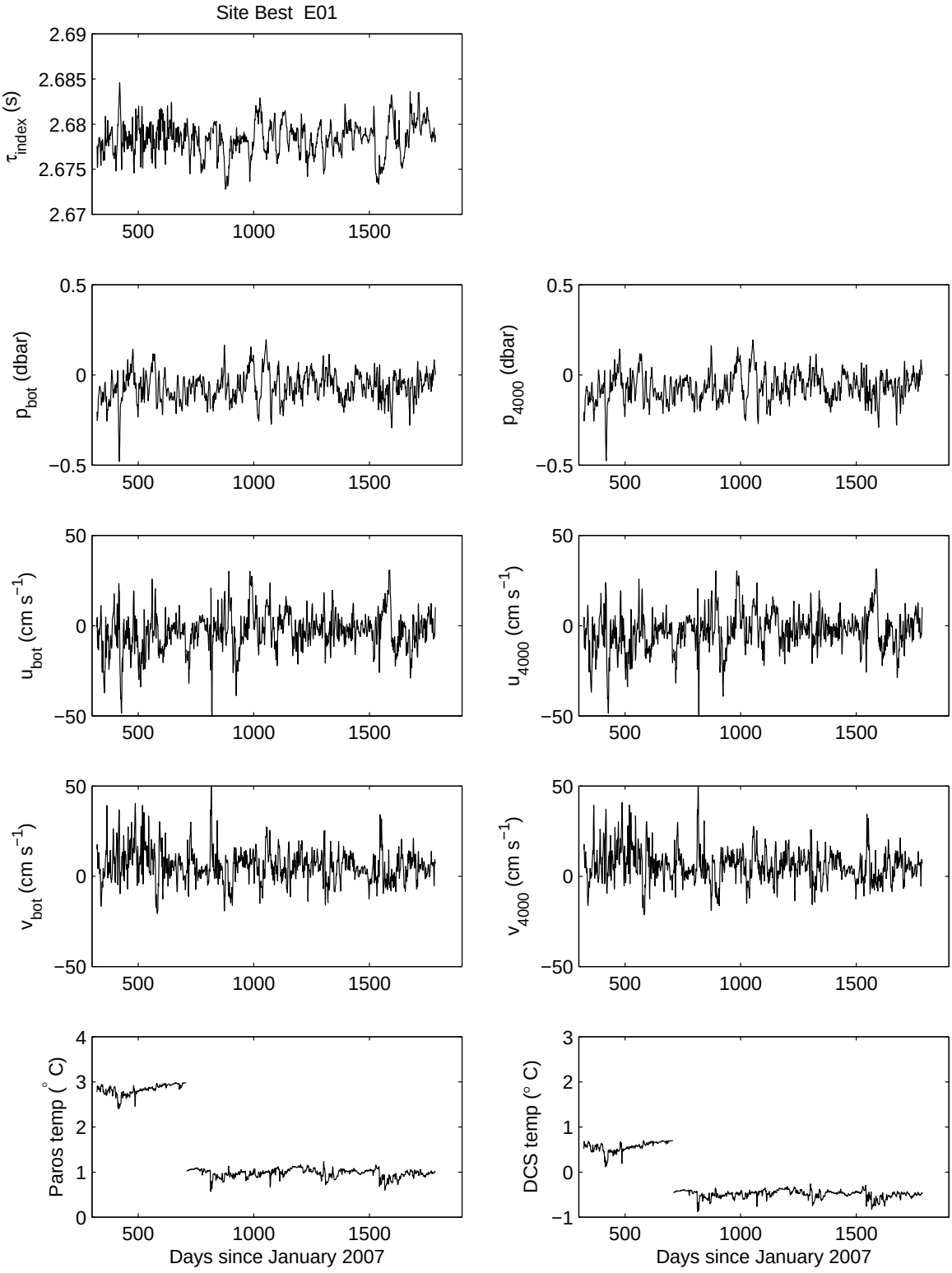

Figure 40: Time series of the 3-day low-pass filtered data obtained at site E01.

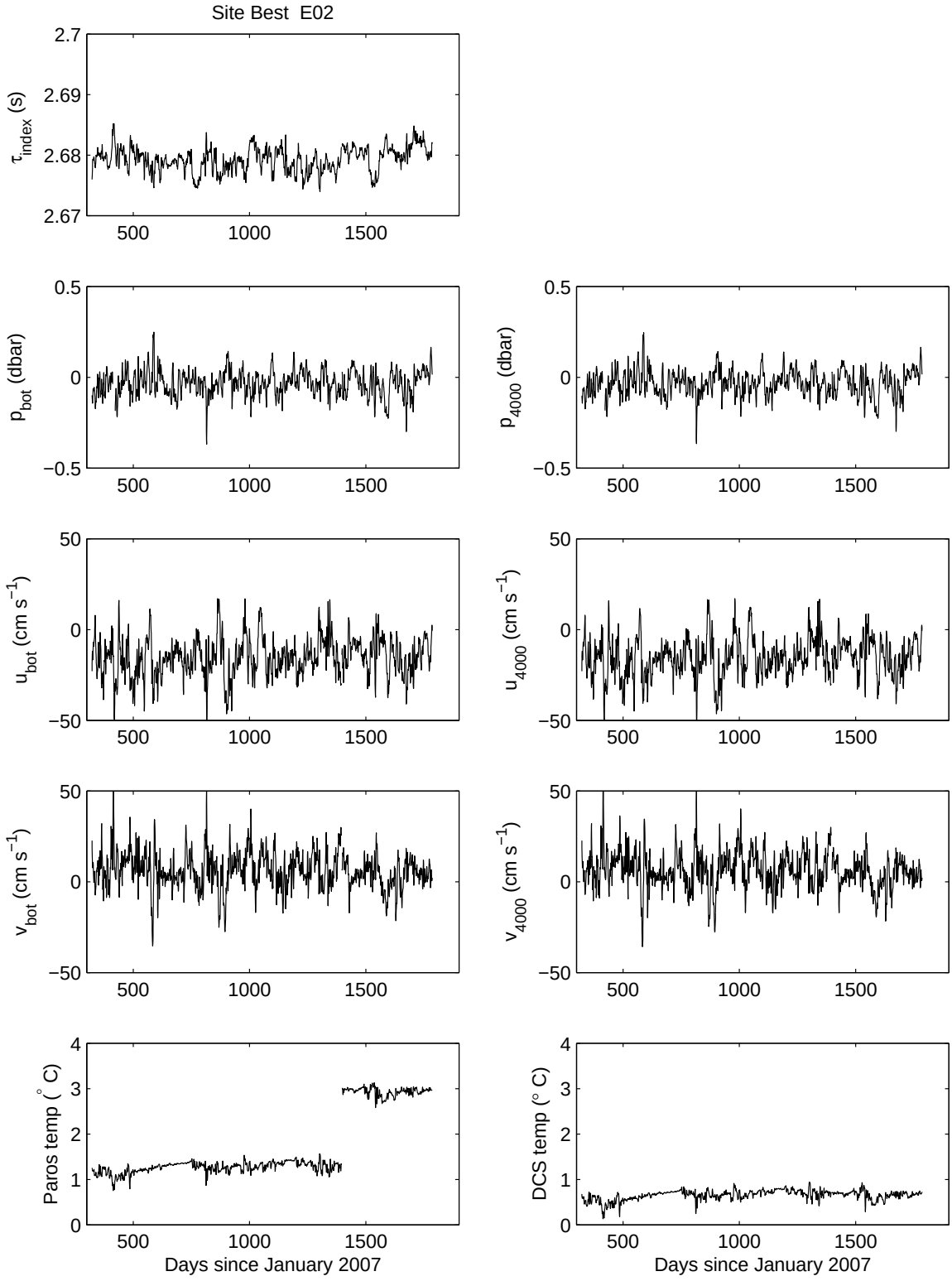

Figure 41: Time series of the 3-day low-pass filtered data obtained at site E02.

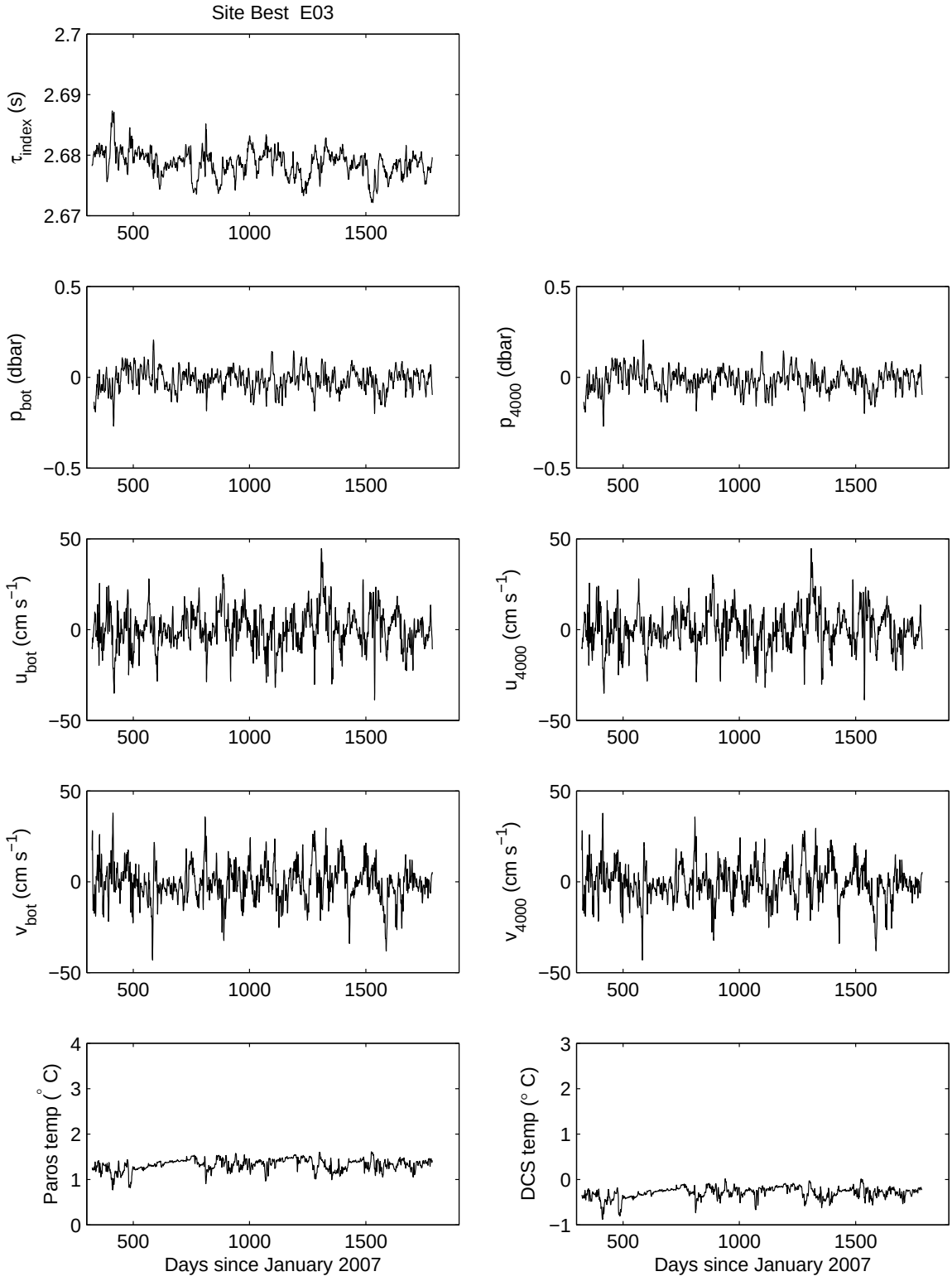

Figure 42: Time series of the 3-day low-pass filtered data obtained at site E03.

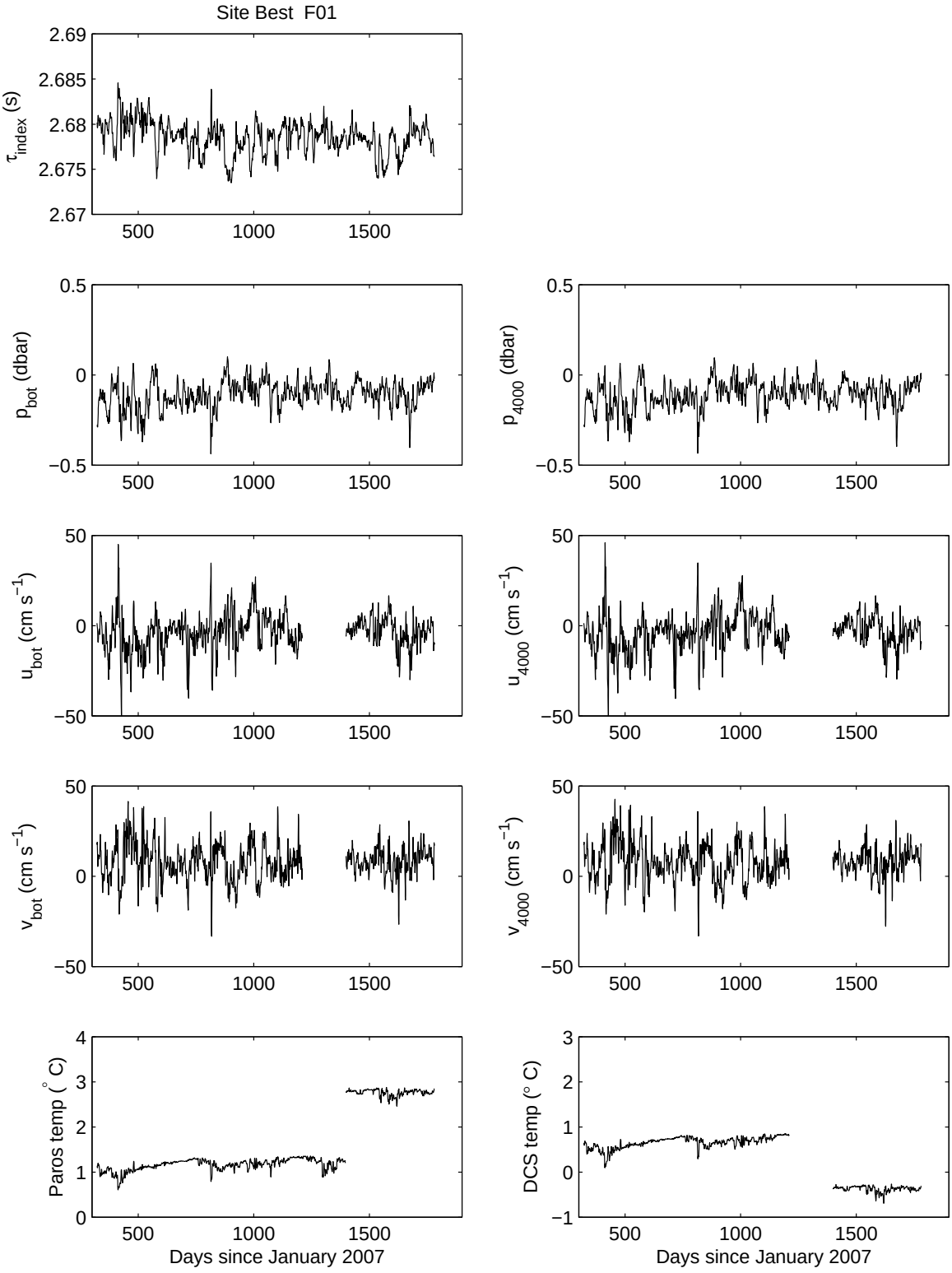

Figure 43: Time series of the 3-day low-pass filtered data obtained at site F01.

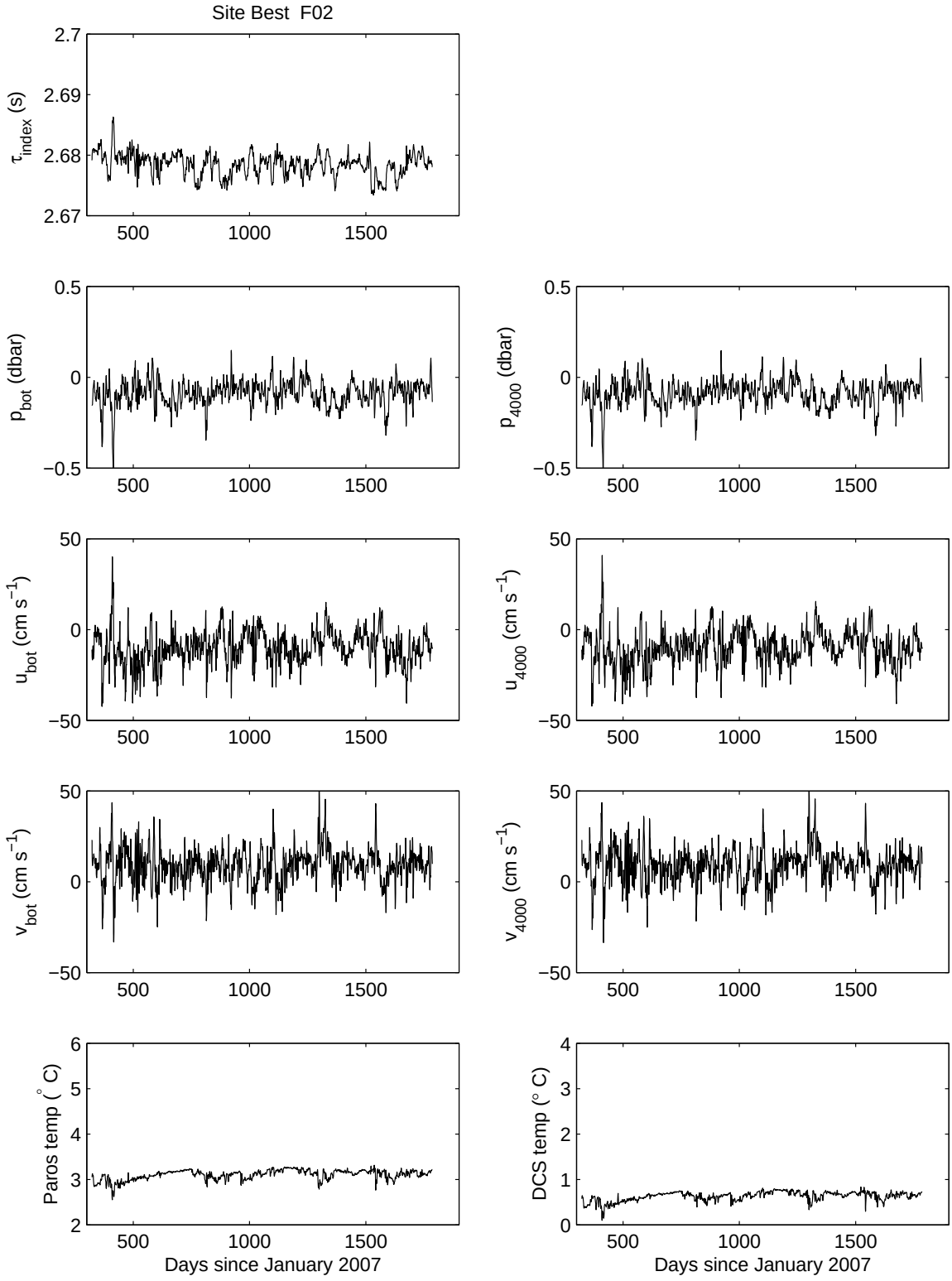

Figure 44: Time series of the 3-day low-pass filtered data obtained at site F02.

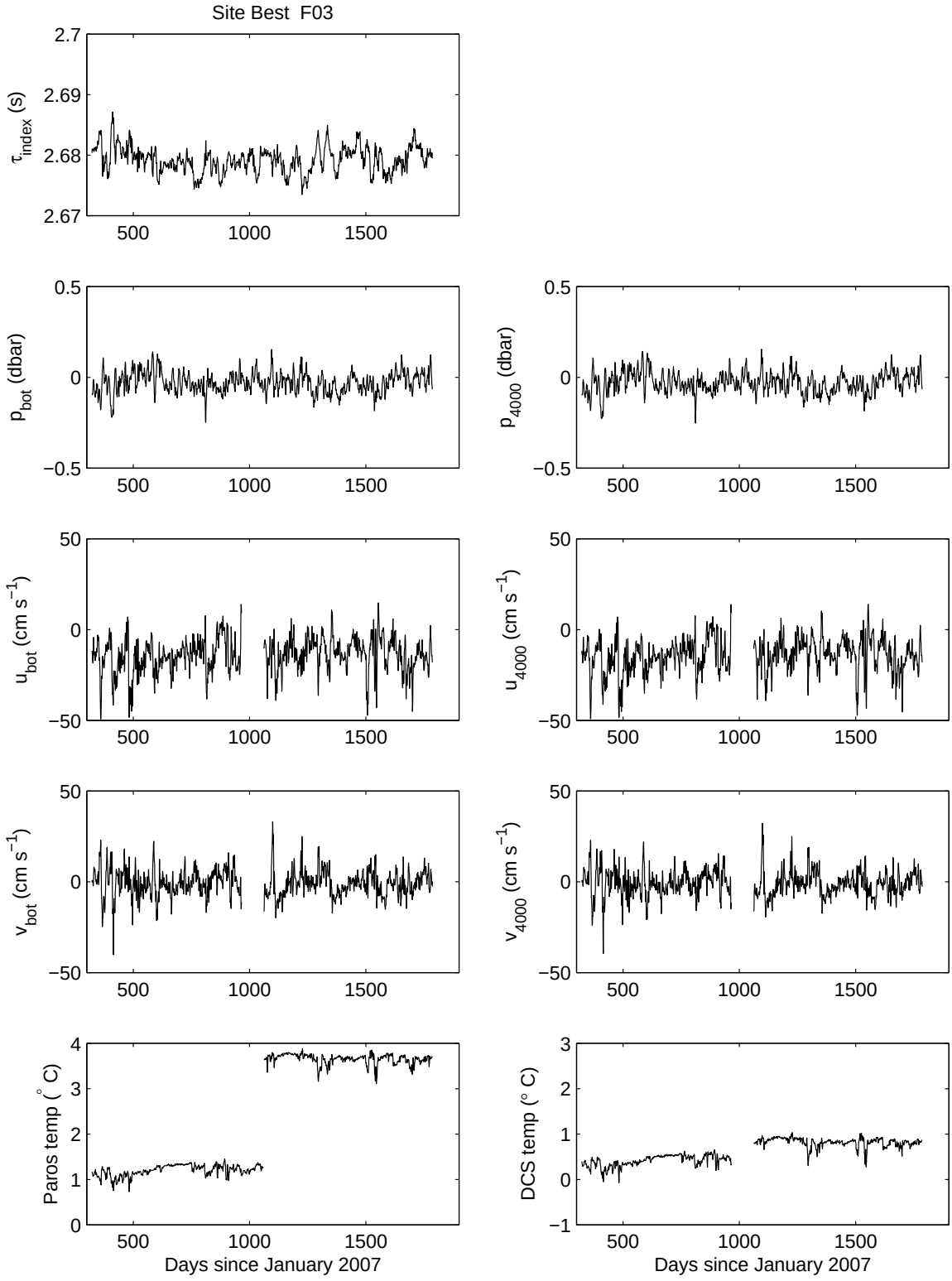

Figure 45: Time series of the 3-day low-pass filtered data obtained at site F03.

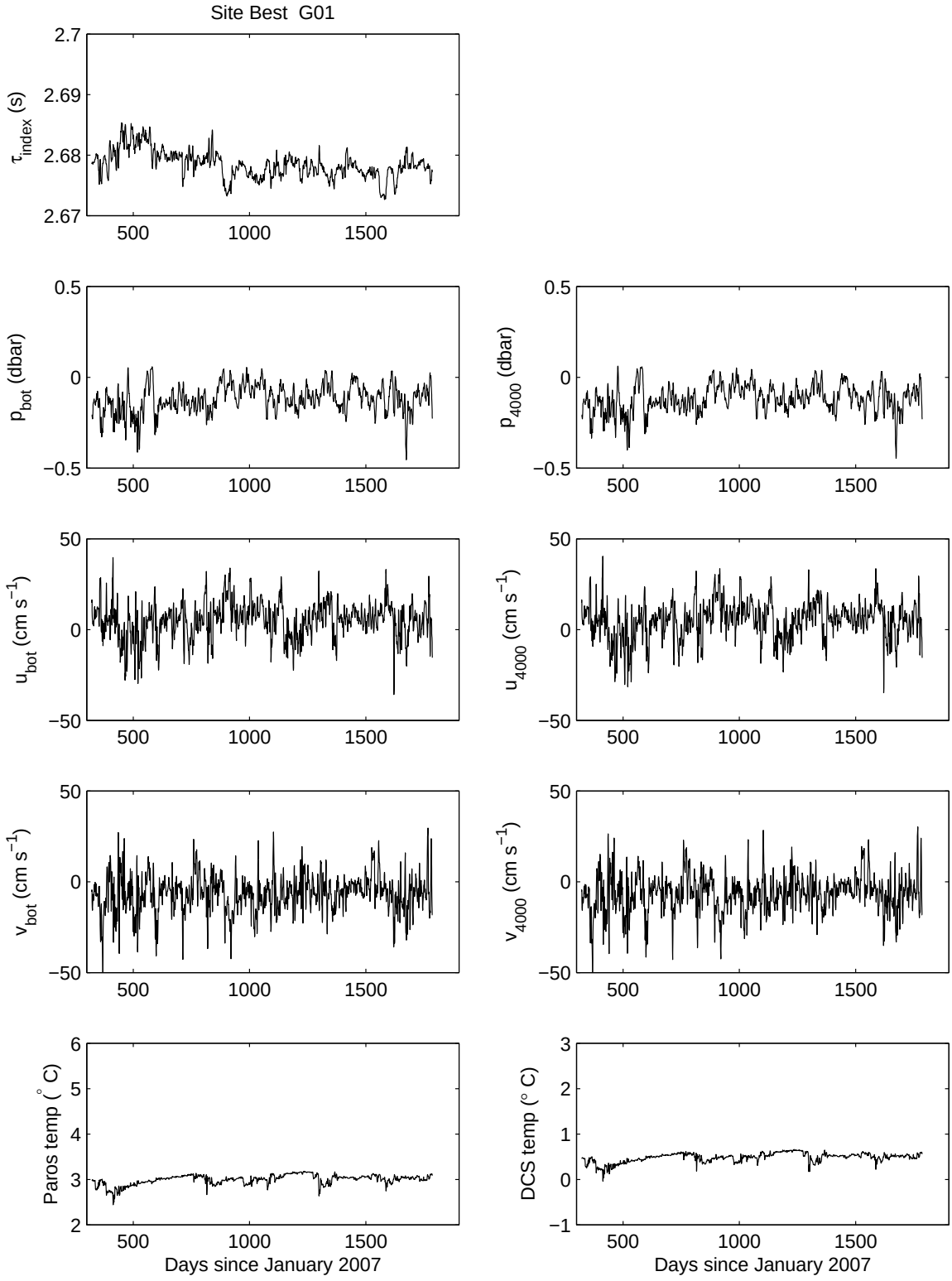

Figure 46: Time series of the 3-day low-pass filtered data obtained at site G01.

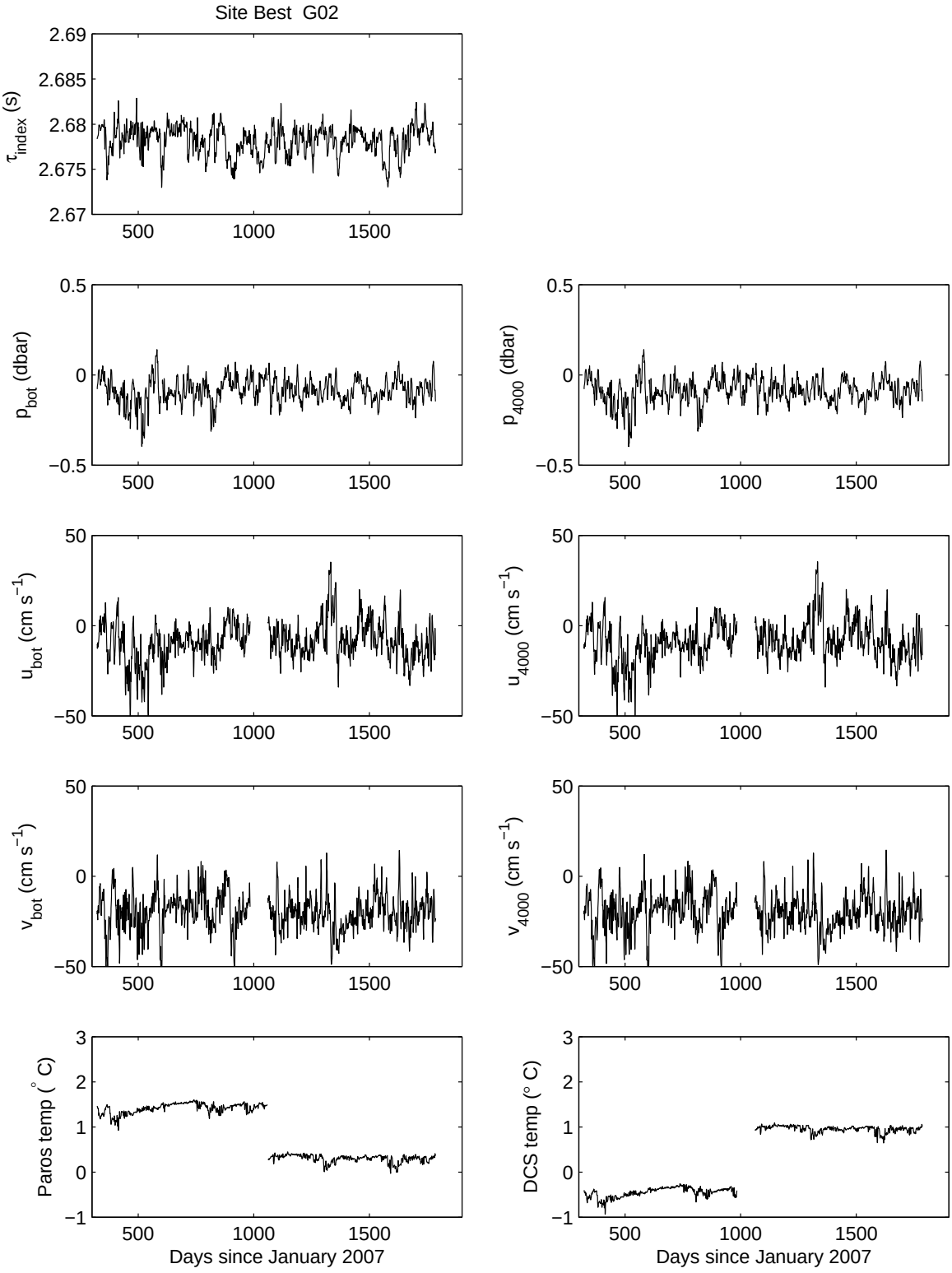

Figure 47: Time series of the 3-day low-pass filtered data obtained at site G02.

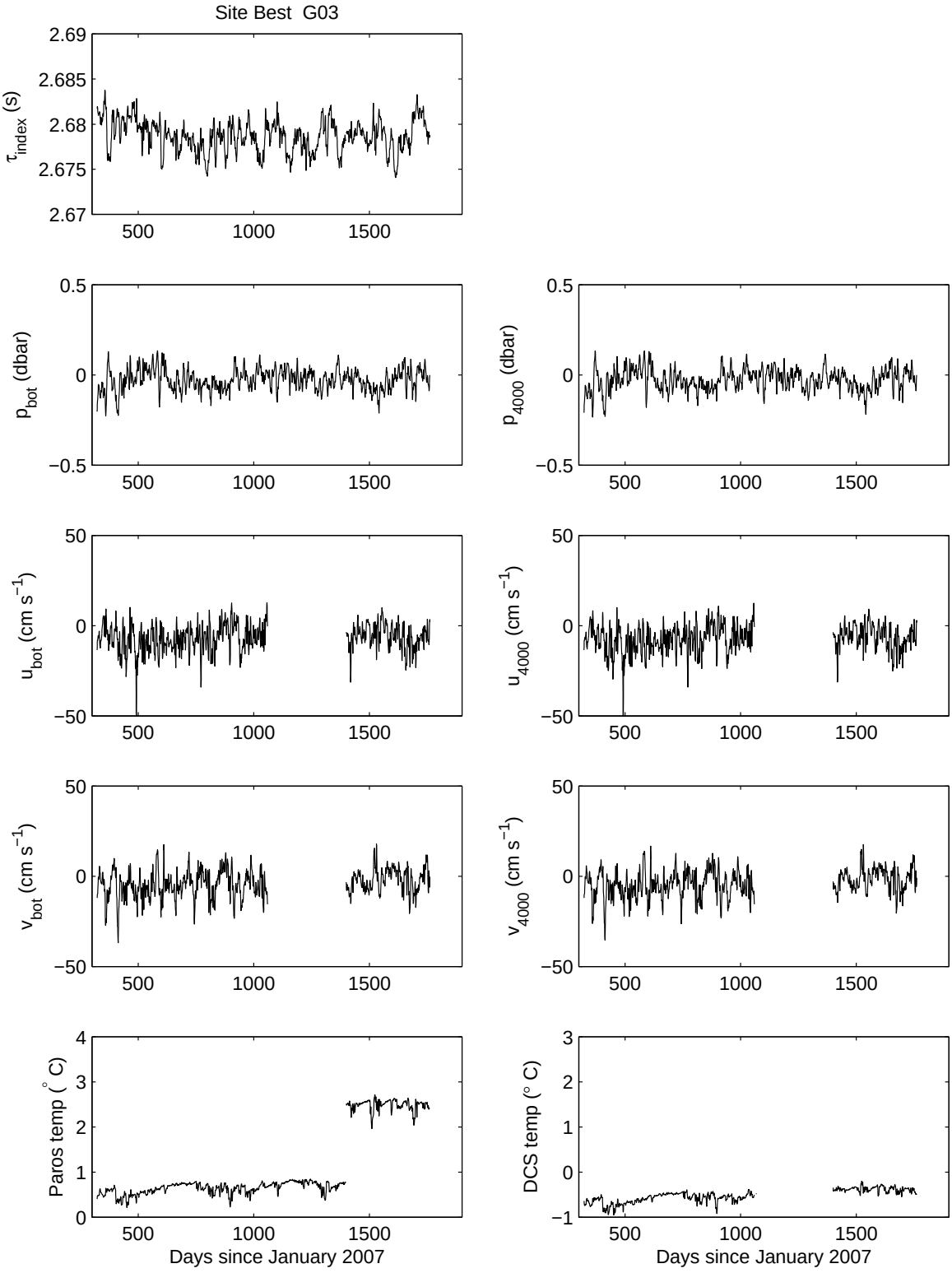

Figure 48: Time series of the 3-day low-pass filtered data obtained at site G03.

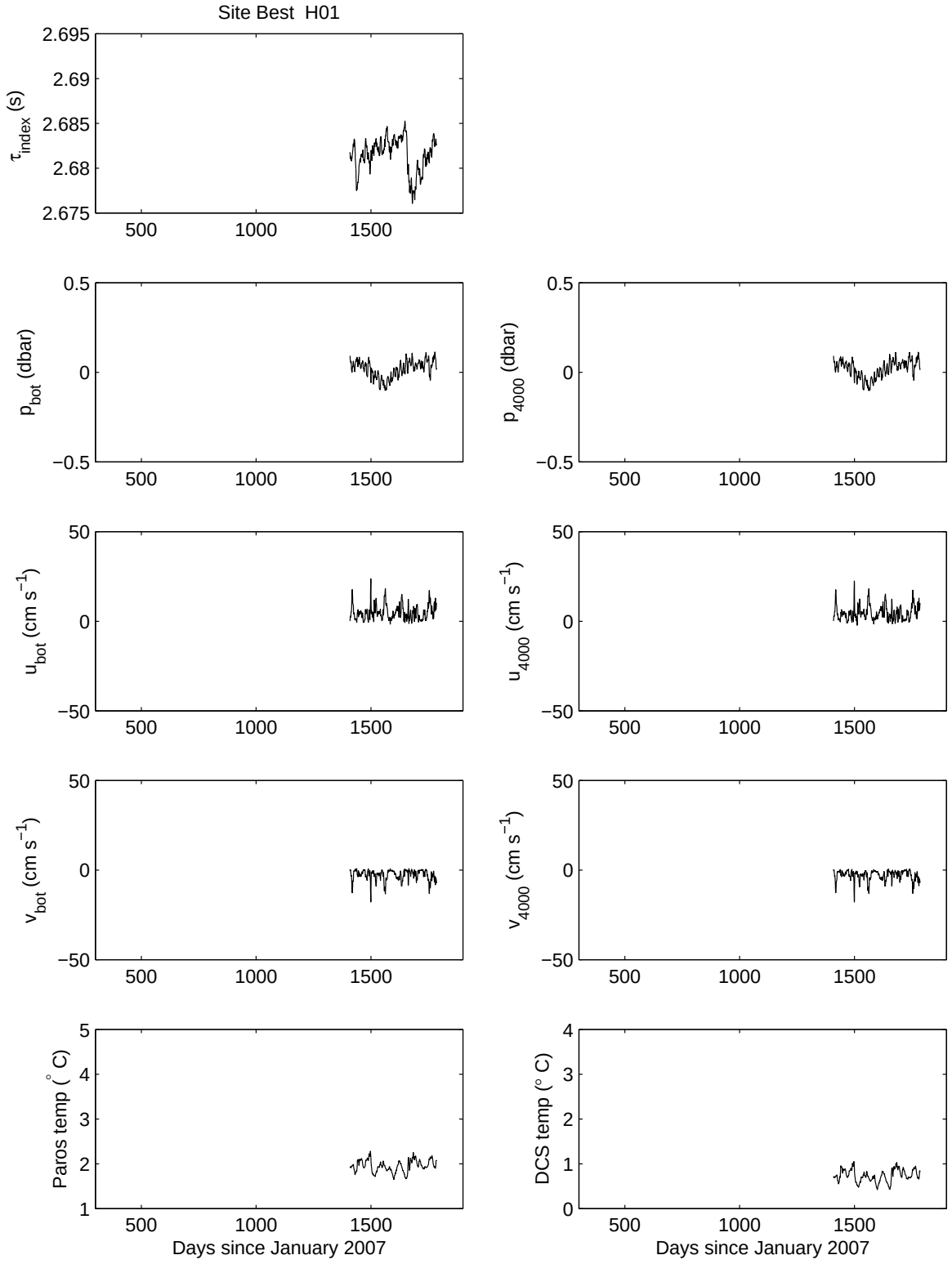

Figure 49: Time series of the 3-day low-pass filtered data obtained at site H01.

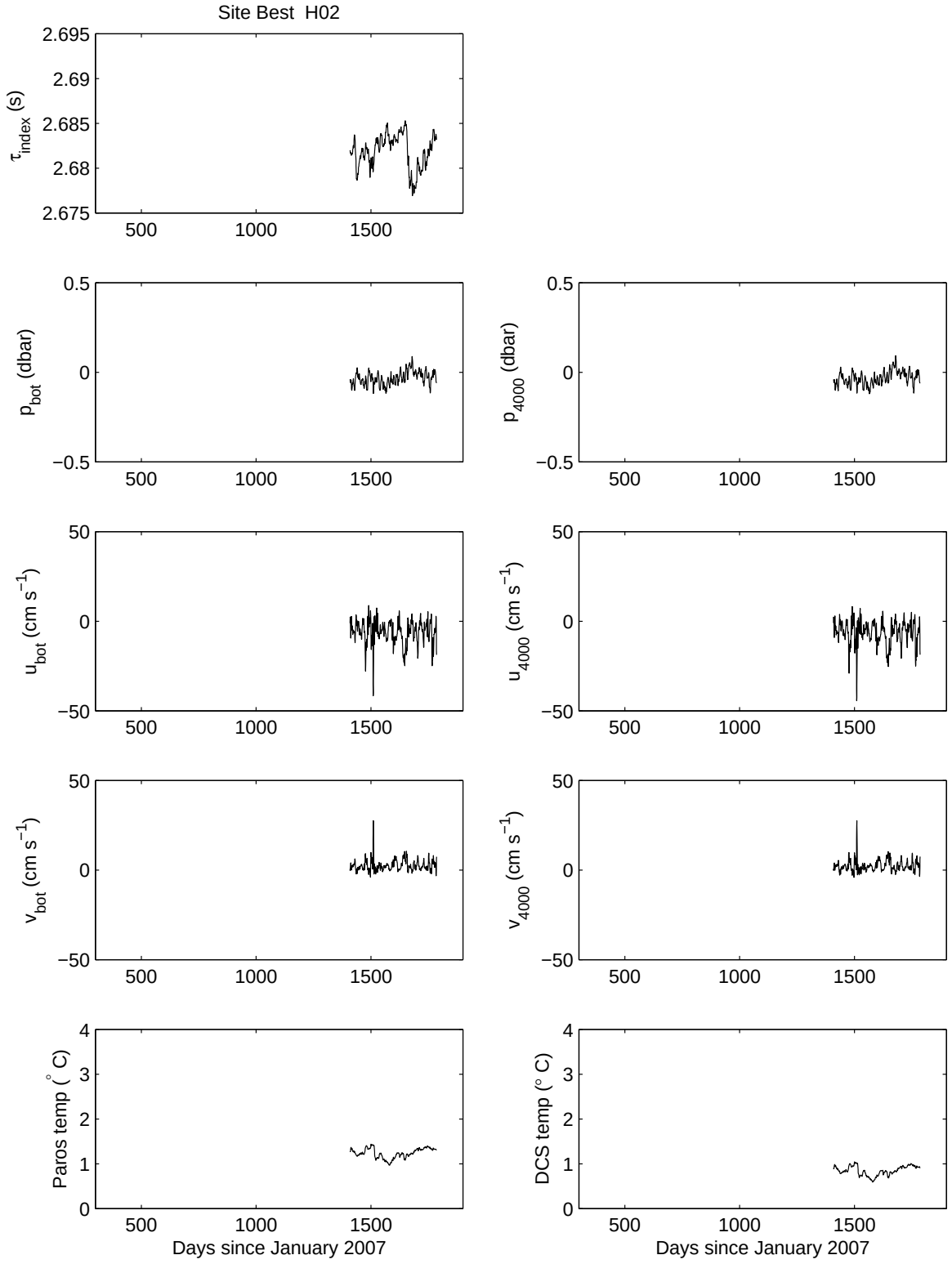

Figure 50: Time series of the 3-day low-pass filtered data obtained at site H02.

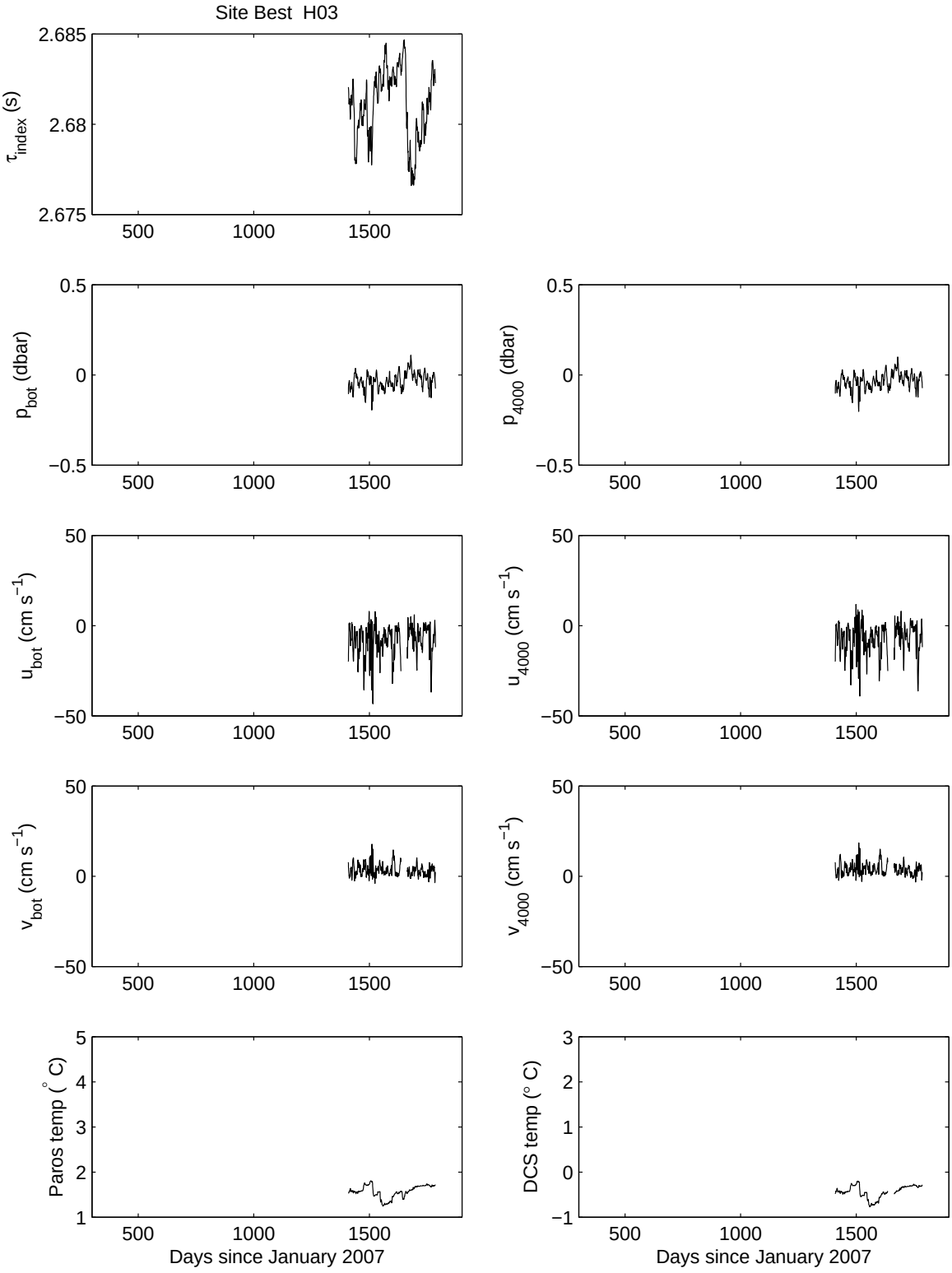

Figure 51: Time series of the 3-day low-pass filtered data obtained at site H03.

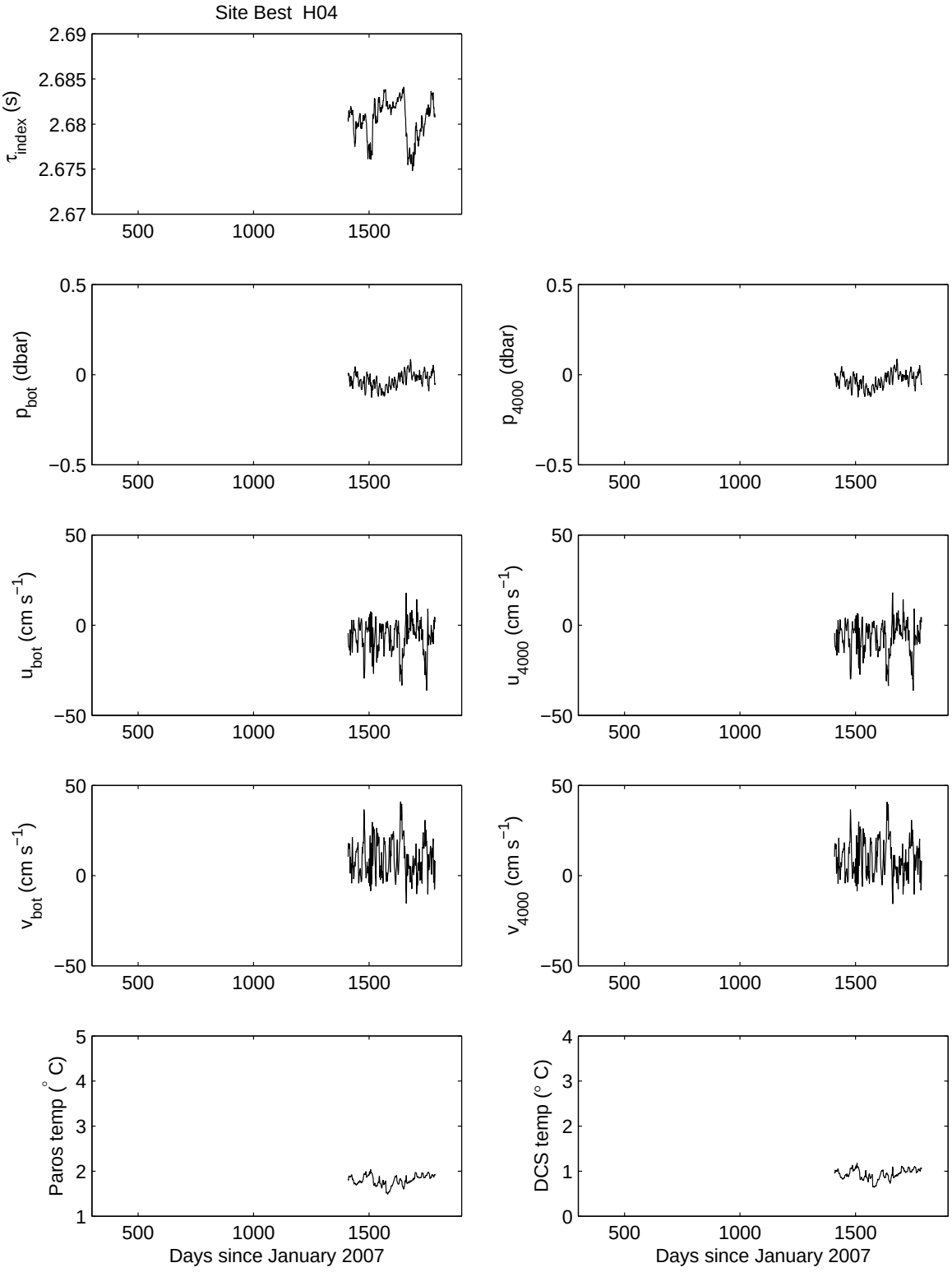

Figure 52: Time series of the 3-day low-pass filtered data obtained at site H04.

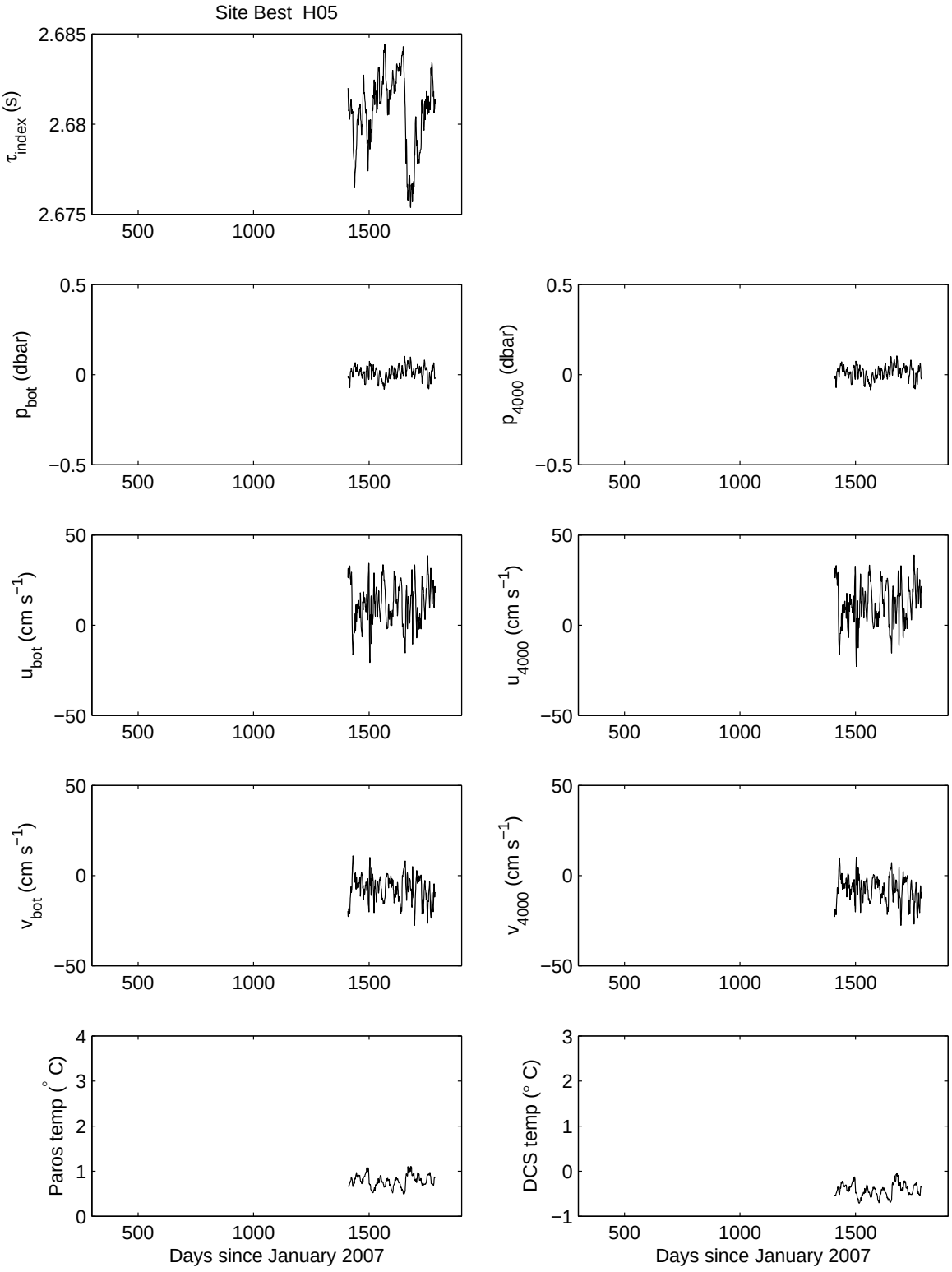

Figure 53: Time series of the 3-day low-pass filtered data obtained at site H05.

4 Acknowledgments

We gratefully acknowledge the captains and crew of the RVIB Nathaniel B. Palmer and the staff of Raytheon Polar Services for their support during the five cruises. The successful deployment and recovery of the CPIESs is due to the instrumentation development and careful preparation done by Erran Sousa, Gerard Chaplin, and Dan Holloway, who were aided by Cathy Cipolla and Gary Savoy at URI's Equipment Development Laboratory.

We thank Janet Sprintall for suppling the XCTDs, taken as part of the Scripps High Resolution XBT Program in the Drake Passage, that were used by Amy Cutting to make the seasonal GEMs. ECMWF ERA-Interim data used in this study have been obtained from the ECMWF data server (http://data.ecmwf.int/data/). University of Hawaii provided the Matlab programs to apply time-dependent declination corrections (obtained from http://www.ngdc.noaa.gov/geomag). Yvonne Firing wrote the objective mapping codes used for cDrake.

The National Science Foundation Office of Polar Programs supported this work under NSF grants ANT-0636493 and ANT-0635437.

5 References

Cutting, A. 2010. *Constituents of sea surface height variability in Drake Passage.* M.S. Thesis, University of Rhode Island. 68 pp.

Donohue, K. A., D. R. Watts, K. L. Tracey, A. D. Greene, and M. Kennelly. 2010. Mapping circulation in the Kuroshio Extension with an array of current and pressure recording inverted echo sounders. *J. Atmos. Oceanic Technol.,* **27,** 507–527.

Firing, Y. L. 2012. Structure and dynamical balance of the Antarctic Circumpolar Current in Drake Passage. Ph.D. dissertation, University of California, San Diego. 172 pp.

Godin, G. 1972. *The analysis of tides.* University of Toronto Press. 264 pp.

Hogg, N. G., and D. E. Frye. 2007. Performance of a new generation of acoustic current meters. *J. Phys. Oceanogr.,* **37,** 148–161.

Kennelly, M. A., K. L. Tracey, and D. R. Watts. 2007. Inverted echo sounder data processing manual. *GSO Technical report 2007–02.* University of Rhode Island. [Available online at http://www.digitalcommons.uri.edu/physical_oceanography_techrpts/2/.]

Kennelly, M. A., D. R. Watts, K. L. Tracey, and K. A. Donohue. 2012. An inter comparison of four models of current meter in high current conditions in Drake Passage. *GSO Technical report 2012–04.* University of Rhode Island. [Available online at http://www.digitalcommons.uri.edu/physical_oceanography_techrpts/3/.]

Munk, W. H., and D. E. Cartwright. 1966. Tidal spectroscopy and prediction, *Phil. Trans. Roy.*

Soc. London, **259,** 533–581.

Meinen, C. S., and D. R. Watts. 1998. Calibrating inverted echo sounders equipped with pressure sensors. *J. Atmos. Oceanic Technol.,* **15,** 1339–1345.

Smith, W. H. F, and D. T. Sandwell. 1997. Global seafloor topography from satellite altimetry and ship depth soundings. *Science,* **277,** 1957–1962.

Sprintall, J., T. K. Chereskin, and C. Sweeney, 2012. High-resolution underway upper ocean and surface atmospheric observations in Drake Passage: Synergistic measurements for climate science. *Oceanography,* **25,** 70–81, http://dx.doi.org/10.5670/oceanog.2012.77.

Sun, C. and D. R. Watts. 2001. A circumpolar gravest empirical mode for the Southern Ocean hydrography. *J. Geophys. Res.,* **106,** 2833–2855.

Watts, D. R., X. Qian, and K. L. Tracey. 2001. Mapping abyssal current and pressure fields under the meandering Gulf Stream. *J. Atmos. Oceanic Technol.,* **18,** 1052–1067.